

**The Effect of Boundary Conditions on the
Polymerization Shrinkage Vectors of Light-Cured
Dental Resin Composites**

vorgelegt von

Dalia Adel Mahmoud Kaisarly

2014

Aus der Poliklinik für Zahnerhaltung und Parodontologie
der Ludwig-Maximilians-Universität München

Direktor: Prof. Dr. Reinhard Hickel

**The Effect of Boundary Conditions on the Polymerization Shrinkage
Vectors of Light-Cured Dental Resin Composites**

Dissertation

zum Erwerb des Doktorgrades der Zahnheilkunde an der
Medizinischen Fakultät der
Ludwig-Maximilians-Universität zu München

vorgelegt von

Dalia Adel Mahmoud Kaisarly

aus

Kairo, Ägypten

2014

Mit Genehmigung der Medizinischen Fakultät der
Universität München

Berichterstatter: Prof. Dr. Karl-Heinz Kunzelmann

Mitberichterstatter: Priv. Doz. Dr. Andreas Fottner
Priv. Doz. Dr. Jan-Frederik Güth

Mitbetreuung durch den promovierten
Mitarbeiter: ---

Dekan: Prof. Dr. med. Dr. h.c. M. Reiser, FACR, FRCR

Tag der mündlichen Prüfung: 17.12.2014

TO MY FAMILY

Acknowledgement

I would like to express my deepest thanks to Prof Dr Karl-Heinz Kunzelmann for giving me the opportunity to conduct this unique research under his meticulous and devoted supervision in the field of medical image registration and to use the exclusive software for performing this research. He gave me the flexibility in taking my own path and encouraged me to pursue my ideas.

Furthermore, I would like to thank Prof Dr Reinhard Hickel, director of the Department of Restorative Dentistry, Periodontology and Pedodontics, Ludwig-Maximilians-University Munich, Munich, Germany for hosting me as a guest researcher.

I would also like to thank Prof Dr Peter Rösch from the Faculty of Computer Science, University of Applied Sciences, Augsburg, Germany, for his support and for giving me more insights into the medical image registration processes.

Special thanks go to both Mrs Evi Köbele for the valuable Micro-CT support and SEM images, and Mrs Gisela Dachs for the SEM images and materials' photos in addition to their never ending kind assistance.

More thanks go to Mr Thomas Obermeier for his continuing technical support and Mr Jian Jin for his help especially in the starting phase of my work, also Mr Stefan Spindler for preparing the non-adhesive cavity model and to Dr Michael Wiseman for helping me with the statistical analysis.

I am very grateful for having found friends in my colleagues at the Tribolabor: Dr Indra Nyamaa, Dr Yu-Chih Chiang, Antonia Chouliara, Dr Jury Malyk, Dr Guangyun Lai, Xiaohui Xu, Chen Quan, Liya Zhao and Dr Nataliya Deyneka Dupriez.

I would also like to thank Prof Dr Sayed Saniour, chief of the Department of Biomaterials and my colleagues at the Department of Biomaterials at the Faculty of Oral and Dental Medicine, Cairo University, Cairo, Egypt, for accepting my research vacation with the purpose of performing research at the Faculty of Dentistry at the LMU Munich, Germany.

I owe deep thanks and gratitude to all people who contributed to the success of my work, even those I failed to mention here. Finally, I would like to thank my whole family, especially my dear mother and my late father, for supporting me and believing in me; without their endless help this project would never have been completed.

Contents

1	General Introduction and Literature Review.....	1
1.1	Historical background of dental resin composites	1
1.2	Composition of dental resin composites	1
1.2.1	Polymer matrix.....	1
1.2.2	Fillers.....	4
1.2.3	Coupling agent	5
1.2.4	Initiator-accelerator system.....	6
1.2.5	Polymerization kinetics	7
1.3	Polymerization shrinkage	8
1.4	Methods for measuring polymerization shrinkage stress	9
1.5	Methods for measuring polymerization shrinkage	13
1.5.1	Volumetric shrinkage measurement.....	13
1.5.2	Linear shrinkage measurement.....	15
1.5.3	Cuspal deflection measurement.....	18
1.5.4	Measurement of adverse effects of polymerization shrinkage	19
1.5.5	Finite element analysis (FEA).....	20
1.5.6	Methods employing micro-CT data for the evaluation of polymerization shrinkage	20
2	Aim of the study.....	28
	Hypothesis.....	29
3	Shrinkage Vectors in Different Cavity Configurations	30
3.1	Abstract	30
3.2	Introduction	31
3.3	Aim of the study	33
3.4	Materials and Methods	33
3.4.1	Specimen preparation.....	33
3.4.2	Preparation of the experimental traceable resin composite.....	33
3.4.3	X-ray micro-computed tomography measurements	34
3.4.4	Data processing	37
3.4.5	Scanning electron microscopy.....	38
3.5	Results	40
3.5.1	Qualitative presentation of polymerization shrinkage: Visualization of shrinkage vectors in the displacement vector fields and SEM.....	40
3.5.2	Quantitative presentation of polymerization shrinkage: values of shrinkage vectors and statistical analysis	46
3.6	Discussion	50
	Conclusions	59
4	Composite Shrinkage Vectors in Ceramic Cavities with Different Boundary Conditions	60

4.1	Abstract	60
4.2	Introduction	61
4.3	Aim of the study	62
4.4	Materials and Methods	62
4.4.1	Specimen preparation	63
4.4.2	Statistical analysis	64
4.5	Results	65
4.5.1	Qualitative presentation of polymerization shrinkage: Visualization of shrinkage vectors in displacement vector fields and SEM	65
4.5.2	Quantitative presentation of polymerization shrinkage: values of shrinkage vectors and statistical analysis	69
4.6	Discussion	72
	Conclusions	75
5	Composite Shrinkage Vector Patterns In Non-Adhesive Teflon Cavities	76
5.1	Abstract	76
5.2	Introduction	77
5.3	Aim of the study	78
5.4	Materials and Methods	78
5.4.1	Specimen preparation	78
5.5	Results	80
5.5.1	Qualitative presentation of polymerization shrinkage: Visualization of shrinkage vectors in the displacement vector field	80
5.5.2	Quantitative presentation of polymerization shrinkage: values of shrinkage vectors and statistical analysis	81
5.6	Discussion	83
	Conclusions	87
6	Shrinkage Vectors in an Experimental Cavity with Enamel Floor	88
6.1	Abstract	88
6.2	Introduction	89
6.3	Aim of the study	90
6.4	Materials and Methods	90
6.4.1	Specimen preparation	90
6.4.2	Statistical analysis	91
6.4.3	Scanning electron microscopy	91
6.5	Results	93
6.5.1	Qualitative presentation of polymerization shrinkage: Visualization of shrinkage vectors in the displacement vector field and SEM	93
6.5.2	Quantitative presentation of polymerization shrinkage: values of shrinkage vectors and statistical analysis	97
6.6	Discussion	101

Conclusions	105
7 Summary	106
Conclusions	109
Recommendations for future research.....	109
8 Zusammenfassung.....	110
5 List of tables	113
6 List of figures	114
7 Annex	121
7.1 Materials and equipments.....	121
7.2 Protocol for the silanization of the traceable glass beads.....	124
8 References	127

1 General Introduction and Literature Review

1.1 Historical background of dental resin composites

Dental resin composites are composed of at least two different materials, an organic resin matrix and inorganic fillers. They were first introduced by Raphael L. Bowen in 1962 with the synthesis of a Bis-GMA monomer formulation filled with finely ground quartz (Bowen, 1962; 1963). Composites were preceded by unfilled acrylic resin and epoxy resins as direct restorative materials for the use in the anterior regions (Bowen, 1956). At about the same time, Michael G. Buonocore worked on acid etching and dentin conditioning targeting to bond unfilled acrylic resin to tooth structure (Buonocore, 1955; Buonocore et al., 1956). From this point onward, research on resin composites and bonding materials and techniques has been continuously conducted to improve the performance and longevity of these restorations.

1.2 Composition of dental resin composites

A resin composite is composed of four major components: organic polymer matrix, inorganic filler particles, coupling agent, and the initiator-accelerator system.

1.2.1 Polymer matrix

The organic polymer matrix in most commercial composites is a cross-linked matrix of dimethacrylate monomers typically selected from Bis-GMA (bisphenol A-glycidyl-dimethacrylate), BisEMA (ethoxylated bisphenol A-dimethacrylate) and/or UDMA (urethane dimethacrylate). Bis-GMA is one of the most frequently used monomers, only in small amounts, as it has an affinity for water absorption that leads to swelling and discoloration. UDMA has the advantage of being less viscous than Bis-GMA, so it can be used undiluted, and having no hydroxyl groups (OH-groups), therefore, exhibiting less water sorption (Sakaguchi and Powers, 2012; Scientific Documentation Tetric EvoCeram® Bulk Fill, 2013). TEGDMA (triethylene glycol dimethacrylate), a low-viscosity reactive diluent, is used to lower the viscosity of the resin and enable sufficient filler incorporation (Figure 1). Although it increases conversion, the modulus is decreased and finally polymerization shrinkage and stress are increased (Cramer et al., 2011).

The most common monomers are aromatic dimethacrylates that undergo polymerization by free-radical initiation via the double bonds at the end of the molecules that results in 2-6% shrinkage (Sakaguchi and Powers, 2012). The reduction of the polymerization shrinkage is the main aim of manufacturers and clinicians as the contraction brings with it many adverse effects like microleakage, marginal gaps and postoperative hypersensitivity which can all lead to failure of the restoration. Therefore, manufacturers have attempted to reduce the shrinkage by synthesizing new blends of fillers and monomers, while on the clinical part, researchers try to reduce the shrinkage effects by clinical restorative techniques as for example incremental filling, slow start polymerization (Lee et al., 2005).

More recently, siloranes, low-shrink composites, have been introduced that contain monomers with epoxy (oxirane) functional groups. The polymerization of these monomers is initiated by cations and proceeds by the ring-opening mechanism resulting in lower shrinkage values even <1 vol% by the bonded-disc method (Filtek™ Silorane, Silorane System Adhesive, Technical Product Profile, 2007; Sakaguchi and Powers, 2012; Weinmann et al., 2005).

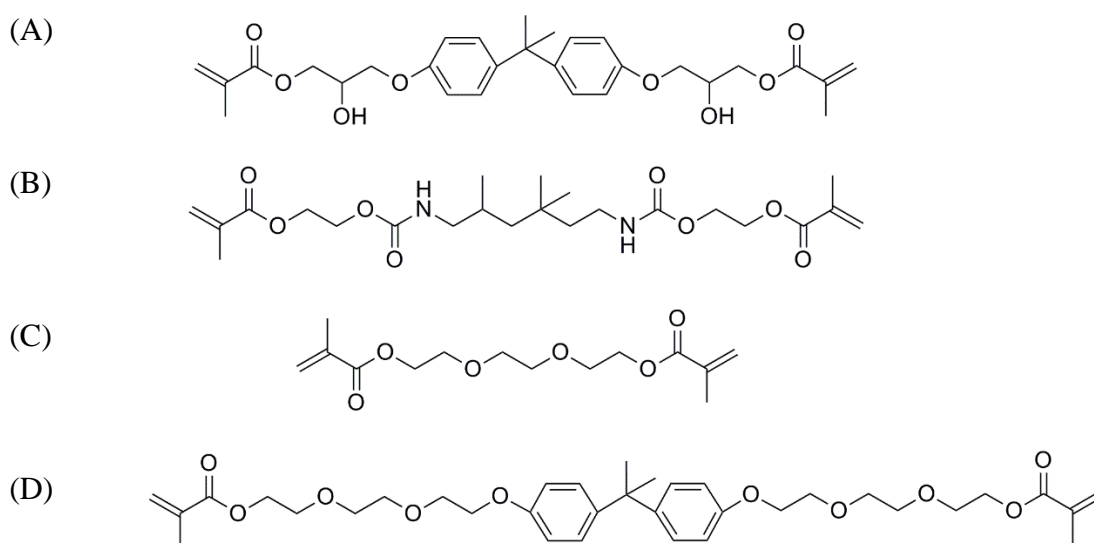


Figure 1 The chemical structure of Bis-GMA (A), UDMA (B), TEGDMA (C) and Bis-EMA6 (D).

Table 1 Classification of composites according to the functional group determining their cure (Kunzelmann, 2008)

Matrix according to the functional group	Chemical system	Properties of composites with this matrix	Examples
Pure methacrylates	Classical dental matrix, e.g. Bis-GMA, UDMA, TEGDMA	Polarity of the matrix varies depending on the composition High strength	Tetric Ceram/Vivadent, Charisma/Kulzer, P60/3M , Z100/3M, 250/3M, TPH- Spektrum/Dentsply, Pertac II/Espe
	Classical ormocers, differ from classical monomers in the non-reactive part (Si-O-network)	Hydrophobic Low elution of monomers	Definite/Degussa
Acid modified methacrylates	Compared with the classical dental matrix it has more hydrophilic monomer components e.g. polar side groups (COOH=compomers)	More hydrophilic than the pure methacrylate matrix	Dyract AP/Dentsply, Compoglass F/Vivadent, Hytac/Espe
	Ormocers with carboxylic function	Low elution of monomers	Admira/Voco
Ring opening epoxides	oxirane	Low shrinkage High strength	Not available commercially
	Silorane (siloxane with oxirane function)	Low shrinkage High strength hydrophobic	P90 Silorane/3M ESPE

1.2.2 Fillers

Fillers constitute the major portion of the composite by weight. They are added to the resin matrix to reduce polymerization shrinkage and stress, to reinforce the resin matrix, and to provide an appropriate degree of translucency. The fillers consist of inorganic material such as finely ground quartz or glass, sol-gel derived ceramics, microfine silica, or nanoparticles. Most glasses contain heavy-metal oxides such as barium, zinc, yttrium fluoride, or ytterbiumtrifluoride for radiopacity. Fillers are usually silanized to bond to the organic matrix and transfer the stresses to the fillers. However, some researchers kept fillers nonbonded for stress reduction (Condon and Ferracane, 1998).

Composites are classified according to the filler system. Fillers influence the materials' properties through even minute addition of separate components. Therefore, mixtures of large and small fillers are used in order to incorporate as many fillers as possible. Small fillers are located in the spaces between larger ones. Some fillers are added for radioopacity, for example ytterbium fluoride, Table 2 (Kunzelmann, 2008).

Table 2 Kunzelmann's classification of composites according to filler system (Kunzelmann, 2008)

Filler system	Examples
SiO ₂	Isosit, Vivadent
SiO ₂	Durafill, Kulzer; Silux Plus, 3M
Quartz + SiO ₂	Pertac II, Espe
Compact glasses + SiO ₂	TPH Spektrum, Dentsply; Charisma, Kulzer, etc.
Compact glasses + SiO ₂ + spherical, sintered mixed oxides	Tetric Ceram, Vivadent
Porous glasses + compact glasses + SiO ₂	Solitaire, Kulzer; Solitaire 2, Kulzer
Fibres + compact glasses + SiO ₂	Alert, Jeneric Pentron
Ion-releasing fillers + compact glasses + SiO ₂	Ariston, Vivadent
Compact glasses + SiO ₂ + spherical, sintered mixed oxides + prepolymerized fillers with [compact glasses + SiO ₂ + spherical, sintered mixed oxides]	Tetric EvoCeram, Vivadent
Multimodal, spherical fillers prepared according to the sol-gel-method	Palcifique Estelite, Tokuyama Dental; P60, 3M; Z100, 3M; Z250, 3M
Nanofiller-primary-particle + calcined nanofiller agglomerates	Filtek Supreme (XT), 3M-Espe
Nanofiller-primary-particle + compact glasses	Grandio, Voco

Composites are classified according to the particle size, shape, and the particle-size distribution of the filler into macrofilled, hybrid and microhybrid composites, nanofill and nanohybrid composites, Table 3, (Sakaguchi and Powers, 2012).

Table 3 Traditional classification of resin composites (Sakaguchi and Powers, 2012)

Type of composite	Filler size
Macrofilled (early composites)	average filler diameter of 20-30 μm
Hybrid	two types of fillers blended together: 1) fine particles of average particle size 2-4 μm and 2) 5-15% of microfine particles, usually silica, of particle size 0.04-0.2 μm
Microhybrid (60-70% filler by volume translates into 77- 84% by weight)	1) fine particles of a lower average particle size 0.04-1 μm are blended with microfine silica 2) The fine particles may be obtained by grinding glass (borosilicate glass, lithium or barium aluminum silicate glass, strontium or zinc glass), quartz, or ceramic materials and have irregular shapes
Nanofill	nanometer sized particles 1-100 nm
Nanohybrid	1) these consist of large particles 0.4-5 μm with added nanometer sized particles 2) they are hybrid materials, not true nanofilled composites

1.2.3 Coupling agent

The manufacturers surface-treat the fillers by a silane coupling agent to form a bond between the inorganic and organic phases of the composite. One end of the molecule, that contains functional groups, hydrolyzes to generate hydroxyl groups and then reacts with the hydroxyl groups on the surface of the filler through condensation reaction. The other end has a methacrylate double bond that copolymerizes with the monomers during curing of the composite (Figure 2). The coupling agent strongly binds the filler to the resin matrix, thereby enhancing the mechanical properties of the composite by transferring the stresses from the mechanically weak matrix to the stronger filler in addition to providing a hydrophobic environment that minimizes water absorption. A typical silane coupling agent is 3-methacryloxypropyltrimethoxysilane (MPTS), while in the low-shrink silorane composite,

an epoxy functionalized coupling agent, 3-glycidoxypropyltrimethoxysilane, is used to bond the filler to the oxirane matrix (Sakaguchi and Powers, 2012).

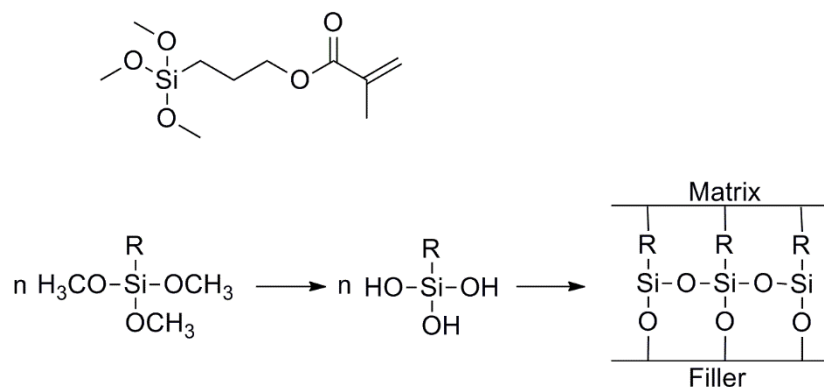


Figure 2 The silane coupling agent.

1.2.4 Initiator-accelerator system

The function of the initiator-accelerator system is to initialize the network forming polymerization. The polymerization reaction can be started by light-activation, chemical activation, and dual curing which is chemical and light-curing together. Light activation is usually achieved with blue light at a peak wavelength of 470 nm, that is absorbed by a photosensitive agent, most commonly camphorquinone 0.1-1.0%. The free radical reaction is accelerated in the presence of an organic amine. The disadvantage of camphorquinone is its yellowish tint and the toxicity concerns over the amine co-initiator that is used with camphorquinone (Cramer et al., 2011). In the silorane composite, camphorquinone, iodonium salts and electron donors generate cations that start the ring opening polymerization process (Sakaguchi and Powers, 2012).

Alternatives to camphorquinone/amine systems are the phosphine oxide initiators. They initiate through a cleavage mechanism that does not require a co-initiator. They absorb in the visible range, however exhibit little absorption beyond 420 nm and are therefore not ideal for use in dental applications, as dental curing lamps are designed to match the absorbance spectrum of camphorquinone at 470 nm. On the other hand, Lucirin TPO is an acyl phosphine oxide that bleaches out after polymerization, therefore it can be used for composite bleach shades or colorless protective varnishes. Another initiation system is based on benzoylgermanium derivatives that undergoes photodecomposition to form radicals

without the need for a co-initiator. Recently introduced bulk fill composites are intended for use in increments up to 4 mm, which is achieved by a combination of camphorquinone, phosphine oxide and a germanium based photoinitiator as Ivocerin. It allows curing in large increments with an absorption maximum in the blue light range around 370-460 nm. It is more reactive than camphorquinone or Lucirin TPO resulting in more rapid polymerization with greater depth of cure (Cramer et al., 2011; Scientific Documentation Tetric EvoCeram® Bulk Fill, 2013).

1.2.5 Polymerization kinetics

The free monomer molecules are loosely bonded by weak van der Waals force and upon polymerization, the monomers are tightly linked by covalent bonds in a polymer with a smaller distance between the molecules leading to polymerization shrinkage.

Polymerization contraction strain is time-dependent and proceeds in two stages: pre-gelation and post-gelation, or rigid contraction (Bausch et al., 1982). Two macroscopic demarcations occur during polymerization: the gel point conversion at which an incipient gel is formed. The second macroscale demarcation is the vitrification point which represents the conversion at which the polymer becomes glassy, accompanied by an increase in modulus. These polymer networks are extremely heterogeneous which grow from microgels arising near sites of initiation (Cramer et al., 2011). Plastic flow occurs during the initial phase and internal stresses within the material undergo stress-relaxation, while stress development occurs beyond the gel point and its magnitude depends on the elastic modulus (Braem et al., 1987).

Hardness is taken as an indirect measure for the degree of cure, and is measured in a longitudinally sectioned specimen from the top of restoration until the bottom, with decreasing hardness values denoting decreasing degree of conversion with increased thickness and distance from the light source (Cho et al., 2011; Onose et al., 1985). Over 20 years ago, the question about anisotropy of the cure pattern was raised with possible variation of shrinkage patterns within the material, relative to the initiating light source, with respect to material thickness and surface area. In cases where material specimens are imperfectly cured, the measured shrinkage will be correspondingly reduced (Onose et al., 1985; Watts et al., 1984; Watts and Cash, 1991).

Recent studies investigated light beam profiles and their effect on the polymerization of the composites. Irradiance values calculated by conventional methods assume power uniformity within the light beam but do not describe the distribution of the irradiance delivered. Beam profilers investigated the optically active emitting area, the mean irradiance, the irradiance

distribution and the top hat factor with differences among various light curing units. This could propose improper curing of deeper parts of a restoration due to beam inhomogeneity (Price et al., 2010e; Price et al., 2011).

1.3 Polymerization shrinkage

Since the use of resin composites as restorative materials, a lot of research has been conducted in the field of polymerization and its effects as shrinkage and stress. In vivo tests focused on indirect evaluation of gap formation by resin replica technique (Opdam et al., 1998; Qualtrough et al., 1991; Roulet et al., 1991). In vitro test methods investigate the resin composite in form of a material sample or applied within a cavity prepared in human teeth (Chiang et al., 2010) or other material such as resin composite or ceramic block (Cho et al., 2011; Li et al., 2011).

Composites undergo volumetric shrinkage of 2-6% upon setting, which creates 5-15 MPa contraction stresses (Feilzer et al., 1987) between the composite and the tooth, straining the interfacial bond, leading to debonding, microgaps and cuspal deflection. This stress can even exceed enamel's tensile strength and result in stress cracking and enamel fractures along the interfaces. Restorative failures as hypersensitivity, pulpitis and secondary caries may occur (Ferracane, 2005; 2008; Kleverlaan and Feilzer, 2005; Labella et al., 1999).

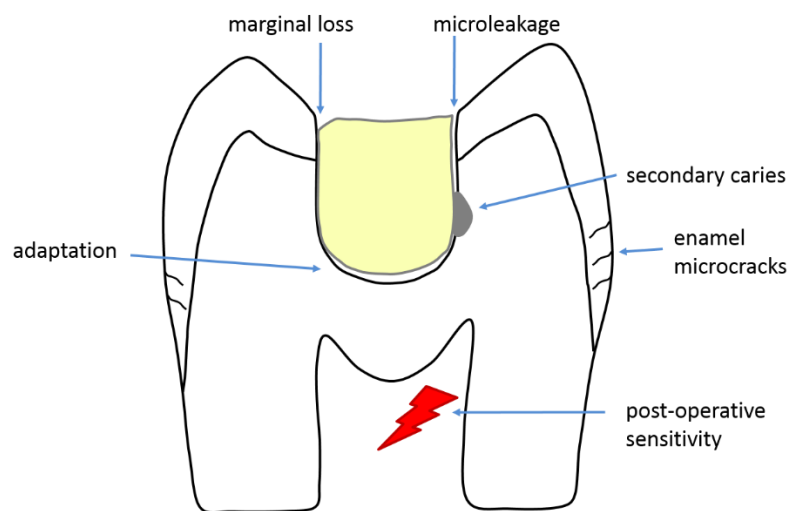


Figure 3 Failures that may occur after application of a composite restoration, modified after Tantbirojn et al., 2004 (Tantbirojn et al., 2004)

The greater the volumetric shrinkage is, the greater is the shrinkage stress for a comparable elastic modulus. The development of shrinkage stress depends on the volumetric shrinkage strain and the stiffness of the composite at the time of shrinkage; even low-shrinkage composites might exhibit high stress when having a high elastic modulus. A 2 mm incremental application of composite and polymerizing each increment independently is usually advised to ensure a full depth of cure and to reduce the net effect of polymerization shrinkage. Net shrinkage stress is assumed to be less because a smaller volume of composite is allowed to shrink before successive additions. (Sakaguchi and Powers, 2012). On the other hand, Versluis et al., 1996 showed that the incremental application combined with a well-established bond to the tooth increased the deformation of the restored tooth and in turn the stress level within the tooth-restoration complex (Versluis et al., 1996).

Feilzer et al., 1987, showed that the stress development in a bonded composite restoration depends on the restoration geometry, in that the pregelation flow of the material is inhibited when the ratio of the bonded surface exceeds a certain limit; the magnitude of stress can be estimated through the C-factor (configuration factor) which is the ratio of bonded to unbonded areas. The higher the C-factor, the greater the stress level. This observation is related to the description of shrinkage as a vector, having both magnitude and direction (Feilzer et al., 1987). Other studies criticized that the C-factor does not take into account the volume of the applied composite and Braga et al., 2006, related shrinkage stress to microleakage in restorations of larger size (Braga et al., 2006; Watts and Satterthwaite, 2008).

1.4 Methods for measuring polymerization shrinkage stress

Early shrinkage stress measurements were performed by Bowen (Bowen, 1967; Bowen et al., 1983) and Hegdahl (Hegdahl and Gjerdet, 1977) using a **Universal Testing (Instron) machine** (UTM), while a **servo-hydraulic UTM** was used by the ACTA group of Davidson, Feilzer, de Gee and Alster who achieved major insights and developments, including the effect of C-factor on the stress magnitudes and eliminating the effect of system compliance. Unfortunately this approach was expensive and complex, in addition to the basic limitation of eliminating compliance for load measurement systems as they imply finite compliance. (Alster et al., 1997; Davidson and de Gee, 1984; Davidson and Feilzer, 1997; Feilzer et al., 1988; 1989; 1990; Watts et al., 2003). An apparatus with a controlled compliance to measure contraction stress was developed by Sakaguchi et al., 2004, in which the composite specimen

was located between a glass plate and a steel rod that measured the developed force upon curing (Sakaguchi et al., 2004a).

Polymerization shrinkage stress was also determined by a **tensilometer** (Davidson and de Gee, 1984; Davidson et al., 1984; Feilzer et al., 1987) and **strain gauges** (Sakaguchi et al., 1992). A **stress-strain-analyzer testing machine** was developed by Dullin, 1998, during his master's thesis under the supervision of Kunzelmann and Stockhausen (Dullin, 1998) and used for the shrinkage stress measurement with and without compliance (Chen et al., 2001; Chen et al., 2003).

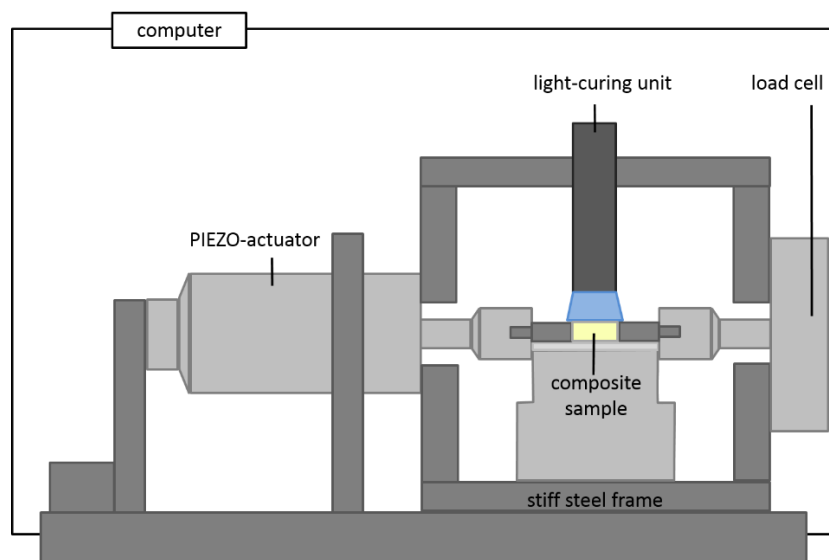


Figure 4 stress-strain analyzer machine designed by Dullin, modified after Chen et al., 2001 (Chen et al., 2001; Chen et al., 2003; Dullin, 1998).

Photo-elastic and **Moire methods** are based on optical fringes (Ernst et al., 2004; Kinomoto and Torii, 1998; Kinomoto et al., 1999; 2000; Oliveira et al., 2012; Rullmann et al., 2012). Another method is the **finite element modeling (FEA)** which consists of a computer based model that determines the type and location of stresses in the model structures (Ausiello et al., 2002; Rodrigues et al., 2012). Shrinkage strain-rate and stress was measured during polymerization with a **tensometer** which is based on the cantilever beam deflection theory (Lu et al., 2004a; b; Sun et al., 2009b).

The “**ring-slitting method**” was used to evaluate residual shrinkage stresses in composite. Ring-shaped specimens were cured and slit for the evaluation of the gap distance due to

stress release and gap measurements were evaluated with an image analyzer program (Park and Ferracane, 2005; Park and Ferracane, 2006).

The **Bioman shrinkage-stress instrument** was designed and constructed at the University of Manchester to overcome the difficulties encountered with the servo-hydraulic UTM and its function is based on the fixed beam compliance (Watts et al., 2003; Watts and Satterthwaite, 2008).

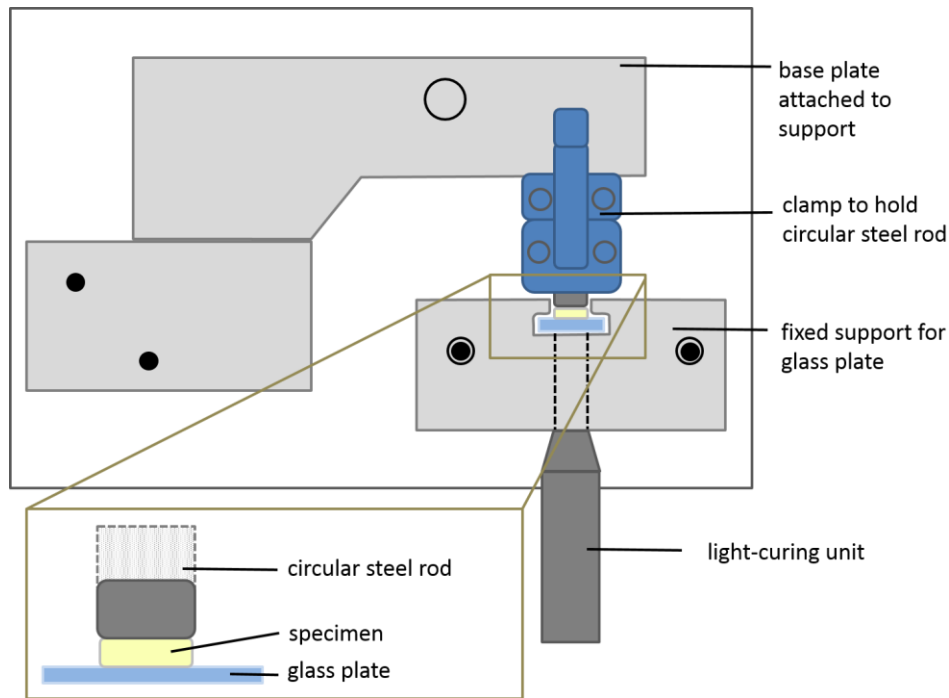


Figure 5 The Bioman shrinkage-stress instrument, modified after Watts et al., 2003 (Watts et al., 2003).

Variations in final stress values are found in the literature which can be attributed to the various testing techniques and system compliances. In order to obtain data that can be related to the clinical situation, the instrument compliance should preferably be similar to that of the prepared tooth (Schneider et al., 2010).

Polymerization shrinkage stresses are also evaluated by **FEA**. Among the advantages of FEA are the rapidity of work and the ability to vary the conditions ranging from perfect to unfavourable. None or only a few teeth specimen are needed as one tooth is enough for generating a tooth model which can then be manipulated to host different conditions. A detailed stress analysis is possible which makes it attractive for use. Nevertheless, FEA models need direct experimental validation and they do not consider that biological systems

have a high degree of variability between specimens (Morin et al., 1988). In the early 70s of the last century, stresses in biological structures were analyzed (Brekelmans et al., 1972), in human teeth (Thresher and Saito, 1973), restored molar (Farah et al., 1973), then in teeth under different loading conditions (Takahashi et al., 1980).

Versluis et al., 2004, investigated shrinkage stresses associated with tooth deformations upon restoration by FEA, and they used reported strain gauge measurements and occlusal deformation patterns for validation. It was concluded that shrinkage stresses depend on the location as well as properties of the tooth and restoration, the geometry, constraints and the restorative procedures; stresses were in the tooth rather than the restoration or the tooth-restoration interface (Versluis et al., 2004b). Rodrigues et al., 2009, explained in detail the workflow for generating such model and analyzed class I restoration with different boundary conditions and found stress concentrations in the vicinity of the tooth-restoration interface (Rodrigues et al., 2009). One study evaluated the effect of the C-factor on the shrinkage stresses, but the stress peaks did not increase with increasing C-factor (Rodrigues et al., 2012), while it was stated that not only the C-factor but also the longitudinal compliance and the elastic modulus of the substrate play a role in the stress generation (Meira et al., 2007). Another study investigated the correlation between C-factor, shrinkage stress and volumetric shrinkage both experimentally and by FEA (Pabis et al., 2012).

1.5 Methods for measuring polymerization shrinkage

Various devices have been used for measuring polymerization shrinkage in terms of volumetric and linear shrinkage, cuspal displacements, indirect techniques as microleakage, finite element analysis and through the use of micro-CT-data sets (Figure 6).

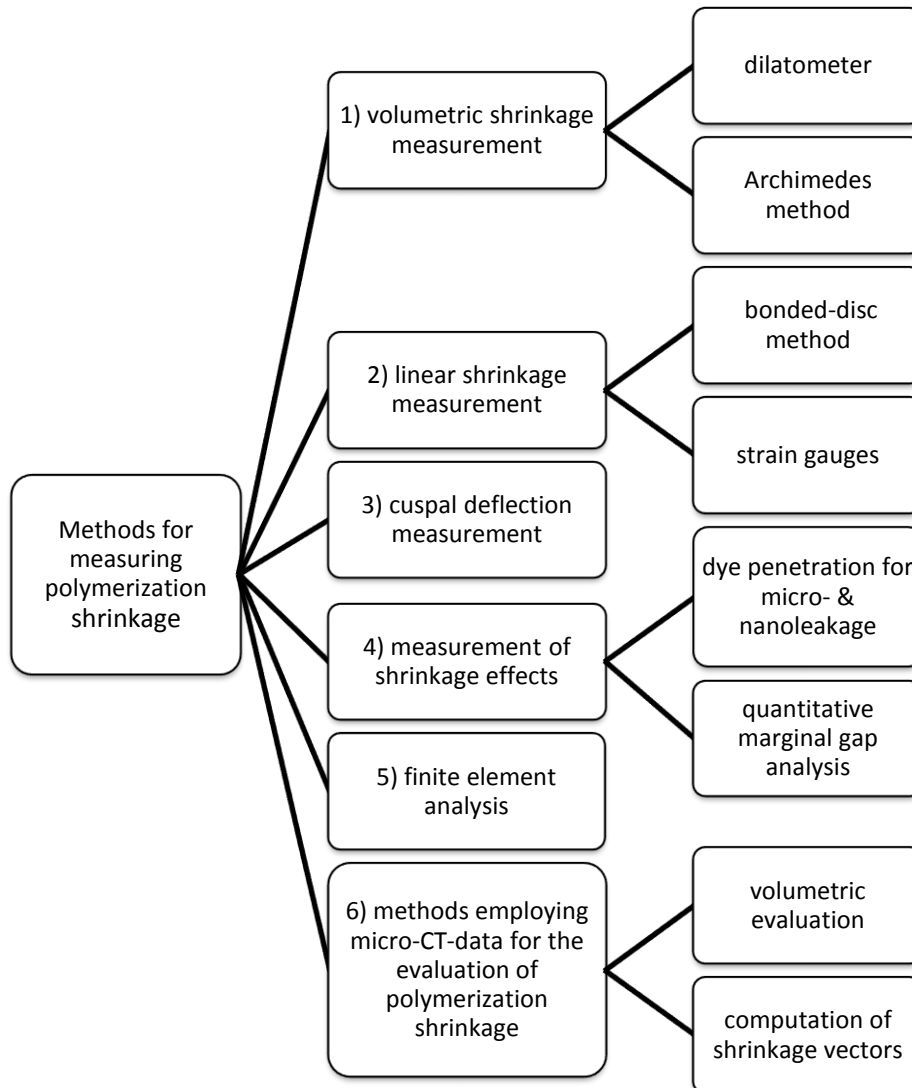


Figure 6 Overview of the methods for measuring the polymerization shrinkage strain.

1.5.1 Volumetric shrinkage measurement

Volumetric shrinkage can be measured in a **mercury dilatometer** by determining the linear height changes of a column of fluid connected to a reservoir surrounding the sample. The capillary tube is read like a thermometer (Bekkedahl, 1949; Rodriguez et al., 2006; Smith and Schoonover, 1953). The disadvantages of this method are the potential for errors due to

small temperature changes by composite polymerization which can affect the liquid volume; tedious specimen preparation is needed and flowables cannot be measured (de Gee et al., 1981; Kullmann, 1989; Penn, 1986). Access of the light source and opacity of the mercury were difficulties with light-cured dental materials (Watts and Cash, 1991). Due to the potential for environmental mercury contamination and toxic mercury vapors, water filled dilatometers were used for polymerization shrinkage measurement. However, the most critical factor for the successful application was maintaining a constant temperature environment for the dilatometer during shrinkage test (Lai and Johnson, 1993; Rees and Jacobsen, 1989). The heat from the light source in addition to the heat of the exothermic polymerization reaction contribute to an unavoidable increase in temperature upon curing.

Yamamoto et al., 2007, measured the polymerization shrinkage of flowables in a water-filled dilatometer and with speckle contrast measurement. The flowable composite was condensed into a glass tube, irradiated, and the laser-speckle field was recorded in a digital frame (Yamamoto et al., 2007). The water-filled dilatometer is also indicated for shrinkage measurement of other types of composites, not only flowables.

Measuring the **density change** of composites before and after polymerization can be done by a gas pycnometer that determines the volume of samples before and after polymerization without contact, and the difference in volume is calculated (Cook et al., 1999) or by measuring the specific gravity differences between cured and uncured composite test specimens using a modified version of ASTM method D792 "Specific Gravity and Density of Plastics by Displacement" (Puckett and Smith, 1992). Buoyancy (density in water) measurements were used to evaluate the volumetric polymerization shrinkage of composites in real time by measuring the buoyancy change of the specimen in distilled water (Lee et al., 2005). The **Archimedes method** measures the actual shrinkage in volume according to the buoyant force principle (Weinmann et al., 2005). The Archimedes method was recently developed into a German Standard (DIN 13907/2005) (Filtek LS, Technical Product Profile, 2007; Soltesz et al., 1986; Watts and Marouf, 2000). When testing hydrophilic materials, e.g. compomer or flowables, water sorption is a disadvantage with the Archimedes method that can be overcome by the use of an alternative medium to water, such as oil or mercury.

Naoum et al., 2012, measured polymerization shrinkage with an electromagnetic balance that recorded changes in the composite buoyancy during polymerization which permitted real time volumetric shrinkage measurements at small intervals (Naoum et al., 2012). Volumetric shrinkage was obtained by video imaging using AcuVol (Bisco Inc.,

Schaumburg IL, USA) and sample imaging by a digital video-camera (Labella et al., 1999; Sharp et al., 2003).

It was stated that the volumetric shrinkage is approximately equal to three times the linear shrinkage provided the shrinkage occurs identically in all directions as derived from the formula:

$\gamma_p = 1^3 - (1 - \alpha_p)^3 = 3\alpha_p - 3\alpha_p^2 + \alpha_p^3$ (γ_p , volume shrinkage; α_p , linear shrinkage strain), where α_p is very small (Lee et al., 2005; Lee et al., 2012). Isotropic shrinkage is shrinkage equal in all directions, which is hardly the case in a restorative material applied into a tooth cavity, as it is confined by the cavity's boundaries and boundary conditions.

1.5.2 Linear shrinkage measurement

Early measurements of linear shrinkage were determined on a cylinder of material using a dilatometer, and the % shrinkage = $\frac{\Delta L}{L} \times 100$ where ΔL = change in length and L = uncured length (Lee et al., 1969).

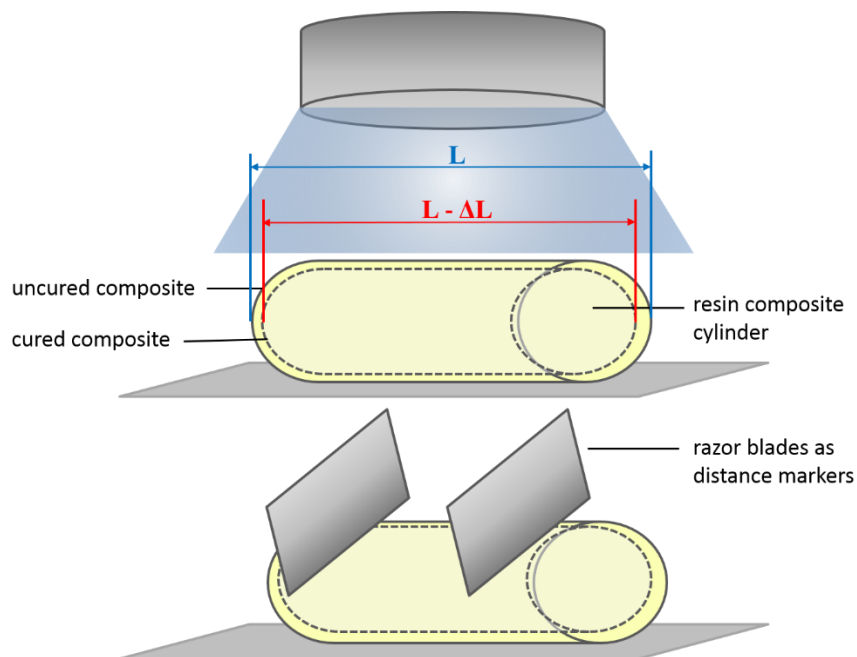


Figure 7 Measurement of the linear polymerization shrinkage of a composite cylinder.

The most common measurement for polymerization shrinkage is the **bonded-disc method** by Watts and Cash, also referred to as the “Watts method” (Watts and Cash, 1991). Earlier precursor was described by Wilson (Wilson, 1978) and Bausch (Bausch et al., 1982). Linear

shrinkage measurements are performed with linear displacement transducers such as LVDT (linear variable differential transformer) and the bonded-disc method has been internationally adopted by a number of academic and industrial research laboratories (Watts and Cash, 1991; Watts and Hindi, 1999; Watts and Marouf, 2000): a disc-shaped specimen of uncured composite is positioned at the center of a ring attached to a glass slide and covered by a flexible microscope coverslip on which the LVDT probe is placed for measuring the plate deflection; the material is light cured and data are recorded over time by a computer. The bonded-disc method results in lower shrinkage values because only the linear shrinkage of a bonded composite disc is measured and then converted into volume percent. However, the Archimedes method measures the actual volumetric shrinkage according to the buoyant force principle, with both methods showing a high correlation (Weinmann et al., 2005). Advantages of the bonded-disc method include the adjustment of a defined C-factor, the shrinkage direction is governed by the configuration rather than the direction of light application, axial shrinkage strain corresponds to volumetric shrinkage, specimen diameter matches that of the light guide tip, complete cure of the specimen due to low thickness, and lastly ease and convenience of use (Watts and Hindi, 1999).

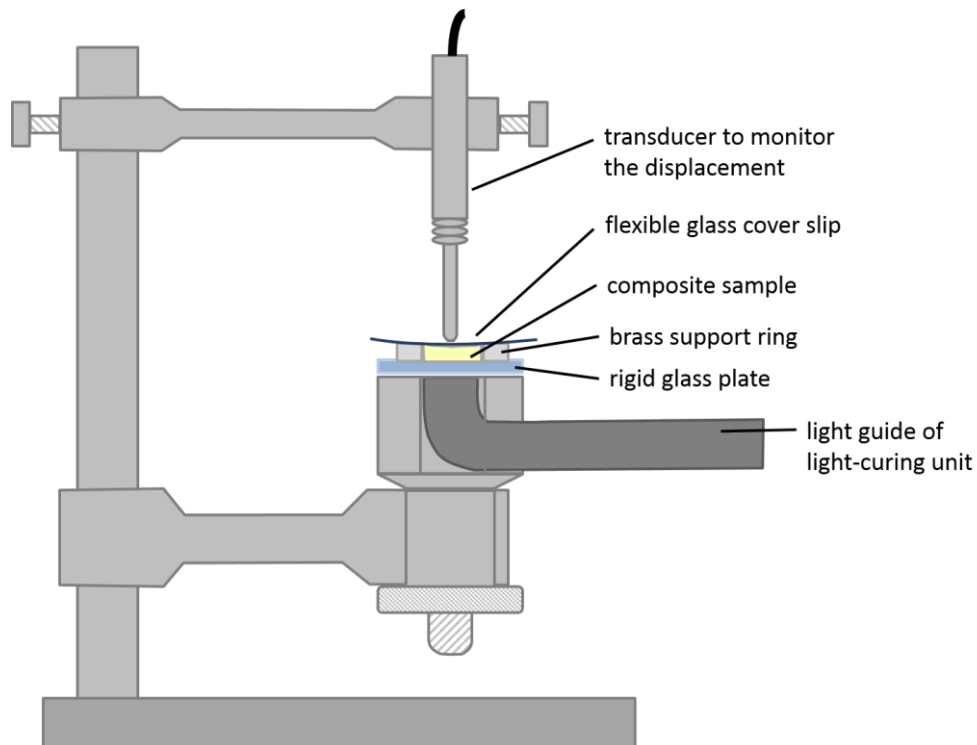


Figure 8 The bonded-disc method for measurement of the linear polymerization shrinkage, also referred to as “Watts method”, modified after Watts and Cash, 1991 (Watts and Cash, 1991).

Various techniques for linear polymerization measurements include **strain gauges** (Sakaguchi et al., 1991; Sakaguchi et al., 1992; Sakaguchi et al., 1997), the use of a microscope (Davidson and Feilzer, 1997) and the linometer whose results were in agreement with those obtained with the mercury dilatometer (de Gee et al., 1993). When a direct contact displacement transducer such as a strain gauge is used, some mechanical resistance must be overcome to produce deformation of the gauge. Consequently, the polymerization shrinkage before the gel-point is compensated by flow of resin and only post-gel contraction is measured (Sakaguchi et al., 1991).

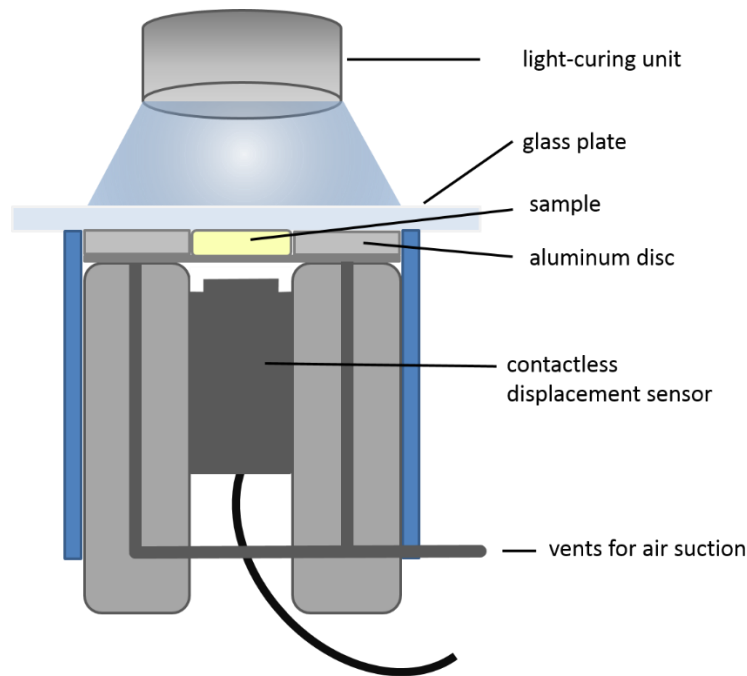


Figure 9 Linometer for the measurement of linear polymerization shrinkage, modified after de Gee et al., 1993 (de Gee et al., 1993).

A **scanning laser beam** was used to measure linear polymerization shrinkage of light-cured composites. The advantages of this method are: the sample is unaffected by the measurement technique and small samples could be analyzed with great accuracy (Fano et al., 1997). A laser interferometric method consisted of a low power Helium-Neon laser, a Michelson interferometer, amplified photodiode detectors, and a computer data acquisition system. The method measured linear polymerization shrinkage in dental restoratives and evaluated as the percent linear contraction (Fogleman et al., 2002).

The **2D particle tracking method** measured the linear polymerization shrinkage of composites by an optical instrument without directly contacting the specimen and the images were processed by a custom made software for image processing and analysis (IMAQ Vision and Labview 7.0, National Instrument, Austin, TX, USA). An update of that method involved the fluorescent particle tracking method with computer vision during curing and a software for multi-particle tracking. (Kweon et al., 2013; Lee et al., 2012). Another study determined polymerization shrinkage using a video-imaging device (Simon et al., 2008; Yamamoto et al., 2012).

1.5.3 Cuspal deflection measurement

The previously mentioned methods measure the gross shrinkage of resin composite samples as such, but they do not represent or consider the boundary conditions that occur in a tooth cavity, and in turn do not predict clinical performance. The measurement of cuspal deflection is indicative of the measurement of polymerization shrinkage of bonded resin composite inside a tooth cavity, in an attempt to correlate to the clinical situation. Polymerization shrinkage was greater when measured by a dilatometer than cuspal movement where the composite was restricted by being bonded to the cavity walls (Suliman et al., 1994) and it was previously confirmed that shrinkage strains changed with the boundary conditions (Sakaguchi et al., 2004b).

Cuspal deflection has been thoroughly investigated for class II cavities restored with resin composites using a variety of techniques including photography/microscopy (microscope with a micrometer stage) (Gonzalez-Lopez et al., 2004; Rees et al., 2004; Suliman et al., 1993b), Michelson interferometry (Suliman et al., 1993a), strain gauges (Alomari et al., 2001; Donly et al., 1989; Morin et al., 1988; Taha et al., 2009; Versluis et al., 2004a), linear variable differential transformers (LVDT) (Lee et al., 2007; Meredith and Setchell, 1997; Pearson and Hegarty, 1989), contact stylus profilometry together with computer graphics (DeLong et al., 1985; Tantbirojn et al., 2004), digital-image-correlation (DIC or texture correlation) (Chuang et al., 2011a; b) or electronic speckle pattern interferometry (Bouillaguet et al., 2006; Lang et al., 2004). DIC method analyzes an object's displacement based on the comparison of two similar speckled images; one before deformation and one after. Images are recorded using a CCD camera through an optical microscope, and the local displacements between the images are found out (Chuang et al., 2008; Chuang et al., 2011b; Huang et al., 2005; Li et al., 2009).

The measured cuspal deflections averaged 15 μm up to 50 μm , but varied according to the technique used. Absence of standardization of tooth size, cavity preparation and restoration technique renders comparison of results difficult, since contraction of cusps depends on the remaining tooth structure. Some studies combined cuspal deflection with microleakage analysis (Moorthy et al., 2012) or shrinkage stress determination (Kwon et al., 2012).

The methods used are not standardized among the various testing labs. For this reason comparisons of the results should be done with caution. One group of researchers have performed various investigations with standardized cavity configurations that allow the comparison of the results among their studies (Abbas et al., 2003; Cara et al., 2007; Fleming et al., 2005; Fleming et al., 2007a; Fleming et al., 2007b; Moorthy et al., 2012; Palin et al., 2005). Another difficulty of the interpretation of the results is when partial debonding of the restoration happens, because it would decrease the cuspal movement, while the bond has failed, thus, giving misleading results.

1.5.4 Measurement of adverse effects of polymerization shrinkage

A traditional method of determining the adverse effects of polymerization shrinkage includes in vitro assessments of interfacial adaptation based on dye penetration, or quantitative marginal gap analysis by the replica technique and SEM (Lutz et al., 1977; Qvist and Qvist, 1985; Roulet et al., 1991; van Dijken et al., 1985). Bond strength tests are also used to evaluate the composite-dentin-bonding-agent-complex. There are various tests like the shear, the tensile bond strength test, as well as the micro-shear and microtensile bond strength tests (Armstrong et al., 2010; Braga et al., 2010). Data from labs worldwide using various tests on the same material achieve different results, even microtests could not eliminate the high degree of variations among results (Scherrer et al., 2010). Other in vitro phenomena are used to evaluate the effects of polymerization shrinkage such as microleakage, nanoleakage, structure and mechanical properties of the bonding interface. These can also be related to bond strength values, but they do not necessarily correlate with results of microleakage tests or gap formation at the cavity margin, whereas nanoleakage tests and morphological and chemical characteristics of the bonding interface could be indicative of future dentin bond durability (Tagami et al., 2010).

However, the clinical reliability of these tests were considerably questioned. It was suggested to develop more appropriate bond test and analysis of in vitro phenomena (Tagami et al., 2010), while others suggested to use an interfacial fracture mechanics approach for the analysis of the dentin-adhesive bond for better agreement of test results (Scherrer et al.,

2010). In this regards, it was reported that the use of hydrophilic DBAs the dye penetration method bore some difficulties in differentiating between the stained bonding agent and true gaps. Furthermore, the accuracy of the replica technique was found to depend largely on the quality of both the impression and replica for the margin analysis. In addition, it gives information on the length but not the depth of defect, same applies to SEM (Chiang et al., 2009).

1.5.5 Finite element analysis (FEA)

Polymerization shrinkage is also analyzed by methods like the finite element analysis. A well known study is presented by Versluis et al., 1998, in which they questioned that composites shrink toward the light. They proposed a cylindrical cavity with different boundary conditions that were simulated by FEA and which stated that the shrinkage direction of light cured dental composites depends on the boundary conditions, specially the bonding between the restoration and the tooth rather than the light source (Versluis et al., 1998). In an attempt to predict shrinkage stresses volumetric shrinkage was measured and related to the C-factor; the stress peak correlated with the volumetric shrinkage but not with the C-factor (Pabis et al., 2012).

1.5.6 Methods employing micro-CT data for the evaluation of polymerization shrinkage

The microcomputed tomography is a cone beam tomography producing **3-dimensional images** of high resolution up to 6 μm . The micro-CT scans have been extensively used for bone density investigation (Bouxsein et al., 2010; Wagner et al., 2011), mineral content assessment in caries research (Clementino-Luedemann et al., 2006; Clementino-Luedemann and Kunzelmann, 2006; Huang et al., 2007; Schwass et al., 2009; Zou et al., 2009), and tooth modeling in finite element analysis (Magne, 2007).

Data acquisition for the evaluation of polymerization shrinkage has been performed by different researchers and could be divided into two distinct parts: on one hand the assessment of volumetric changes and resulting gap analysis or detachment of the restorative material from the cavity interface, and on the other hand the shrinkage vector calculations by the use of particle tracing before and after polymerization.

1.5.6.1 Volumetric evaluation of polymerization shrinkage

Non-destructive investigation of the marginal adaptation and the adhesive interface were performed (De Santis et al., 2005; Kakaboura et al., 2007; Meleo et al., 2012), in addition to

the evaluation of the internal adaptation of adhesive restorations (Kwon and Park, 2012). The research group at the ADA Foundation in Gaithersburg, USA, published studies on volume loss of resin composites (Sun and Lin-Gibson, 2008; Sun et al., 2009a; Zeiger et al., 2009) and volume loss in association with direct non-destructive microleakage investigation (Sun et al., 2009a; Sun et al., 2009b). The disadvantage of this method is that gaps are detectable at x 2.5 voxel size which is a rather insensitive method. Currently a typical micro-CT resolves 6-8 μm which corresponds to a detectable gap size of 25-30 μm .

1.5.6.2 Methods utilizing the shrinkage vectors methods

The visualization of polymerization shrinkage in form of shrinkage vectors is a technique that has been introduced and improved by the research group at the Tokyo University, Japan (Cho et al., 2011; Inai et al., 2002). The basic concept of this technique has been adopted and furtherly developed by the research group at the Ludwig-Maximilians-Universität (LMU) in Munich, Germany (Chiang et al., 2009; Chiang et al., 2010; Rösch et al., 2009).

Medical image registration

The use of radiological images has increased in medical research and healthcare. Generally, image registration can be used for combining images of one subject, therefore compensating for example for motion between scans. This is performed by registration algorithms that automatically register images by a rigid body transformation. On the other hand, non-rigid registration algorithms compensate for tissue deformation or align images from different subjects (Fischer and Modersitzki, 2008; Hill et al., 2001).

Medical image registration methods are important in brain tumor studies for tumor visualization and observation (Bauer et al., 2013). In dentistry, Kunzelmann, 1996, was one of the first to visualize 3D data for wear analysis and quantification of filling materials in vitro and in vivo (Kunzelmann, 1996). Swennen et al., 2007, have applied the rigid registration method for detailed visualization of the interocclusal relationship in the course of 3D virtual planning of orthognathic surgery. They designed a 3D splint with the double CT scan procedure to obtain an anatomic 3D virtual augmented model of the skull with detailed dental surface (Swennen et al., 2007). Sandholzer et al., 2013, used quantitative micro-CT data for studying the 3D shrinkage and shape preservation of human teeth upon heating which is relevant information for forensic investigators (Sandholzer et al., 2013).

Methods for acquiring polymerization shrinkage vectors

Shrinkage vectors represent the magnitude and direction in which shrinkage occurs (Watts and Cash, 1991). The **Tokyo-group** invented the filler-tracing-method for visualization of polymerization shrinkage by obtaining real polymerization shrinkage vectors. They embedded radioopaque zirconia fillers into a resin composite, scanned the restoration before and after light-curing, identified the fillers manually in both scans and calculated the movement 2-dimensionally (Inai et al., 2002).

The first automated process was conducted by the **Munich-group** in which micro-CT datasets were combined with the images registration approach to determine and visualize the direction and amount of polymerization shrinkage vectors 2-dimensionally then 3-dimensionally. Radiolucent glass fillers were embedded into a flowable resin-composite to avoid reconstruction artifacts in the micro-CT, then scanned with a micro-CT before and after light-curing, and traced.

In the **2D-study** the displacement vector field was calculated with an elastic registration algorithm using vector-spline regularization combined with B-spline based elastic registration (Arganda-Carreras et al., 2006; Chiang et al., 2008; Chiang et al., 2009; Kybic and Unser, 2003; Sorzano et al., 2005). The basic idea of the elastic registration is the application of a grid to both pre-and-post-polymerization scan images, where the regular grid is applied to the pre-polymerization situation, and the deformed grid to the post-polymerization. The grid itself is elastic and its deformation costs energy; with larger deformations requiring more energy. One of the images is the elastically deformed version of the other. The main goal of elastic registration is fitting the grid to the new position by using the least possible energy, where the points of grid deformation are identical to the tracer markers. To register two images, it was assumed that one the images, the source image, is an elastically deformed version of the other, the target image; elastic fields can be expressed in terms of B-splines. Image registration can be carried out using landmark-based or landmark-independent registration algorithms, the latter being superior when the image exhibits major deformations or when the information is unevenly distributed. The grid is fit to the tracer markers that constitute landmarks that are identical to the points where the grid is deformed and being fit to new position based on tracer markers by elastic registration. However, tracer markers are not evenly distributed in every 2D section of the 3D scan and the missing deformations are assumed. Consequently, the elastic registration based on B-splines regularization is highly dependent on its parameter values and in case of improper

assumptions might lead to incorrect results. For visualization purposes, the shrinkage vectors were displayed as glyphs (Chiang et al., 2008; Chiang et al., 2009).

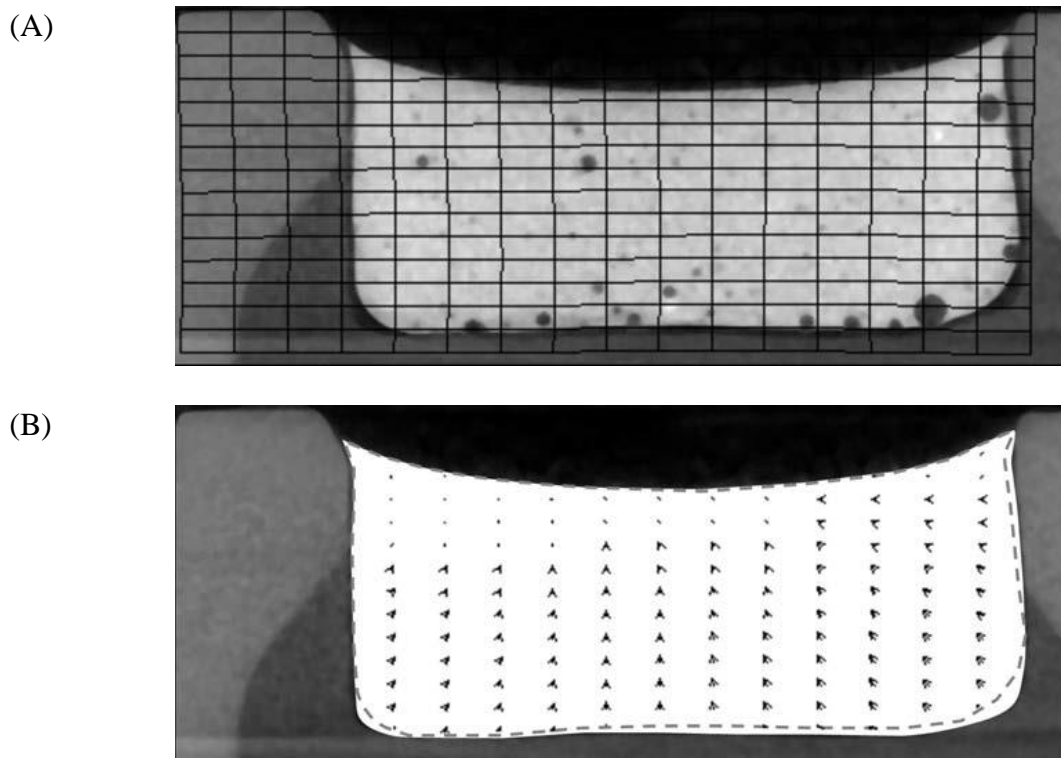


Figure 10 The image processing of the **2D shrinkage vector evaluation**: (A) the original source image of the uncured resin composite with the deformation grid. (B) The displacement field obtained from the elastic registration is superimposed to the output source-target image of the registered target image. The vector field displays the deformation due to the mass movement of the polymerization shrinkage and the dotted line marks the deformed shape after light-curing of the composite (Chiang et al., 2009). Reuse of the images is with written permission by Dr Yu-Chih Chiang (2014).

Moreover, they analyzed **3D shrinkage vectors** using the same experimental flowable composite, but implementing a different method of image registration based on a block-matching algorithm. It consisted of a three-step approach: first, the subimage selection from the micro-CT scans with the software InsightSNAP (www.itknap.org), second, the sphere segmentation, which is the identification and separation of glass spheres from the rest of the restoration in the uncured image, depending on the grey value, and third, the registration of the individual spheres through local rigid registration (the block-matching) to determine the segmented spheres' displacement during the polymerization process. They visualized the deformation 3-dimensionally field using VTK (www.vtk.org) and vector lengths were obtained (Chiang et al., 2009; Chiang et al., 2010; Rösch et al., 2009).

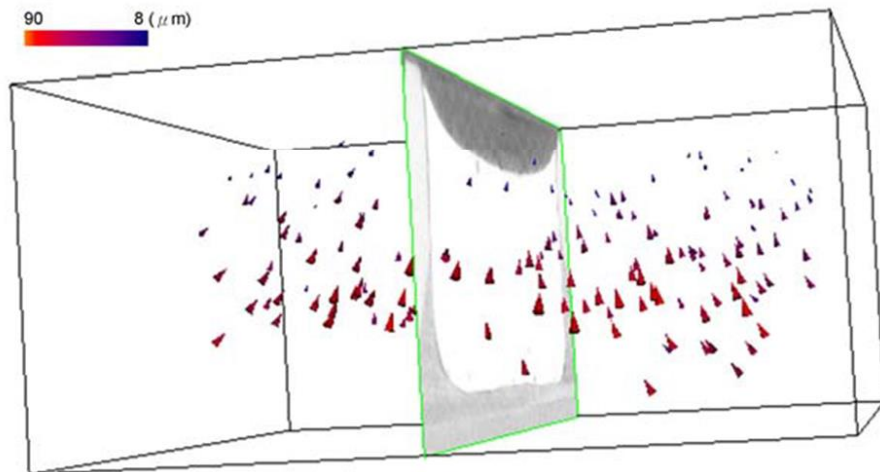


Figure 11 The **3D deformation field** by Chiang et al., 2009 (Chiang et al., 2009). Reuse of the images is with written permission by Dr Yu-Chih Chiang (2014).

The results of the **Munich-group** in the 2D investigation were in agreement with those of the 3D analysis. The composite was applied in a cylindrical class I cavity. In the unbonded group, composite adhered to one side and pulled from the other wall, thereby forming a compensatory gap. In the bonded group, cavities with equal enamel thickness at both margins the displacement vectors showed upward shrinkage, with small vectors near the enamel and a translucent area was detected at the bottom. In the bonded group with unequal enamel margins the main orientation of the displacement vector field was toward the bottom of the cavity and to the side with greater amount of enamel with a compensatory mass movement at the top of the restoration. In a further study, they applied the composite in a trapezoidal class I cavity with dentin walls only to study the effect of different self-etch bonding systems on the polymerization shrinkage direction. The displacement vector fields and vector lengths varied depending on the bonding agent used. With ClearFil SE Bond and OptiBond the vectors moved downward, while with Xeno V it was the opposite (Chiang et al., 2009; Chiang et al., 2010).

In the second study of the **Tokyo-group**, they imported the micro-CT-scan data of the composite restorations before and after polymerization into a custom made software, the 3D-BON software (Ratoc Systems Engineering, Tokyo, Japan) and used a cluster-labeling algorithm to extract the fillers and perform the pairing procedure as has been introduced earlier by the **Munich-group** (Chiang et al., 2008; Cho et al., 2011; Rösch et al., 2009). Images were reconstructed from the data by a 3D data visualization tool Avizo 6.2

(Visualization Sciences Group, Burlington, MA). The movement distance of each filler after polymerization was obtained 3-dimensionally. However, the analysis of filler movement was limited to the axial direction, i.e. in relation to the light source, by dividing filler movement data into 165 regions within the restoration. In the bonded condition, their findings showed downward shrinkage at the superficial part (1 mm), and an upward shrinkage, toward light, in the deeper part of the restoration, whereas the unbonded restorative material completely shrunk upward, toward light, (Cho et al., 2011). One drawback of this method is the radioopacity of the zirconium dioxide fillers introducing reconstruction artifacts in the micro-CT.

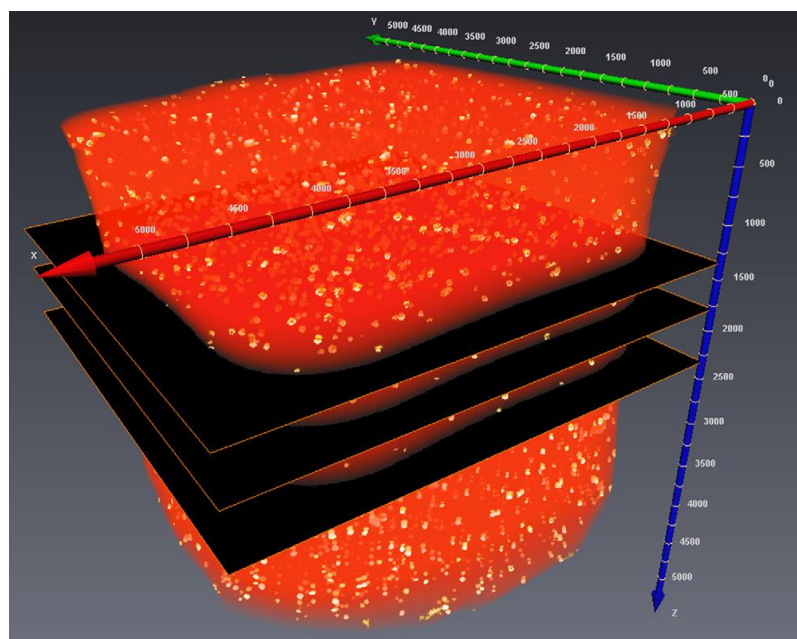


Figure 12 The 3D image obtained by superimposing micro-CT scans from the composite before and after polymerization. The three slices are representative of the 165 slices that were analyzed for the filler movement in the axial direction by Cho et al., 2011 (Cho et al., 2011). Reuse of the images is with written permission by Elsevier/RightsLink (2014).

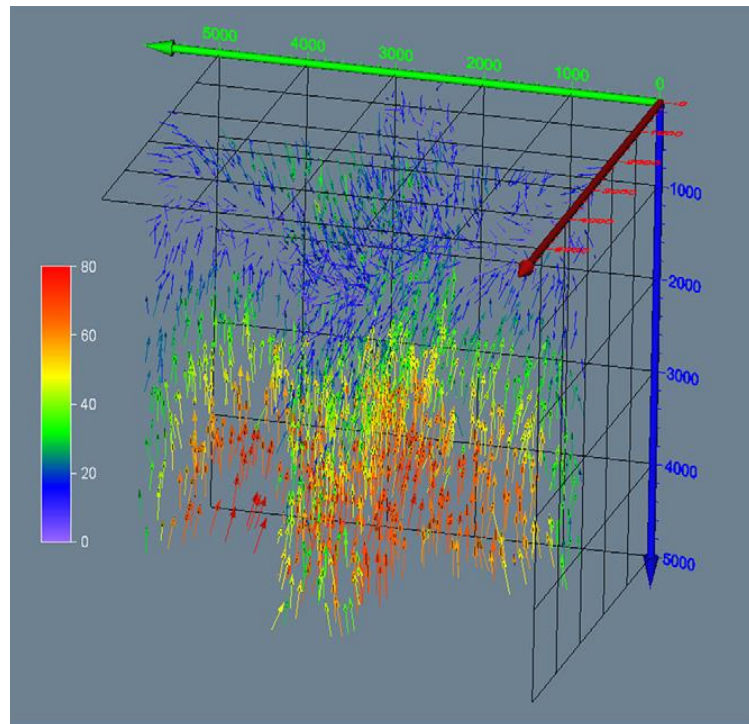


Figure 13 The 3D vector field image represents the filler movement direction in the bonded group by Cho et al., 2011 (Cho et al., 2011). Reuse of the images is with written permission by Elsevier/RightsLink (2014).

Polymerization shrinkage is generally related to the material's properties, the light source and the boundary conditions. Flowable resin composites have a lower modulus of elasticity and exhibit greater amounts of volumetric shrinkage, thus, facilitating the visualization of shrinkage vectors. A more flexible material generates less shrinkage stresses at the tooth-restoration-interface than a stiffer one as the pre-gelation flow compensates for the shrinkage. Moreover, the polymerization is affected by aspects related to the light source. The power output varies among light-curing units, the distance between the light-guide and the restoration should be as small as possible so that more photons reach the full depth of the restoration (Price et al., 2010b; Price et al., 2010e; Price et al., 2011). Also, the direction of light application might have an influence on the shrinkage. In the presented studies the light was applied perpendicular to the long axis of the tooth, while Versluis et al., 1998, have added a 45 degree angulation which resulted in only small changes of the shrinkage direction in their FEA evaluation (Versluis et al., 1998).

The available data on the shrinkage vectors give insight into the shrinkage direction of light-cured composites using micro-CT data sets. Only few aspects of boundary conditions were

reported such as bonded and unbonded restorations, the use of various self-etch adhesives and the effect of unequal enamel margins on the shrinkage direction (Chiang et al., 2009; Chiang et al., 2010; Cho et al., 2011). Yet, further investigations are needed to clarify the effect of the boundary conditions on the shrinkage vectors.

2 Aim of the study

The 3D evaluation method of shrinkage vectors in light-cured composites was proposed by Rösch et al., 2009, and employed by Chiang et al., 2009, 2010 (Chiang et al., 2009; Chiang et al., 2010; Rösch et al., 2009). It is an accurate tool for the quantification of polymerization shrinkage vectors and it displays the internal movements within the restoration that could not be seen otherwise. Therefore, the aim of this study was to investigate the effect of boundary conditions on the polymerization shrinkage of a light-initiated resin composite in form of displacement vector fields. Polymerization shrinkage was visualized 3-dimensionally and shrinkage vectors were also analyzed in the axial direction. Boundary conditions consisted of the cavity configuration, the bonding condition and the bonding substrate (Figure 14).

Each chapter addressed a certain topic related to the boundary conditions. In **Chapter 3** the specific aim was to study the effect of different cavity configurations on the shrinkage vectors which is of clinical relevance. The prepared cavities could be standardized, while human teeth could not. For this reason, **Chapter 4** was proposed to study the shrinkage vectors with the least possible influence by the substrate in etched and silanized ceramic cavities with and without a dentin bonding agent. In contrast, **Chapter 5** aimed at evaluating the effect of a nonbonded boundary condition on the shrinkage in a non-adhesive Teflon mold. Here, only the cavity configuration played a role, independent of the adhesion.

“Bonding to enamel is stronger than bonding to dentin”. How does this statement translate into the shrinkage behavior of composites upon light-curing? To find out, the effect of the tooth’s coronal bonding substrates, enamel and dentin, was studied by using an experimental cavity model where enamel was located at the cavity floor in opposition to the traditional cavity with enamel at the cavity margins, **Chapter 6**. Additionally, the effect of a self-etch versus a total-etch adhesive was analyzed. Figure 15 summarizes the specific objectives of the current study.

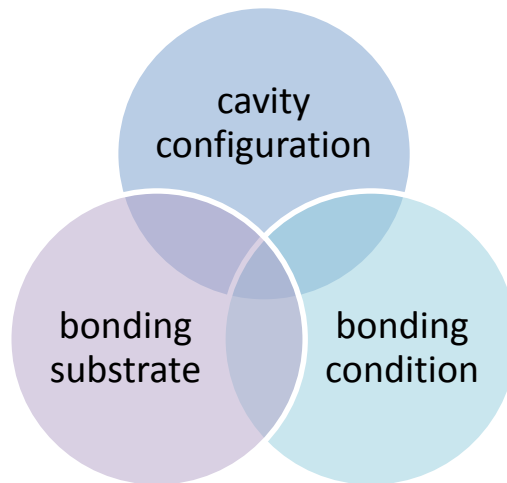


Figure 14 The investigations of the current study were based on the boundary conditions which include the cavity configuration, the bonding condition and the bonding substrate.

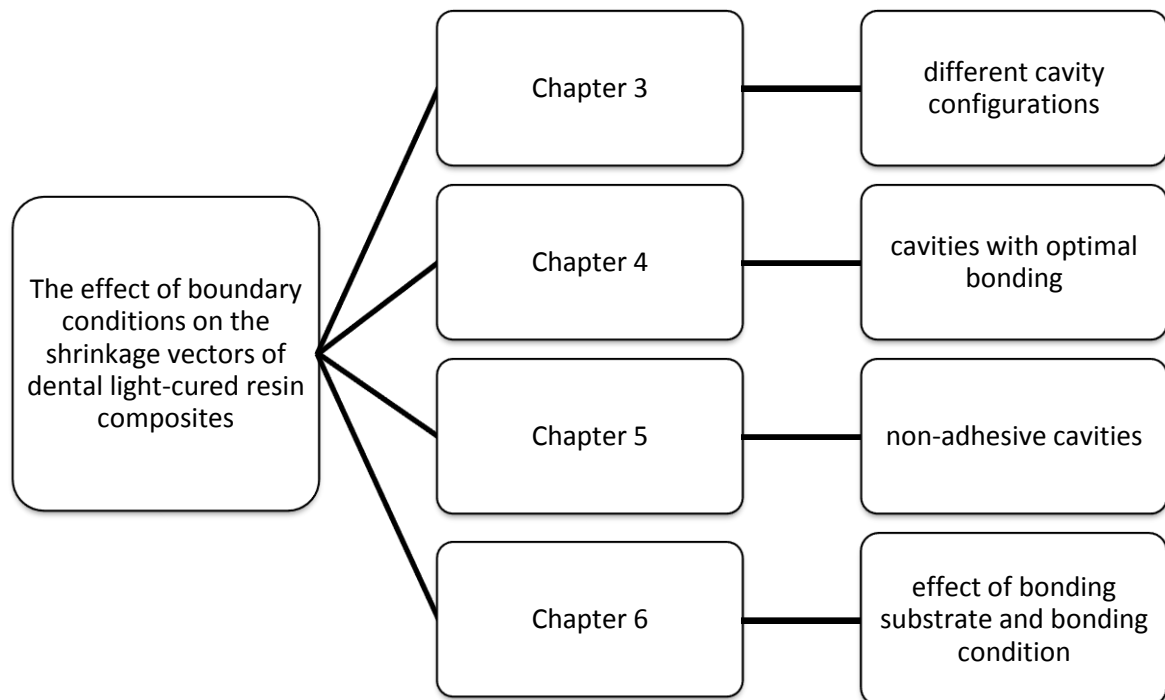


Figure 15 Overview of the different study parts.

Hypothesis

The hypothesis of the current work is that the shrinkage direction in the form of shrinkage vectors is influenced by the restoration's boundary conditions rather than the light source. Boundary conditions can be divided into the cavity form, the bonding condition and the bonding substrate, as displayed in Figure 14.

3 Shrinkage Vectors in Different Cavity Configurations

3.1 Abstract

Objectives: To detect the effect of different cavity configurations on the shrinkage direction in relation to the light source and to visualize polymerization shrinkage of a light-initiated resin composite in form of displacement vector fields.

Methods: 27 human teeth were equally divided into three groups and labeled according to the cavity-configuration as “adhesive”, “diverging“ and “cylindrical”. All class I cavities were axially symmetric and 3 mm deep. The “adhesive” cavity configuration represented beveled enamel-margins, occlusally converging walls and a floor-diameter of 6 mm, the “diverging” cavity had a floor-diameter of 5 mm and a margin-diameter of 7 mm, and the “cylindrical” group had cylindrical walls (diameter 6 mm). 2 wt% traceable glassbeads were added to a commercial composite (Tetric EvoFlow, Ivoclar Vivadent) and bonded with a self-etch one-step adhesive (Adper Easy Bond, 3M ESPE). Two micro-CT scans were performed of each specimen (uncured, cured), subjected to image segmentation for extraction of glass beads followed by a registration process (rigid registration and subsequent block-matching algorithm). The resulting displacement vector fields obtained by tracing the movement of the tracer beads elucidated the distribution of shrinkage vectors three-dimensionally. Furthermore, the shrinkage vector components regarding the vertical dimension, i.e. in relation to the light source, were quantitatively evaluated, too.

Results: Mean vector lengths were computed irrespective of their direction, where the “adhesive” showed highest vector lengths ($31.1 \pm 10.9 \mu\text{m}$), followed by the “diverging” ($27.4 \pm 12.1 \mu\text{m}$) and were least in the “cylindrical” group ($23.3 \pm 11.1 \mu\text{m}$), displaying significant differences between all pairs of groups (one-way ANOVA with Tamhane’s T2). To investigate the composite shrinkage direction the filler movement was analyzed along the z-direction. Negative values denoted shrinkage towards the light-source (upward movement), while positive ones indicated downward shrinkage. Greatest mean filler movement was observed in “adhesive” ($-13.7 \pm 12.1 \mu\text{m}$), followed by “diverging” ($-5.7 \pm 17.2 \mu\text{m}$), while “cylindrical” showed the least mean filler movement ($-3.7 \pm 13.6 \mu\text{m}$) toward the light source; all pairs of groups showed significant differences (one-way ANOVA with Tamhane’s T2).

Conclusion: Shrinkage amount and direction varied according to cavity configuration, where the upper part of all restorations showed downward shrinkage away from light and the lower part shrank upward with variable degrees. Bond disruption occurred at different sites: in the “adhesive” group at the floor, in the “diverging” group at the enamel margin, and in the “cylindrical” group at one side of enamel margin and the floor.

3.2 Introduction

For many decades, an important assumption in dentistry has been that chemically-cured composites shrink to the center of mass, while light-cured resin composites shrink toward the light source. Based upon this hypothesis, methods and techniques like the use of light-reflecting wedges and curing light application from different sides for guiding the shrinkage towards the cavity walls have been recommended (Ciamponi et al., 1994; Lutz et al., 1986). However, an obvious scientific proof confirming this hypothesis was long missing.

Shrinkage vectors represent the amount and direction of composite mass movement due to polymerization shrinkage (Watts and Cash, 1991). Polymerization shrinkage depends on the chemical composition, degree of conversion as well as boundary conditions such as cavity configuration and bonding conditions, and the light intensity and its distribution (Braga and Ferracane, 2002; Ferracane, 2008; Price et al., 2004; Price et al., 2010b; Price et al., 2010c; Price et al., 2010d; Price et al., 2010e; Price et al., 2011; Price et al., 2013; Versluis et al., 1998). The shrinkage effects are indirectly determined by marginal adaptation, gap formation, microleakage and bond strength tests for evaluation and comparison of restorative systems formed of tooth structure, composite and adhesive bonding systems.

The cavity design proposed for adhesive restorations features beveled enamel margins and rounded dentin walls. Lutz et al., 1976, observed polymerization shrinkage of an adhesive restoration toward the light source and assumed it could be attributed to the curing light itself (Lutz et al., 1976; Porte et al., 1984). They referred to Lambert-Beer's law which states that light attenuates as it travels through matter. The presence of a higher photon density at the surface of the materials leads to a better polymerization. With increasing distance to the surface, the light intensity is attenuated. The reduced light intensity is associated with less photons and therefore less polymerization initiating sites, resulting in delayed gelation and build-up of the mechanical properties. As a consequence, the mass movement is directed toward the surface of the cavity.

Versluis et al., 1998, conducted a finite element analysis (FEA) and claimed that shrinkage was not necessarily toward the light source, but was rather affected by the bonding of the restoration and free surfaces, in other words, by the boundary conditions (Versluis et al., 1998). FEA is a good predictor but FEA is only as accurate as the parameters and assumptions based upon. Shrinkage usually is simulated in FEA with a heat transfer approach. The volume which represents the composite material is cooled in the simulation to cause a contraction. The consequences of this contraction are assumed to be similar to the consequences of curing contractions. This approach does not include light attenuation as a function of the distance to the light source. In addition, the boundary conditions usually are assumed to be constant during the loading phase. Only recently the analysis of crack propagation was added to the finite element models for contraction stress analysis but for a different topic (Yamamoto et al., 2009). Even with refined FEA models the outcome always has to be validated with adequate experiments.

The first real visualization of polymerization shrinkage was demonstrated by Inai et al., 2002, who embedded radioopaque zirconia fillers into a resin composite and scanned the restoration before and after light-curing. The fillers in both scans were identified manually and the movement was calculated 2-dimensionally (Inai et al., 2002). Chiang et al., (2009) were the first to investigate the polymerization shrinkage direction with an automated process first 2-dimensionally and later even 3-dimensionally, based on a block-matching algorithm. They used radiolucent glass fillers which were embedded into a flowable resin-composite, scanned with a micro-CT before and after light-curing, and then the movement of each individual particle was traced. The shrinkage vectors were displayed as glyphs (Chiang et al., 2009; Chiang et al., 2010). The radiolucent glass fillers are advantageous, as they do not result in reconstruction artefacts. Due to the high radiopacity the zirconia fillers cause extensive scattering which affects the reconstruction negatively.

Do composites shrink toward the light? Is the shrinkage direction influenced by the attenuation of light as it travels through matter or does the beveling hinder the composite from moving downward? The boundary conditions depend on several variables as for example the shape of the cavity (= cavity configuration), the bonding conditions and the bonding substrates. In order to clarify whether the adhesive cavity design influences the shrinkage direction, two other cavity configurations were proposed. The “diverging” cavity (cone trunk shaped) represented no configurational influence if composite would shrink towards light, while the “cylindrical” cavity could have frictional effects upon composite shrinkage, but is neutral regarding any possible movement in axial direction.

3.3 Aim of the study

The aim of this study was to analyze the effect of different cavity configurations on the shrinkage direction in relation to the light-source, to visualize the polymerization shrinkage of a light-initiated resin composite qualitatively in the form of displacement vector fields 3-dimensionally and to analyze the axial filler movement quantitatively.

3.4 Materials and Methods

The experimental composite and the self-etch adhesive listed in Table 4 were used for the restorative procedure. The extracted teeth were collected and stored in sodium azide in the dark. The experimental procedures were approved by the ethics committee of the medical faculty of the Ludwig Maximilians University, Munich, Germany.

3.4.1 Specimen preparation

27 human teeth were divided into three groups which will be labeled in the following text as "adhesive", "diverging" and "cylindrical" cavities. All samples were 3 mm deep class I cavities. Outside the cavity without contact to the cavity margin the occlusal cups of the teeth were slightly flattened for easier perpendicular light application.

The "adhesive cavity" design, as proposed by Lutz, displayed narrow beveled occlusal margins as indicated for the adhesive restorations and the dentin walls of the cavity were rounded (Lutz et al., 1976). The "diverging" cavity had occlusally diverging walls, with the outer cavity margin 7 mm in diameter and the cavity floor 5 mm in diameter. This cavity design was included to allow for unimpeded upward movement of the composite in case it would shrink toward the light source. The "cylindrical" cavity was prepared according to Chiang with parallel walls, being neutral to any direction of shrinkage (Chiang et al., 2009; Chiang et al., 2010; Versluis et al., 1998).

The teeth were embedded in an acrylic resin (Technovit 4000, Heraeus Kulzer, Germany) and fixed to the sample holder with composite to prevent any movement during the scanning procedure.

3.4.2 Preparation of the experimental traceable resin composite

A flowable resin composite (Tetric EvoFlow, Ivoclar Vivadent, Schaan Liechtenstein), was mixed with 2 wt% silanized radiolucent glass fillers with an average particle size of 40-70 μm (Sigmund Lindner GmbH, Warmensteinach, Germany). Silanization of the glass fillers

was performed to ensure a durable bond between the fillers and the resin matrix (Liu et al., 2001).

Adper Easy Bond, 3M ESPE, a self-etch one step bonding agent was applied for 20 s, air thinned for 5 s and light cured for 20 s using the light-curing unit Elipar FreeLight2, 3M ESPE (power output 1200 mW/cm² according to the manufacturer, checked for constant light intensity once/week with a dental radiometer). The composite was applied into the prepared cavity and remained uncured. There was no specific reason for the selection of Tetric EvoFlow or Adper Easy Bond. The flowable was used to ensure a good marginal adaptation. The depth of cure at 3 mm was confirmed by Lindberg et al., 2004 (Lindberg et al., 2004). We used a modified commercial composite instead of a self-mixed model composite to ensure a constant quality and allow the comparison of the results of studies by Chiang et al. (Chiang et al., 2009; Chiang et al., 2010). In addition to that Tetric EvoFlow has by accident the perfect radioopacity for the segmentation of the glass beads.

3.4.3 X-ray micro-computed tomography measurements

A high resolution micro-computed tomography apparatus (Micro-CT 40, Scanco Medical AG, Switzerland) was used for scanning the samples (Figure 16). The settings for the micro-CT were: acceleration voltage 70 kVp and cathode current 114 μ A. The samples were scanned with high ($8^3 \mu\text{m}^3$) resolution using an integration time of 600 ms. A few drops of water were added to the sample holder to prevent dehydration and subsequent cracking of the tooth during tooth scanning. The sample holder was covered with a radiolucent and dark cap to avoid premature polymerization of the uncured resin composite material during the scanning procedure, and placed inside the micro-CT machine for the first micro-CT scan.

Then the composite was light-cured for 40 s and the sample was scanned again using the same parameters as before (Figure 17). During the whole process the sample remained in the sample holder to avoid a gross displacement of the tooth to facilitate and speed up the subsequent registration of the datasets. After the raw micro-CT scans were reconstructed and saved a 16-bit datasets of the attenuation coefficient per voxel. Each dataset was approximately 3.9 GB large. Details of the workflow are presented in the scheme below (Figure 18).

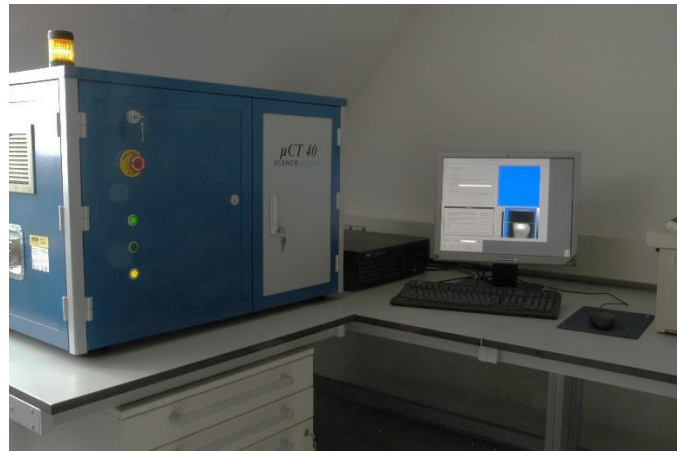


Figure 16 The high resolution micro-computed tomography, μ CT 40, Scanco Medical AG, Switzerland, was used for the 3D scanning procedure of the restorations.

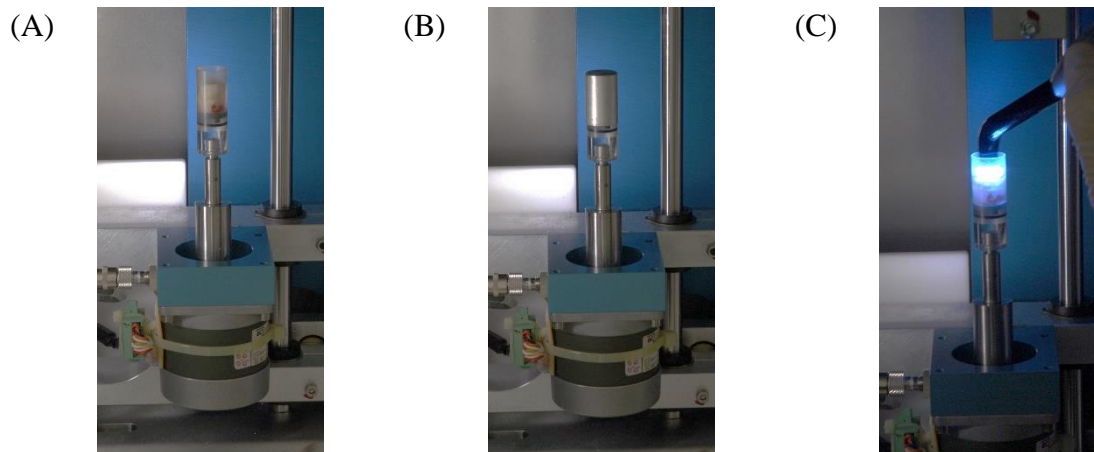


Figure 17 The prepared and filled tooth in the sample holder in the micro-CT (A), covered with a radiolucent and dark cap to avoid premature polymerization during the first scan (B). Light curing (20 s) of the composite was performed while the sample remained in the micro-CT machine (C).

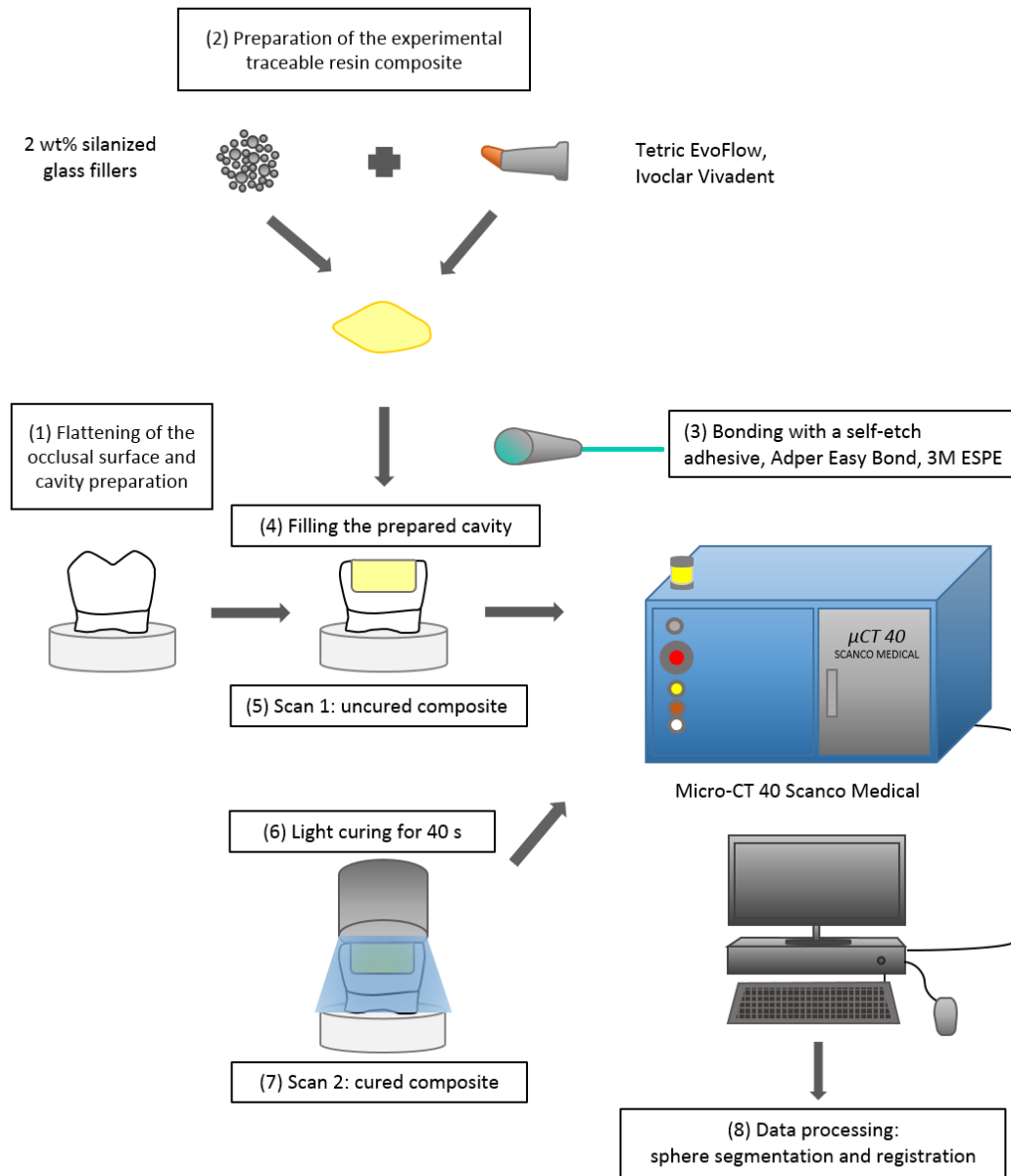


Figure 18 Scheme of the workflow for obtaining the digital 3D-data sets from the micro-CT.

3.4.4 Data processing

The basic idea was to identify each individual embedded glass sphere and follow the position change of the glass spheres due to polymerization shrinkage in both scans. Data processing was performed in different steps consisting of a rigid registration, followed by sphere segmentation and registration of each individual sphere based on a block-matching algorithm, as shown in Figure 19 (Chiang et al., 2008; Chiang et al., 2009; Chiang et al., 2010; Rösch et al., 2009).

3.4.4.1 Rigid registration

Rigid registration was first performed to perfectly match the pre- and post-polymerization scans via the outer tooth contours of each sample. The enamel shell and the dentino-enamel junction served as references which ensured the exact matching of both scans. Implementation was based on the Insight Toolkit, ITK (www.itk.org).

3.4.4.2 Sphere segmentation and sphere registration

This step was performed to detect the change in position of each glass filler that occurred due to the polymerization shrinkage. Data were prepared for calculations using Fiji (<http://fiji.sc/Fiji>).

Sphere segmentation was performed for the extraction of glass fillers based on the greyvalues of the micro-CT scans. Glass beads have a characteristic diameter of 40-70 μm and they can be identified via the tensor of inertia. Only those glass fillers were registered that have been distinctly identified. Each identified spherical structure (glass filler) was labeled and traced in both scans of each sample, where non-spherical structures were discarded.

Sphere registration involved the identification of fillers and the location of each filler in both corresponding scans was calculated.

Starting with the larger glass fillers of the pre-polymerization scans, the search proceeds in the neighboring areas of the post-polymerization scans as the larger glass fillers are assumed to be located in close proximity. This gives a clue about the change in position of the glass fillers due to the contraction movement. Thus, if glass fillers overlap in the pre- and post-polymerization scans, they are assumed to form a “pair”. Taking the orientation of the larger glass filler, smaller ones are searched for by the same method on the basis of the tensor of inertia of each glass filler. The center of each glass filler is determined in the pre-polymerization scan and its corresponding center in the post-polymerization scan. The

Euclidian distance of both centers constitutes the shrinkage vector. These calculations are based on the block-matching algorithm.

3.4.4.3 Visualization of shrinkage vectors

The displacement vector fields were visualized using VTK (www.vtk.org), where each vector was represented graphically in form of a glyph pointing in the direction of shrinkage. All vectors together formed the displacement vector field. For better visibility of the displacement vector fields, the vectors were scaled by the factor 5. The displacement vector fields were analyzed visually for shrinkage patterns.

3.4.4.4 Values of shrinkage vectors

The output of the registration process was in form of a text file that contained the location of each identified filler, defined by the xyz-coordinates, in the pre-polymerization scan as well as in the post-polymerization scan. Absolute values of the displacement vectors were calculated as the Euclidean distance of the centers of gravity of each segmented individual sphere before and after curing:

$$v = \sqrt{(x_{\text{postpolym}} - x_{\text{prepolym}})^2 + (y_{\text{postpolym}} - y_{\text{prepolym}})^2 + (z_{\text{postpolym}} - z_{\text{prepolym}})^2}$$

Analysis of shrinkage in relation to the light source was performed by examining only the z-component of vectors denoting the filler movement along the z-axis:

$$V_{z\text{-component}} = z_{\text{postpolym}} - z_{\text{prepolym}}$$

3.4.4.5 Statistical analysis

The mean vector lengths were computed and subjected to one-way ANOVA with post-hoc pairwise comparisons using Tamhane's T2 (using IBM SPSS Statistics 20).

3.4.5 Scanning electron microscopy

One sample per group was critically point dried, sectioned longitudinally and examined for internal adaptation with a scanning electron microscope (ZEISS GEMINI® FESEM, SUPRA™ 55VP, Carl Zeiss SMT AG, Oberkochen, Germany) at x200 magnification (Figure 66).

Table 4 Composition of the experimental resin composite and the self-etch adhesive

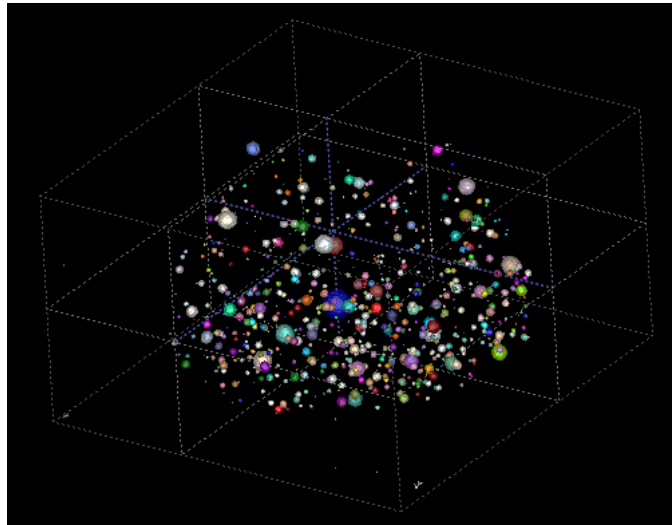
Brand name	Composition	Batch No.	Manufacturer
Tetric EvoFlow (nano-optimized flowable composite)	Bis-GMA, and urethane dimethacrylates (38 wt%) Barium glass filler, ytterbiumtrifluoride, highly dispersed silica, mixed oxide and prepolymers (62 wt%) Particle sizes of the inorganic fillers:40-3000 nm	R36640	Ivoclar Vivadent, Schaan, Liechtenstein
Glass beads (radiolucent spheres, used as traceable markers)	SiO ₂ (72.50 wt%), Na ₂ O (13.00 wt%), CaO (9.06 wt%), MgO (4.22 wt%), Al ₂ O ₃ (0.58 wt%) Diameter: 40-70 μm	Art. No.: 5211	Sigmund Lindner GmbH, Warmensteinach, Germany
Adper Easy Bond (bonding agent)	2-hydroxyethyl methacrylate (HEMA) Bis-GMA Methacrylated phosphoric esters 1,6 hexanediol dimethacrylate Methacrylate functionalized Polyalkenoic acid (Vitrebond™ Copolymer) Finely dispersed bonded silica filler with 7 nm primary particle size Ethanol Water Initiators based on camphorquinone Stabilizers	R461191	3M ESPE, Seefeld, Germany

3.5 Results

3.5.1 Qualitative presentation of polymerization shrinkage: Visualization of shrinkage vectors in the displacement vector fields and SEM

The glass fillers were identified, labeled and extracted from the matrix by sphere segmentation. Then the segmented spheres were registered and shrinkage vectors were computed (Figure 19).

(A)



(B)

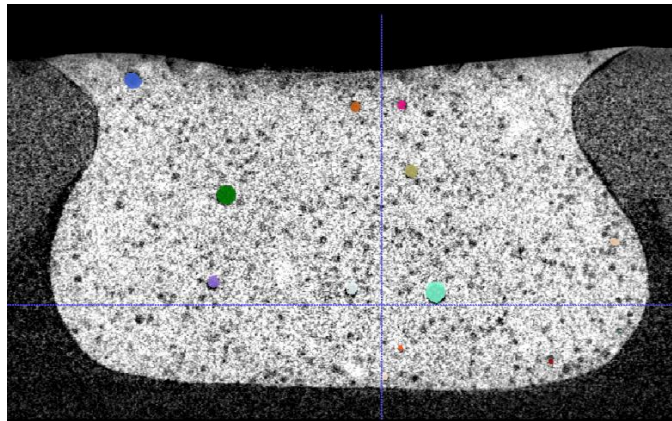


Figure 19 Sphere segmentation and sphere registration based on a block-matching algorithm. Sphere segmentation: set of all identified and extracted glass fillers in a same sample from the “adhesive” group (A), Sphere registration: both scans of one sample (here: "adhesive group") were superimposed. The identified glass fillers in the first scan were simply radiolucent and colorless while the corresponding glass fillers from the second scan were superimposed and color coded (B). Sphere registration was performed based on a block-matching algorithm to determine the displacement of the segmented spheres due to polymerization shrinkage.

3.5.1.1 The displacement vector field in the "adhesive cavity"

The displacement vector field in the “adhesive” cavity showed for all samples an extensive upward movement in the lower part of the restoration with predominantly large vectors, while the upper part exhibited fewer shrinkage vectors with a minimal downward shrinkage (Figure 20). The SEM-images of the arbitrarily selected sample showed a defective and cracked bond at the floor, while an intact bond at the enamel margin was seen (Figure 21).

3.5.1.2 The displacement vector field in the “diverging cavity”

In the “diverging cavity”, the displacement vector field showed in the upper part of the restoration large shrinkage vectors with great downward shrinkage, while the lower part of the restoration had many small vectors with an upward shrinkage (Figure 22). The SEM-images displayed a detached bond at the enamel margin, and an intact bond at the bottom (Figure 23).

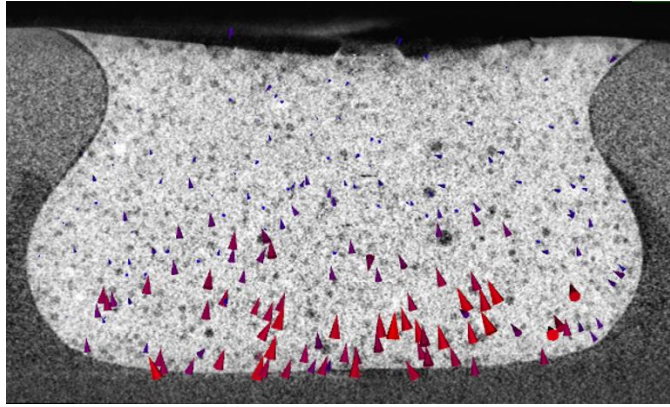
3.5.1.3 The displacement vector field in the “cylindrical” cavity

All teeth in the „cylindrical” cavity group showed a considerable amount of shrinkage vectors in the lower third of the cavity point upwards. The average length of these vectors was 16.7 μm . In contrast to this uniform appearance of the lower part of the cavity, the upper part of the cavity had only a few(er) vectors pointing downwards in the upper third of the cavity for six teeth. The average length of these vectors was 24.5 μm . Three teeth exhibited more shrinkage vectors in the upper third of the cavity pointing downwards with an average size of 34.4 μm . The density of the identified vectors was the same in both groups. The fillers’ density in the lower third was greater than in the upper third. Three teeth revealed a greater number of shrinkage vectors leading downward in the upper part of the restoration (Figure 24).

SEM images showed an intact bond at the enamel margin at one side only and a defective bond at the floor. The atypical shrinkage pattern differed that the upper part showed great downward shrinkage in addition to the great upward shrinkage at the lower part (Figure 25).

The thickness of the adhesive layer varied in the different cavity forms at different locations: in the adhesive form, it was thickest below the enamel margin, while in the diverging, it was thickest at the enamel margin. None of these variations in thickness was observed in the “cylindrical” cavity.

(A)



(B)

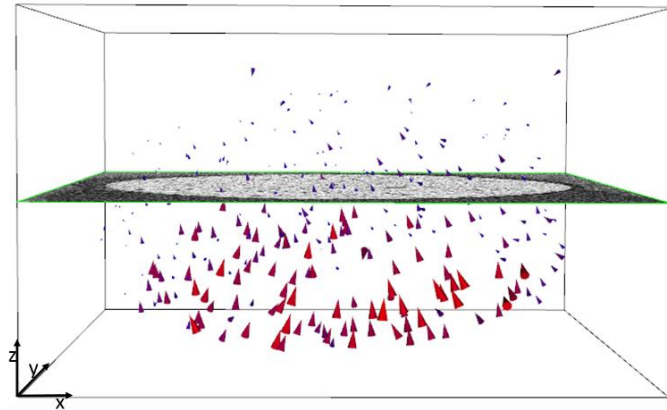
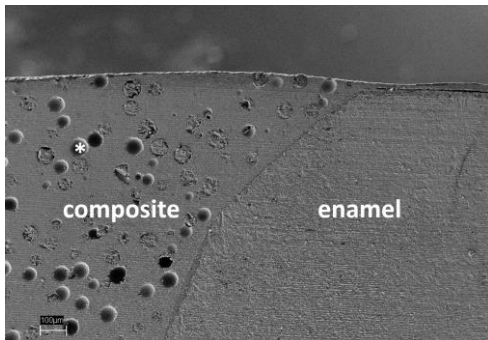


Figure 20 The displacement vector field of the "adhesive" restoration, with the x-plane (A) and the z-plane (B) of the micro-CT scan in the background. Glyphs were scaled by a factor of 5 to enhance visibility. Large shrinkage vectors are seen at the lower restoration part pointing upwards.

(A)



(B)

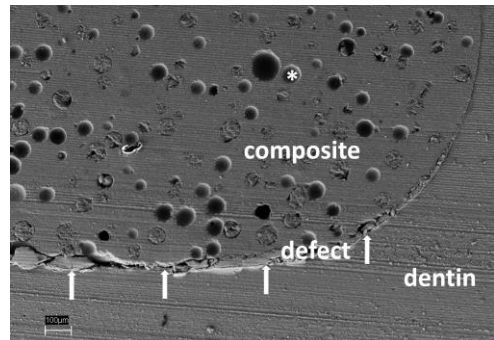


Figure 21 SEM image (x200) of the "adhesive" restoration showing an intact bond at the enamel margin (A) and a defective bond "defect" at the floor of the restoration (B). One traceable glass filler is marked by the star *.

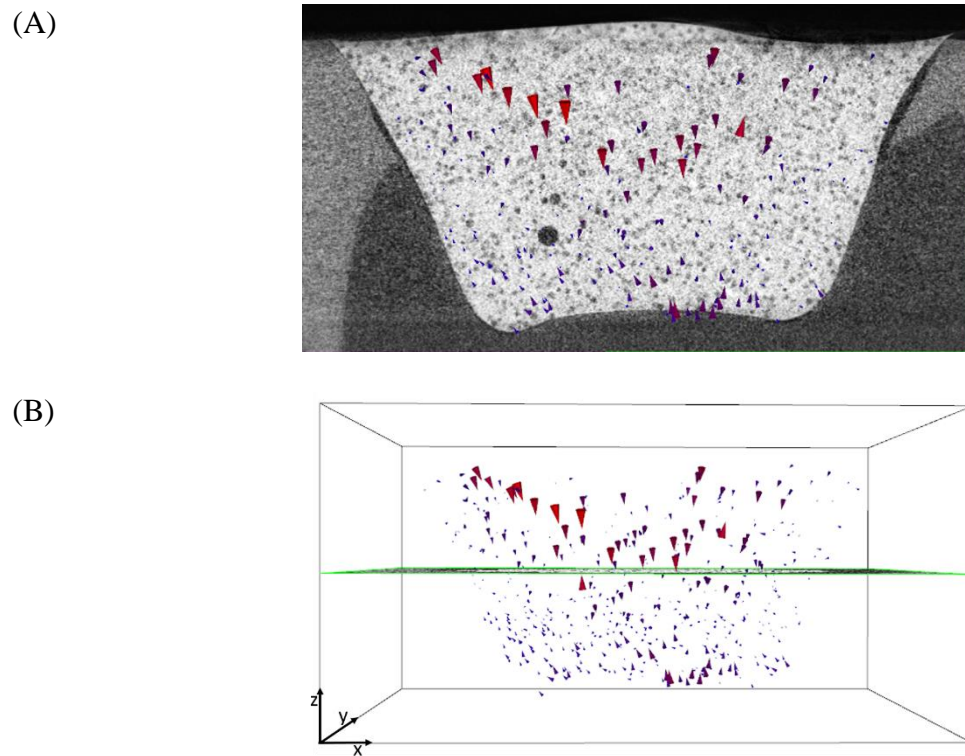


Figure 22 The displacement vector field of the “diverging” restoration, with the x-plane (A) and z-plane (B) of the micro-CT scan in the background. Glyphs were scaled by a factor of 5 to enhance visibility. Large shrinkage vectors point downward near the free surface, and small shrinkage vectors point upward from the restoration floor.

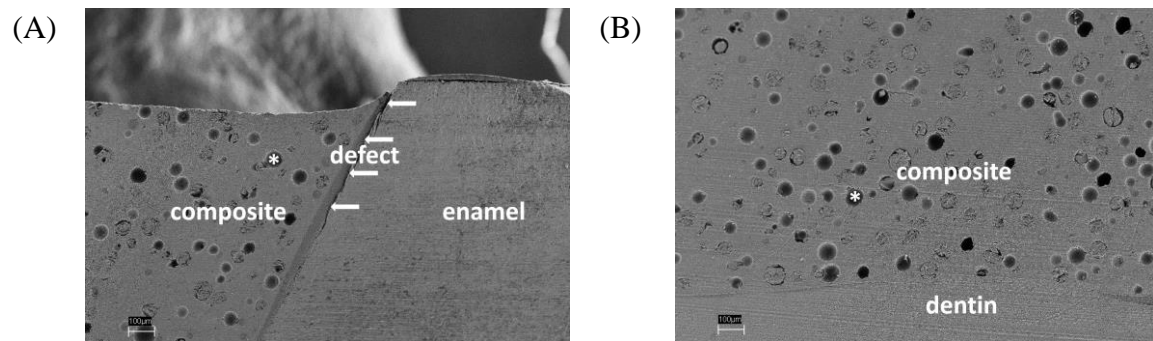


Figure 23 SEM image (x200) of the “diverging” restoration, displaying a defective bond at the enamel margin (A) and an intact bond at the floor of the restoration (B). One traceable glass filler is marked by the star *.

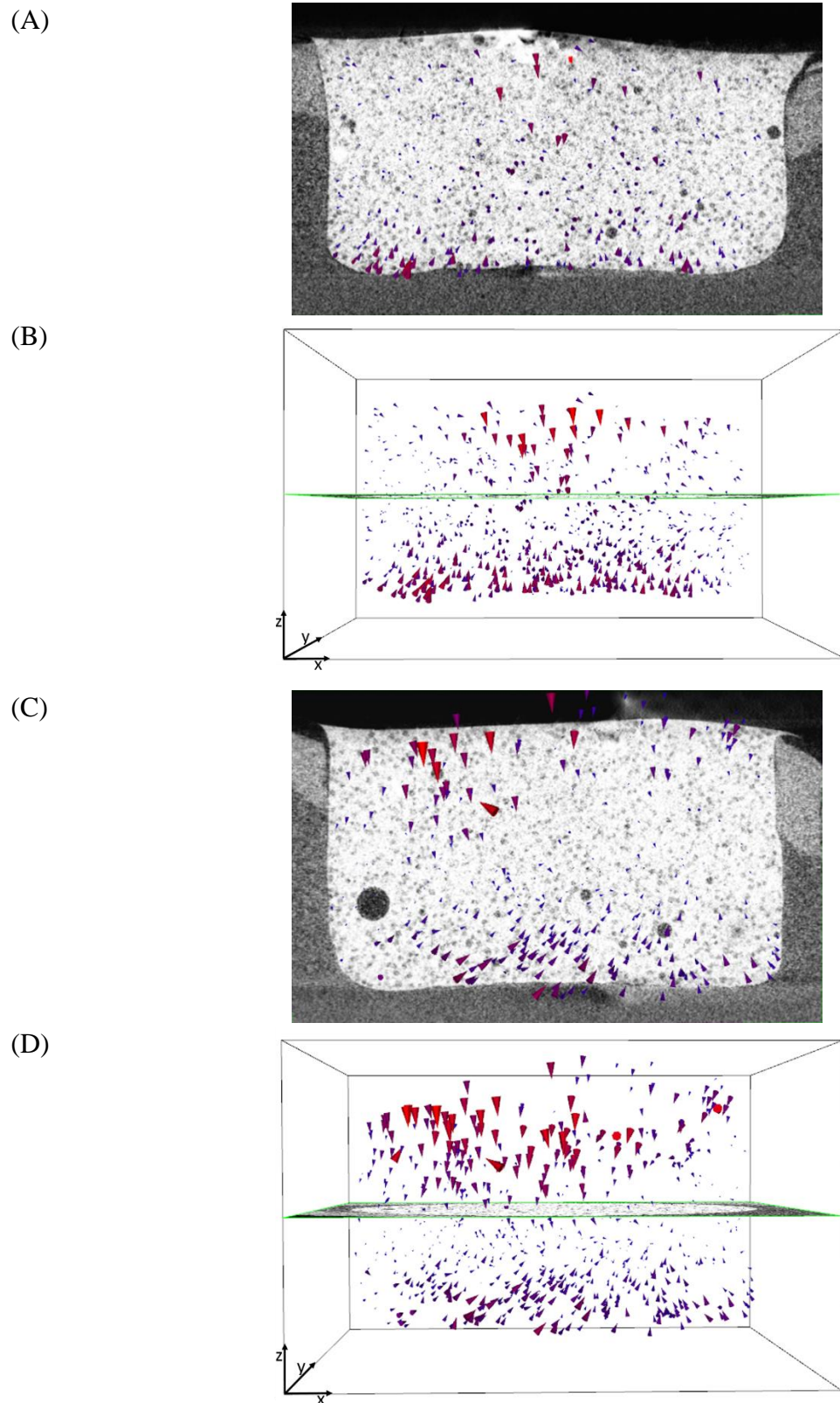


Figure 24 The displacement vector field in the “cylindrical” group with a predominant shrinkage pattern with the x-plane (A) and z-plane (B) of the micro-CT scan in the background showed more vectors in the lower part, while the atypical shrinkage pattern in the “cylindrical” cavity additionally displayed large vectors in the upper restoration part. The x-plane (C) and z-plane (D) of the micro-CT scan displayed in the background. Glyphs were scaled by a factor of 5 to enhance visibility.

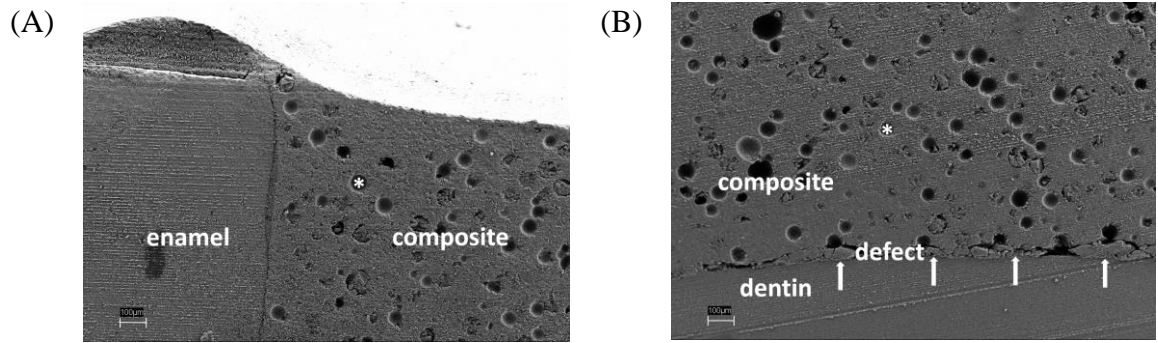


Figure 25 SEM image (x200) of the “cylindrical” restoration showing an intact bond at the enamel margin at one side (A) and a defective bond at the floor of the restoration (B). One traceable glass filler is marked by the star *.

3.5.2 Quantitative presentation of polymerization shrinkage: values of shrinkage vectors and statistical analysis

3.5.2.1 Quantitative non-directional analysis: Probability density function of the vector length values

The results of the mean vector lengths are summarized in Table 3. The "adhesive" cavity had the highest vector length values ($31.1 \pm 10.9 \mu\text{m}$), followed by the "diverging" ($27.4 \pm 12.1 \mu\text{m}$). The "cylindrical" cavity configuration had the least overall vector lengths ($23.3 \pm 11.1 \mu\text{m}$). The probability density function of the vector length values for all groups is displayed in Figure 26. Small vector lengths were most frequent in the "cylindrical" cavity, followed by the "diverging cavity" and large vectors were more often present in the "adhesive cavity".

One-way ANOVA revealed significant differences ($F=179.848$; $Df=2,4370$; $p<0.001$) and the post-hoc pairwise comparison using Tamhane's T2 test showed significant differences between all groups.

In summary, the "adhesive cavity" form had the greatest 3D-shrinkage, the greatest upward and the minute downward movement. In the "diverging cavity", the 3D-shrinkage was intermediate and downward shrinkage was greatest. The "cylindrical" cavity showed the smallest 3D-vectors and the least upward shrinkage.

Table 5 Mean vector length values and mean filler movement in the z-direction in the different cavity configurations

Group	Vector length (μm)	Filler movement in the z-direction (μm)
"adhesive" cavity design	31.1 ± 10.9	-13.7 ± 12.1
"diverging" cavity design	27.4 ± 12.1	-5.7 ± 17.2
"cylindrical" cavity design	23.3 ± 11.1	-3.7 ± 13.6

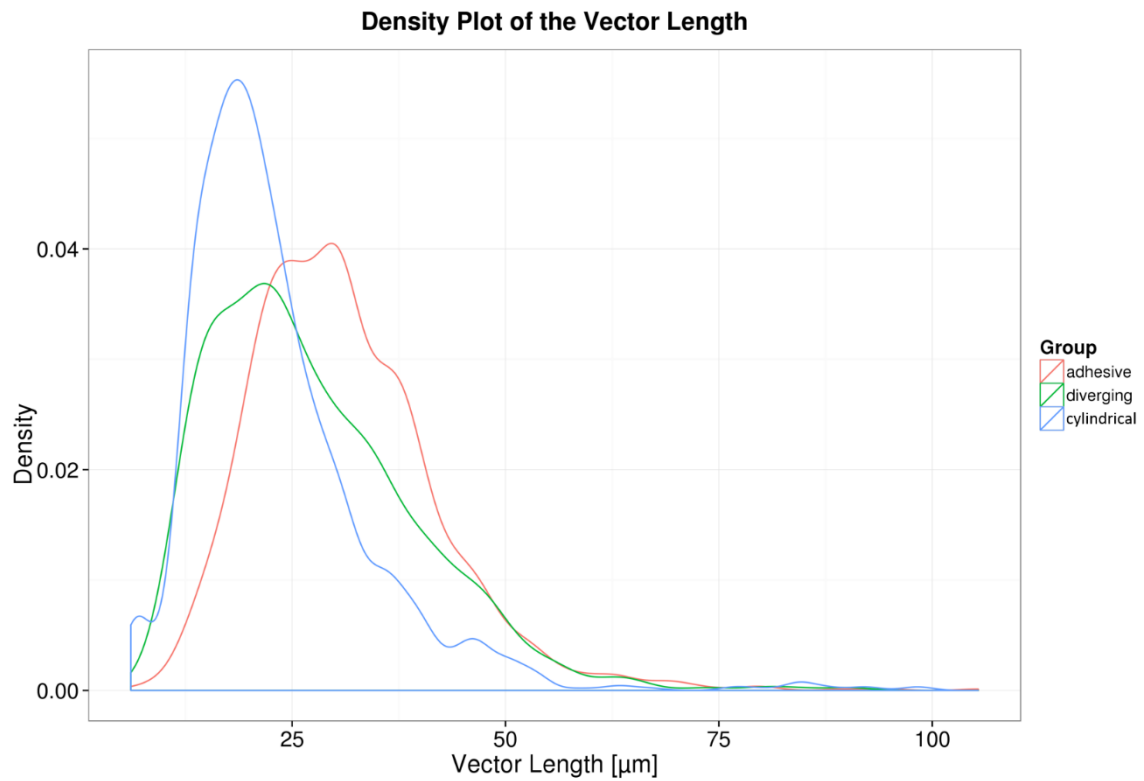


Figure 26 The probability density function of the vector lengths in the “adhesive”, “diverging” and “cylindrical” groups. The “adhesive” group had two maxima above 25 μm and a large vectors were more numerous than in the other groups. The “diverging” group had its maximum at about 25 μm which means that the majority of vectors were in that range. The “cylindrical” group had its peak at about 15 μm which means that the greatest frequency of vectors had that value.

3.5.2.2 Quantitative directional analysis: Probability density function of the z-component of the vectors (Filler Movement in z-direction):

The z-component of the vectors denoting the filler movement was analyzed to investigate whether the composite shrinks towards light or not. Negative values denoted shrinkage towards the light-source (upward movement), while positive ones exhibited downward shrinkage away from light. Greatest mean filler movement towards the light were in the “adhesive cavity” form ($-13.7 \pm 12.1 \mu\text{m}$), followed by the “diverging” cavity ($-5.7 \pm 17.2 \mu\text{m}$), while the „cylindrical” cavity showed the least mean filler movement ($-3.7 \pm 13.6 \mu\text{m}$) toward the light source (Figure 27).

The relative likelihood for the z-component to take on a given value can be described with the probability density function. The area below the curve describes the probability of a z-component having a value in the interval which limits the area to the left and to the right. Considering the interval from negative infinity to zero (equivalent to movement towards the light) the “adhesive cavity” has a higher probability of movement towards the light than by the “parallel cavity”. The “diverging cavity” showed least upward filler movement in z-direction, while its probability of downwards movement was the greatest.

Levene’s test proved equality of variances of the three cavity configurations. The subsequent ANOVA revealed significant differences between the three groups ($F=216.839$; $Df=2,4380$; $p<0.001$). The pairwise comparison with Tamhane’sT2 showed statistically significant differences between all groups.

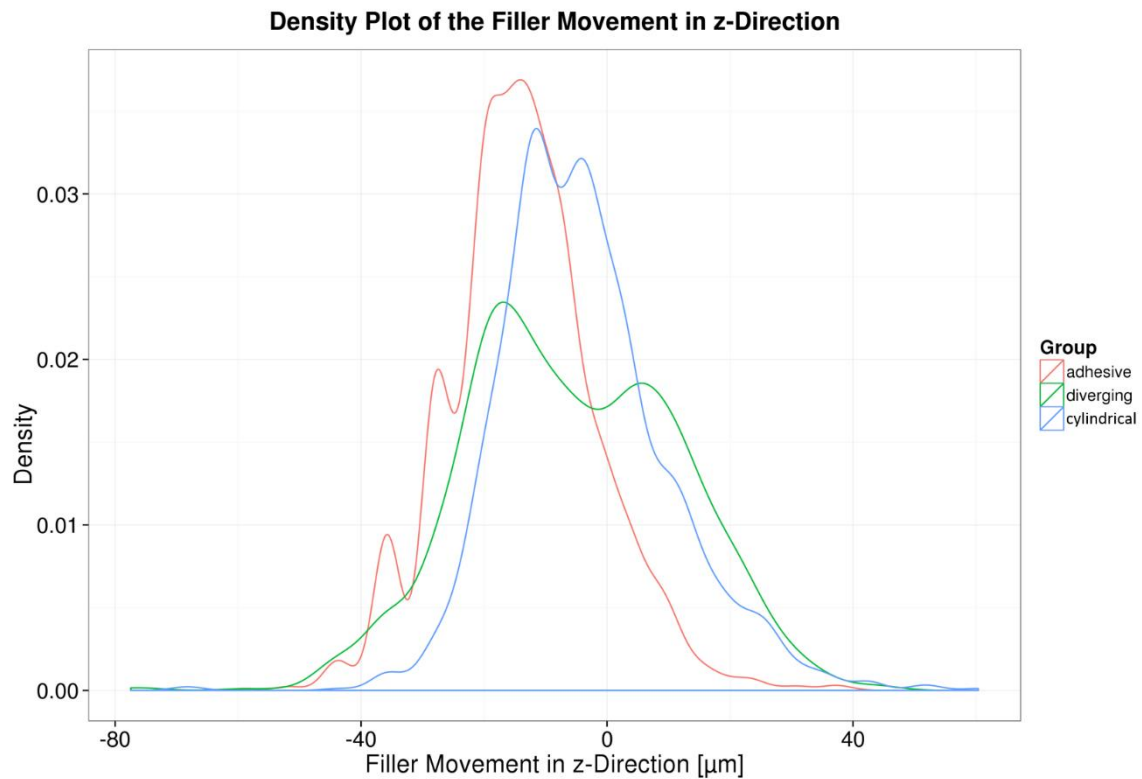


Figure 27 The probability density function of the filler movements in the z-direction in the “adhesive”, “diverging” and “cylindrical” groups. The “adhesive” group showed many peaks which related to the presence of many vectors of that value. The curve is shifted in the negative range that relates to the upward shrinkage movement at the cavity floor. The “diverging” group had a shallower curve with two maxima; the first is in the range of -20 μm that relates to the upward shrinkage at the cavity floor, while the second maximum is located at about 15 μm which can be related to the downward shrinkage seen at the free surface. The curve of the “cylindrical” cavity also has two peaks, but they are close to each other near the zero value. The first peak can be attributed to the upward movement at the lower cavity part and the second peak is related to the downward movement at the free surface.

3.6 Discussion

The computation of polymerization shrinkage vectors of dental resin composites is a relatively recent method. The first attempts were in the form of 2-dimensional shrinkage analysis (Chiang et al., 2009; Inai et al., 2002), then 3-dimensional investigations were developed (Chiang et al., 2009; Chiang et al., 2010; Cho et al., 2011). The evaluation methods have fundamental differences because each is based on a specific mathematical principle.

The 2D displacement vector field calculations of Chiang et al., 2009, were based on an elastic registration algorithm using B-spline regularization (Arganda-Carreras et al., 2006; Chiang et al., 2008; Chiang et al., 2009; Kybic and Unser, 2003; Sorzano et al., 2005). Yet, B-splines regularizations restrict possible deformations, whereas tracing separate fillers in the current study did not have implicit constraints or marginal conditions regarding possible deformations.

Cho et al., 2011, used a cluster-labeling algorithm to extract the fillers and perform the pairing procedure. They obtained the 3D movement distance of each filler after polymerization, but their analysis of filler movement was limited to the axial direction in relation to the light source (Cho et al., 2011).

The 3-dimensional shrinkage analysis of Chiang et al., 2009, 2010, was based on a block-matching method that was previously described in detail (Chiang et al., 2009; Chiang et al., 2010; Rösch et al., 2009). The current study implemented the same method of image registration performed through sphere segmentation and subsequent registration. Sphere segmentation is the identification and separation of glass spheres from the rest of the restoration in the uncured image which depends on the grayvalue of the micro-CT scan. The scan resolution was limited to $8^3 \mu\text{m}^3$, but it was sufficient for the shrinkage analysis. Registration of the individual spheres was performed by a local rigid registration, the block-matching, to determine the segmented spheres' displacement during the polymerization process. Accordingly, each identifiable filler pair before and after curing was represented by a displacement vector which presented the actual movement and was the method's main advantage.

The flowable composite was chosen because the glass fillers were easily added to it. Additionally, it exhibits a greater degree of shrinkage and greater shrinkage vector values are easier to visualize. The use of glass fillers was advantageous as they were silanized for proper chemical bonding and movement with the resinous mass upon polymerization, as

well as avoiding reconstruction artifacts in the micro-CT scans that could occur with zirconium dioxide fillers. The 2 wt% embedded glass fillers were plenty enough to trace the material's movement throughout the restoration and hardly affected the polymerization. However, the flowable composite is not comparable to a hybrid composite regarding the application in posterior teeth as it exhibits greater shrinkage and has a lower modulus of elasticity.

Three cavity designs were proposed to detect their effect on the polymerization shrinkage. The “adhesive cavity” configuration is defect-oriented. It is of clinical relevance, as it is conforming to the spread of pit-and-fissure caries that expands as it penetrates into the enamel passing through the dentino-enamel junction and extending laterally into dentin (Roberson, 2006a). It evolved in a time when there were no dentin bonding agents and with this design, the cavity could be sealed well through bonding to enamel. An enamel bevel was prepared for cutting enamel prisms and to increase the surface area for bonding leading to a tight marginal seal. On the other hand, for many years, adhesive restorations are bonded to tooth structure, although the bond strength to dentin is weaker than to enamel. Consequently, a detachment from the cavity floor would occur resulting in postoperative complains. The “diverging” cavity was proposed as it has no frictional effects in the direction of light, whereas the “cylindrical” does, but the “cylindrical” cavity is neutral regarding the shrinkage movement in axial direction. In case there should be a Lambert-Beer dependence of the composite, the free surface of the “diverging” cavity would harden first and pull the material upward, Figure 28. To settle this query, the “cylindrical” cavity was proposed which could be related and compared to previous experiments (Chiang et al., 2009; Chiang et al., 2010; Versluis et al., 1998).

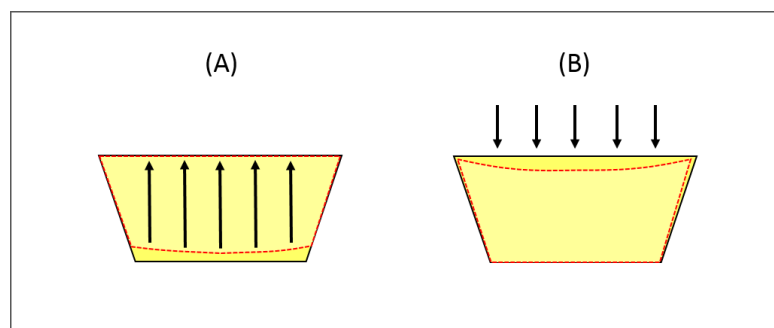


Figure 28 Possible shrinkage directions in the “diverging” cavity configuration: (A) upward shrinkage as composite at the free surface hardens first and pulls the composite upwards as soon as the adhesive bond interface to the tooth is disrupted, or (B) downward shrinkage of the free surface.

It was attempted to choose teeth of similar size and to prepare cavities of alike volumes even though their configuration differed according to each group. However, the “adhesive” group had a mean restoration volume of 72 mm³, whereas the volume of the “diverging” group was smallest with only 52 mm³ and the cylindrical was 58 mm³. Largest vectors were found in the “adhesive” group, followed by the “diverging” and smallest in the “cylindrical” group, also the axial movement was in this sequence. It can be assumed that the direction of shrinkage vectors is not directly related to the volume of the restoration, but rather to the cavity configuration.

The “free shrinkage” is the case when composites are allowed to shrink freely and they will tend to shrink toward the center. This applies only in case there is no contact to a surface. Once the composite contacts a surface, the shrinkage will be directed toward this surface, Figure 29. Whenever composites are bonded, their contraction movement is governed by their boundary conditions such as the cavity configuration, the C-factor, the bonding condition and the bonding substrate. Accordingly, this shrinkage is termed the “effective shrinkage” (Asmussen and Jorgensen, 1972; Hansen, 1982a).

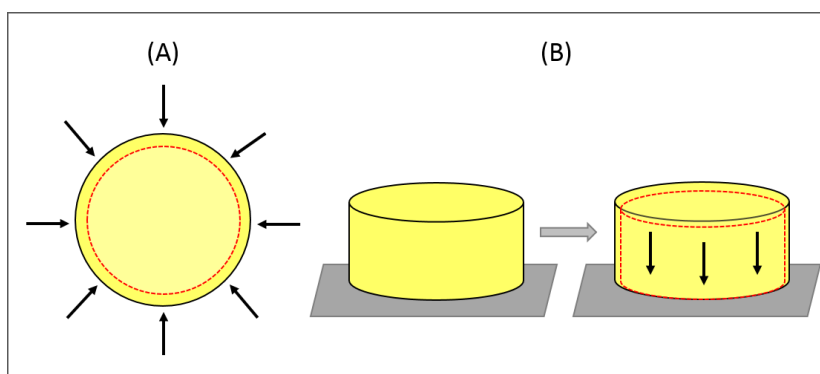


Figure 29 The shrinkage of a floating specimen having no contact with any surface exhibits “free shrinkage” (A), but a specimen in contact with a surface shrinks towards it (B).

All cavity forms showed downward shrinkage, away from the light source, in the upper parts, though to different extents. A fictional zero-line is where downward and upward shrinkage meet and constitutes a range of almost no axial shrinkage. It was located close to the surface in the “adhesive form”, almost in the middle in the “cylindrical restoration” and at the junction between middle and lower one third in the “diverging cavity”. Similar observations were made by FEA in the case presented with perfect bond to enamel and no bond to dentin (Versluis et al., 1998) and in the bonded restoration showing downward shrinkage in the

upper 1 mm, while the remaining fillers shrank upward (Cho et al., 2011). A resin composite has the tendency to shrink toward the center which is limited by a strong bond to the tooth structure. The fictional zero-line can be formed due to the antagonistic movements. The strong bond of the composite to the enamel bevel in the “adhesive” cavity hindered the downward movement, while the large free surface in the “diverging” cavity moved downward and broke the bond with the enamel margin which in turn allowed for even more downward shrinkage that pushed the fictional zero-line to a lower level. Greater discrepancies existed between the boundary conditions of the free surface, the enamel margin and the dentin floor, whereas the bonding conditions and subsequent variations of bond strength values at the cavity walls were more balanced and less prone to great variations. Consequently, axial movements were stronger related to the bonding conditions than movements at the cavity walls.

The main reason for the downward shrinkage can be the large unbonded surface of the restoration. Shrinkage occurs even after the post-gel point due to elastic deformations and in the “diverging” cavity the downward shrinkage was greatest. Beam profile analysis showed that the light intensity is not homogenous throughout the diameter of the light guide which could affect the degree of cure (Price et al., 2011).

In a future study, the polymerization profile analysis and the beam profile analysis could highlight unknown issues in the polymerization process. Many curing lights produce a non-uniform light output that affects microhardness which is a measure for the degree of conversion. Inhomogeneity of light output causes inhomogenous polymerization across the composite restoration. Laser beam analyzers determine the homogeneity within a light beam which characterizes the degree of spatial and spectral uniformity of curing light power distribution. Practical tips for proper curing include placing the light guide tip perpendicular and closest possible to the restoration to optimize light transmission in depth (Leprince et al., 2013; Naoum et al., 2012; Price et al., 2010a; Price et al., 2011; Price et al., 2013). In the current study, the composite was cured at the closest possible distance to ensure best polymerization.

The light source in relation to the different cavity configurations was presented in Figure 30. A cross-sectional view of the “adhesive cavity” elucidated that light could not directly reach the resin composite below the enamel margin in proximity of the dentin walls. This could have affected the polymerization process and might have left the composite less cured there. Stronger bonding to enamel, anchoring through the enamel bevel and more profoundly cured

composite near the surface might be the reasons for the greater shrinkage in the lower cavity part.

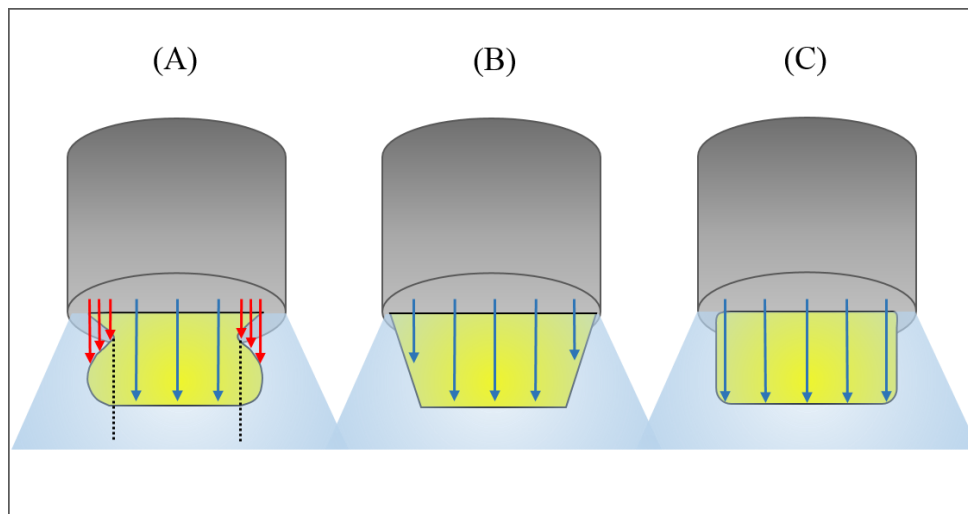


Figure 30 The light source in relation to the “adhesive” (A), “diverging” (B) and “cylindrical” (C) cavity configurations. In the “adhesive” cavity, light did not directly reach the resin composite below the enamel margin. In the “diverging” and “cylindrical” cavities, there was no configurational impedance to the curing-light.

The degree of cure of the composite below the enamel bevel can be related to the enamel translucency and in part to the dentin translucency. The translucency of enamel can be expressed as a transmission coefficient t_c that is dependent on the light wavelength. T_c of enamel is higher at longer wavelengths of light in the visible range and decreases with decreasing wavelengths due to increase in the light scattering as indicated by the Rayleigh scattering equation. Dehydration also reduces the translucency values due to an increased difference in refractive indices between enamel prisms and surrounding medium when water is replaced by air (Brodbelt et al., 1981).

In the current study teeth were dry while manipulation for the bonding procedure and composite application. Few drops of water were added to the sample holder to avoid tooth cracking during the scanning procedure, but did not touch the occlusal surface not to interfere with the filling material. Upon air drying enamel, the relative translucency of enamel decreases to about 80% after only 10 s (Brodbelt et al., 1981), while the scanning procedure lasted 1.5 h. Resultingly, the enamel translucency of the scanned specimen was for sure decreased than in the normal hydrated state, which could explain a possible lesser degree of cure in the undercut area below the bevel. On the other hand, the translucency parameters of

only few high translucent composites are similar to those of enamel and dentin of the same thickness (Yu et al., 2009), meaning that the translucency parameters of tooth structure is usually greater than that of composites. Hence, the undercut area has no impaired access to the curing-light.

Light emission is not homogenously distributed throughout the light beam as there is a light focus that differs from one curing light to another. The light focus of the used curing light, Elipar FreeLight2, 3M ESPE, in relation to the cylindrical cavity is presented in Figure 31. It shows more intense light in the center and less intense light at the peripheries.

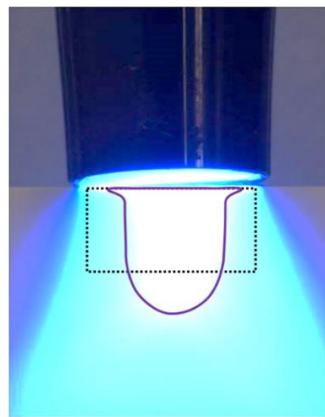


Figure 31 The light focus of Elipar FreeLight2, 3M ESPE, in relation to the “cylindrical” cavity.

The direction of the light curing has been very important in the 70s and 80s of the last century, when curing lamps were less intense, but today, there are enough photons within the cavity. Despite of the light attenuation there are sufficient photons at a depth of 2 mm for photo initiators to start the polymerization reaction (Kramer et al., 2008; Lindberg et al., 2004). For this reason, the direction of light application was not investigated in the current study, though the light was applied perpendicular to the tooth long axis. Until today, this might be critical with increments greater than 2 mm where some studies show the decrease of hardness with increased depth which can be explained by a changed network density. Clinically, Tetric EvoFlow should not be used in increments greater than 2 mm, although the depth of cure of 3 mm was previously confirmed (Lindberg et al., 2004). Further investigations are needed with bulk-fill materials in deeper cavities and with incrementally applied composites.

The enamel bevel in the “adhesive” cavity was prepared so that enamel prisms were almost cut perpendicular yielding higher bond strength values (Swanson et al., 2008). The bonded surface area to enamel was greater in the “adhesive” cavity due to the bevel than in the “diverging”, therefore, restricting the movement in the upper part of the “adhesive” cavity. Additionally, the margins in the “diverging” cavity were furthest away from the mass center of the restoration followed by a decrease of bond strength in their periphery (de la Macorra and Cabrera, 2012).

The course of enamel prisms and the direction of cutting are of great importance for marginal integrity. In the “diverging” cavity a defective bond to the enamel margin was observed which was an unusual finding considering that bonding to enamel is stronger than bonding to dentin. However, the direction of cutting the enamel prisms was almost parallel and according to Ikeda et al., could lead to contraction gaps and/or enamel microcracks (Ikeda et al., 2002; Lutz and Phillips, 1983; Phillips et al., 1983). On the other hand, cutting perpendicular to enamel prisms leads to higher bond strength values (Ikeda et al., 2002) which is in accordance with the statement that margin beveling has a greater effect in minimizing microleakage due to increased bond strength than the type of the adhesive. Therefore, a bevel should be cut as the shrinkage direction is exclusively governed by the bonding (Swanson et al., 2008).

The shrinkage pattern of the “adhesive” cavity resembled that of the „cylindrical” in the “predominant mode” where the filling was attached at the enamel margins and separated from the floor. The “atypical pattern” showed detachment from enamel at one side resulting in less stress at the floor. If composite detached from one site, then the unbonded surface area is increased which in turn decreases the polymerization shrinkage stresses of the remaining bonded surface area. In the “adhesive” and „cylindrical” cavities a defect was observed that could be either adhesive failure or cohesive failure in composite at the cavity floor due to upward movement.

Axial shrinkage constituted only part of the overall shrinkage and should not be taken as the sole measure. In the “adhesive” cavity, numerous vectors were located at the rounded area between floor and walls reflecting deformation in the area of undercut where light was not directly accessible and its intensity was more attenuated than in other areas. The displacement vector field of the „cylindrical” cavity differed from results obtained by Chiang et al., 2009, 2010, while it was in agreement with that obtained by Cho et al., 2011. Shrinkage patterns might be associated with volumetric changes or distribution within each cavity form; greater shrinkage occurred at the area of greater volume in each group.

The “cylindrical” cavity form had no volumetric variation within the cavity, nonetheless detachment happened at one enamel margin which was assumably the point of first detachment (Chiang et al., 2009; Chiang et al., 2010). Earlier, it was observed that contraction due to polymerization is not equal in all directions; in initial stages of setting, the material would adhere to cavity walls and shrinkage occurs exclusively at the free surface until stresses in the material exceed the adhesion. Then the material loses its grip on the cavity wall and a crescent-shaped gap is produced (Asmussen and Jorgensen, 1972). Zeiger et al., 2009, have measured the volumetric polymerization shrinkage and associated leakage in two cavities of equal volume but with different dimensions. They have claimed that neither overall shrinkage nor its spatial distribution are affected by cavity geometry or C-factor (Zeiger et al., 2009). In this study, however, a clear difference in shrinkage direction and vector lengths between the three cavity forms was obvious. Cavities with different C-factors should be investigated in the future.

Flattening of the occlusal surface for obtaining the closest distance for light curing did bear some problems: when removing too much enamel, some dentin was exposed at the cusp tips, and the cavity margins were not fully located in enamel. Acquiring adequate cavity depth caused pulp exposure. In an attempt to avoid these problems, grinding of the occlusal table and removing as little as possible enamel maintained some fissures into which some bonding agent or resin composite material would flow into, possibly interlocking at the surface and affecting the shrinkage direction. The occlusal surface was flattened to ensure the exact location of the focus of the light source. Cusp tips were flattened but the enamel at the cavity margins has not been prepared.

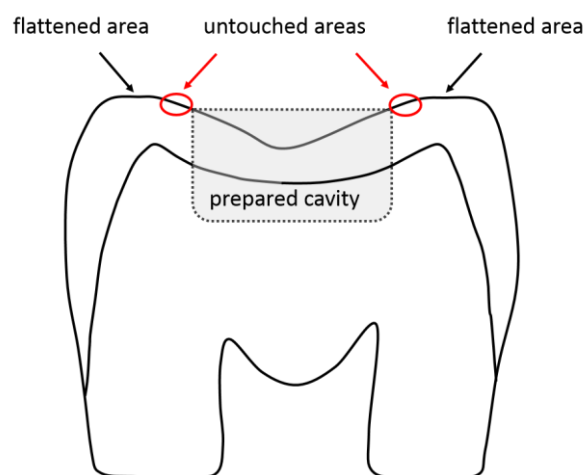


Figure 32 Cusp tips were flattened to allow for light-curing as close as possible to the restoration. Cavity margins were mostly located in enamel.

The thickness of enamel at the cavity margins and cavity walls was not perfectly uniform neither within one sample, nor throughout all samples. Nevertheless, a specific shrinkage pattern for each group could be identified and related to the cavity form. The sample size was sufficiently large (n=9) to report this observation as the resultant shrinkage pattern or in other words, the displacement vector field. Previous observations reported that thick enamel margins promote better adhesion, while thin enamel margins favour detachment and gap formation (Chiang et al., 2009; Chiang et al., 2010). However, this finding was not confirmed in our study. Nevertheless, it might be related to differences in the bonding agents used, or the discrepancies in thickness of enamel margins themselves.

A radiolucent area between the tooth and restoration was observed in some samples of the adhesive and diverging groups which could either be a gap or the adhesive layer in greater thickness. It was seen in both pre- and post-polymerization scans and consequently assumed to be the adhesive, confirmed by SEM. Its thickness varied in the different cavity forms at different locations: in the “adhesive” form, it was thickest below the enamel margin, while in the “diverging”, it was thickest at the enamel margin. In the “adhesive” cavity, it might be explained by an impaired escape of excessive adhesive with an increased tendency towards pooling of the adhesive upon air thinning in comparison with the „cylindrical” and “diverging” cavity forms which have a greater occlusal access and therefore, greater way of escape. Furthermore, shrinkage is greatly determined by the bonding condition (Versluis et al., 1998) which needs more investigations.

To sum up, this investigation could display that the proposed cavity configurations exhibited various displacement vector fields. Also the direction of the shrinkage vectors varied according to the cavity configuration. More research is needed to find out how to best apply composite to avoid the formation of gaps at the cavity floor or the margins.

Conclusions

Within the limitations of this study, the following can be concluded:

1. The shrinkage amount and direction varied according to the cavity configuration, with greatest shrinkage vectors in the “adhesive” cavity, followed by the “diverging” and it was least in the “cylindrical”.
2. Lutz was right in his observation that shrinkage occurred upward in the “adhesive” cavity which was confirmed by the quantitative directional shrinkage analysis.
3. The “diverging” cavity showed large downward movement at the free surface, and in the “cylindrical” cavity, upward and downward shrinkage were seen in the lower and upper restoration parts.
4. Detachment occurred at the areas of greatest shrinkage in each cavity configuration; in the “adhesive” at the cavity floor, in the “diverging” at the cavity margin, in the “parallel” at both floor and one margin.
5. The enamel bevel in the “adhesive” cavity had a strong influence on the shrinkage direction: bevel at great angulation to the long axis of the tooth; enamel prisms should be cut perpendicular to yield higher bond strength values.
6. More investigations on the effect of the light source on the shrinkage vectors are needed.
7. The claim that composites shrink toward the light source is disproved.

4 Composite Shrinkage Vectors in Ceramic Cavities with Different Boundary Conditions

4.1 Abstract

Objectives: Ceramic serves as a homogenous substrate for a cavity model and provides for optimal bonding conditions which stands in contrast to the heterogeneity of enamel and dentin. The objective of this study was to visualize the polymerization shrinkage of a composite in form of displacement vector fields and to detect the shrinkage direction and patterns, in relation to the light source in a silanized ceramic-cavity with different boundary conditions.

Methods: 18 ceramic specimens (IPS Empress CAD, Ivoclar Vivadent) were prepared with a cylindrical cavity (diameter 6 mm, depth 3 mm) and divided into two groups according to the surface treatment into “ceramic+HF+silane” group and “ceramic+HF+silane+DBA” group. In “ceramic+HF+silane”, the cavity was etched (hydrofluoric-acid 5%), silanized (ESPE Sil, 3M ESPE) and filled with a composite (Tetric EvoFlow, Ivoclar Vivadent) to which 2 wt% traceable glass beads were added. In “ceramic+HF+silane+DBA”, in addition a layer of dentin bonding agent (OptiBond FL, Kerr) was applied before the composite application. Two micro-CT scans were performed of each specimen (uncured, cured), subjected to image segmentation and registration based on a block-matching algorithm. The displacement vector field exhibited the distribution of shrinkage vectors three-dimensionally and shrinkage vectors were analyzed in the axial dimension and for any shrinkage patterns.

Results: In “ceramic+HF+silane”, two shrinkage patterns were identified: in “Pattern-1” shrinkage vectors in the upper one third of the restoration were directed downward, then deviated to one side; “Pattern-2” displayed vectors in the upper one third moving downward, then represented a horizontal swirling in the whole lower two thirds of the restoration. Shrinkage vectors were significantly greater in the “ceramic+HF+silane+DBA” ($41.6 \pm 18.9 \mu\text{m}$) than in the “ceramic+HF+silane” ($30.5 \pm 14.4 \mu\text{m}$). Both groups showed downward movement away from the light, which was greater in the bonding ($19.2 \pm 16.0 \mu\text{m}$) than the silane group ($8.4 \pm 15.6 \mu\text{m}$), with statistically significant difference by the Independent Samples T-test.

Conclusion: Displacement vector fields in both groups stated the obvious movement away from the light source, possibly due to the strong bond with silanized ceramic. Identification of two patterns in “ceramic+HF+silane” presented that shrinkage could happen differently even under similar conditions, while the layer of bonding agent produced a more uniform shrinkage pattern. Boundary conditions seem to play an important role in polymerization shrinkage.

4.2 Introduction

The crown of human teeth is composed of an enamel shell covering the underlying dentin. Any defect such as caries, will track its way through enamel into dentin and consequently, a restoration will have an interface with both tissues (Roberson, 2006a). Bonding to enamel is stronger and less technique sensitive than bonding to dentin which is due to the compositional differences between the two substrates (Roberson, 2006b) and it can be assumed that bonding to substrates with different qualities and bond strengths affects the direction of polymerization shrinkage.

Versluis et al., 1998, have investigated this topic in a finite element analysis (FEA). They analyzed the effect of boundary conditions on the polymerization shrinkage direction by changing the bonding conditions in their model, a cylindrical cavity with two substrates representing enamel and dentin. Three conditions were simulated: without any bond, with bond to enamel only and perfect bonding to both enamel and dentin, each condition resulting in a different shrinkage pattern. In the unbounded condition composite shrank to the center; with enamel bond only it shrank downward at the upper restoration part and upward at the lower part, and when bonded to enamel and dentin, it shrank all the way downward, away from the light source. They concluded that shrinkage is not necessarily directed toward the light source, but it is affected by bonding of the restoration and the presence of free surfaces (Versluis et al., 1998).

Chiang et al., 2009, 2010, were the first to visualize the polymerization shrinkage vectors three-dimensionally and to show how the shrinkage direction was affected by the presence of enamel and dentin as different bonding substrates. They used two micro-CT scans of uncured and cured composite in human teeth, subjected them to image registration based on a block-matching algorithm for the calculation of 3D shrinkage vectors (Rösch et al., 2009). The influence of enamel on the shrinkage direction was seen: in cavities, with margins of equal enamel thickness, composite detached from the cavity floor and shrank toward the light source. On the other hand, in cavities with margins of unequal enamel thickness

composite shrank toward the thicker enamel margin, while it detached from the opposite side of the cavity (Chiang et al., 2009; Chiang et al., 2010).

Previous studies have substituted human teeth by an artificial material to avoid the inhomogeneity of substrate and the variations of size and properties among teeth. A glass model cavity was used to assess the shrinkage stress in dental composites (Li et al., 2011), while in another study, a block made of resin composite with a standardized cavity served as the bonding substrate for the evaluation of resin composite polymerization by micro-CT imaging (Cho et al., 2011). The inner surface of glass ceramic restorations such as inlay, onlays, veneers and crowns are indicated for etching by 5-10% hydrofluoric acid and subsequent silanization for obtaining an optimal bond between the restoration and the tooth structure (IPS Empress CAD, Technical Product Profile, 2007). Silane, though not an adhesive, improves adhesion by promoting a chemical bond between the inorganic ceramic material and the organic resin matrix of the composite.

The specific physical properties of enamel and dentin have an impact on the bond quality and consequently might influence the shrinkage direction. In the Chapter 3 human teeth were used for the shrinkage investigations. It was observed that the direction of cutting the enamel prisms influenced the bond quality and subsequent gap formation. Also the thickness of enamel at the cavity margins varied and might affect the resultant shrinkage direction. Ceramic can provide for an optimal bond with a dental resin composite. Therefore, selecting an alternative substrate serving as a model cavity system could be a good option when trying to understand the effect of boundary conditions on the shrinkage direction.

4.3 Aim of the study

The aim of this study was to investigate the polymerization shrinkage of a model light initiated resin composite with the least possible influence by the substrate. Therefore, bonding to ceramic instead of enamel and dentin was investigated, to detect the shrinkage direction in relation to the light source in etched and silanized ceramic cavities with and without a bonding agent and to visualize the shrinkage in form of displacement vector fields. The bonding agent served as a stress breaker and to evaluate if the mean vector length values were influenced by the layer of bonding agent.

4.4 Materials and Methods

The experimental resin composite, Table 4, p.39, and the materials listed in Table 6, p.64, were used in this study.

4.4.1 Specimen preparation

A total of 18 ceramic specimens were cut from ceramic blocks (IPS Empress CAD, Ivoclar Vivadent) and cylindrical cavities with parallel walls (diameter 6 mm, depth 3 mm, n=9) were prepared (Chiang et al., 2009; Chiang et al., 2010; Versluis et al., 1998). The outer surface of the ceramic was trimmed to fit into the micro-CT sample holder and flowable composite was applied and light-cured all around to obtain a reference mark that simulates enamel. This procedure was important for the process of rigid registration (overlay of both scans) at a later step; identification of different substrates depends on the corresponding greyvalue. The specimen was fixed into the sample holder with composite to avoid its movement during scanning.

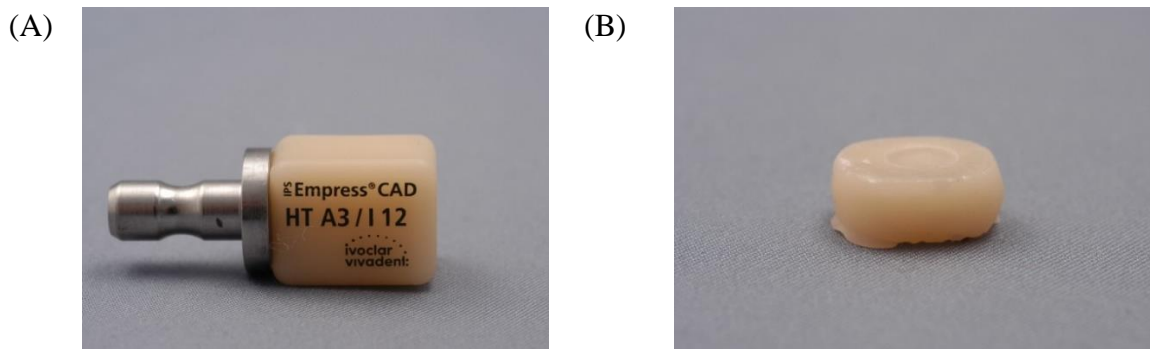


Figure 33 The ceramic block (A) was cut into three slices into which a cylindrical cavity was prepared. The outer margin was trimmed to fit into the micro-CT sample holder and flowable composite was added as a reference landmark for the rigid registration (B).

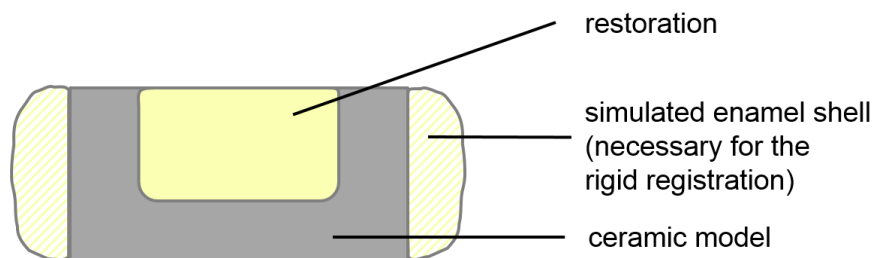


Figure 34 Schematic drawing of the ceramic model.

Specimens were divided into two groups: in the “ceramic+HF+silane” group, the cavity was etched by 5% hydrofluoric acid (VITA CERAMICS ETCH, Vita Zahnfabrik) for 1 min, thoroughly rinsed with water for 1 min, air dried, and silane coupling agent (ESPE Sil, 3M ESPE) was applied and air dried for 5 min. In the “ceramic+HF+silane+DBA” group,

additionally, a layer of dentin bonding agent (OptiBond FL, Kerr) was applied, air thinned for 5 s and light-cured for 20 s using Elipar FreeLight2, 3M ESPE prior to the application of the experimental composite (power output 1200mW/cm² according to the manufacturer, checked for constant light intensity once/week with a dental radiometer). OptiBond FL forms a thick film of adhesive and has good mechanical properties, thus, a good bond is expected.

From this point onward the methodology was following the same protocol as described in Chapter 3. It included the preparation of the experimental composite, the micro-CT measurements, the data processing, polymerization shrinkage evaluation and the SEM analysis.

4.4.2 Statistical analysis

Mean vector lengths were computed and subjected to the Independent Samples T-test (using IBM SPSS Statistics 20).

Table 6 Composition of the ceramic block, hydrofluoric acid, silane coupling agent and the total-etch adhesive

Brand name	Composition	Batch No.	Manufacturer
IPS Empress CAD, A3 Ceramic block for CEREC and Inlab	SiO ₂ Additional contents: Al ₂ O ₃ , K ₂ O, Na ₂ O, CaO, and other oxides, pigments	Ref# 602522 N57913 N52287	Ivoclar Vivadent, Schaan, Liechtenstein
VITA CERAMICS ETCH (In-lab ceramic etchant)	Hydrofluoric acid 5%	14060	VITA Zahnfabrik, Bad Saeckingen, Germany
ESPE™ Sil (Silane Coupling Agent)	3-methacryloxy-propyl-trimethoxy-silane (3-MPTS)	424203	3M ESPE AG, Seefeld, Germany
OptiBond FL (Prime/Adhesive) (Total-etch Adhesive)	Adhesive: HydroxyEthylMethAcrylate (HEMA) 15-20% Disodium Hexafluorosilicate 1-2% Methacrylate Ester Monomers and inert fillers Primer: HydroxyEthylMethAcrylate (HEMA) 25-30% Ethyl Alcohol 20-25%	4462783 (Prime) 4462763 (Adhesive)	Kerr, Italy

4.5 Results

4.5.1 Qualitative presentation of polymerization shrinkage: Visualization of shrinkage vectors in displacement vector fields and SEM

The qualitative presentation of the polymerization shrinkage was in form of displacement vector fields which showed the three-dimensional distribution of the shrinkage vectors. SEM images were added for more details of the effect of polymerization shrinkage on the bond integrity.

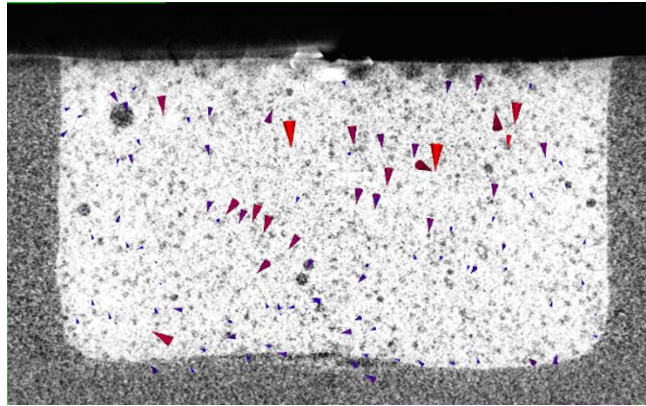
4.5.1.1 The displacement vector field in the “ceramic+HF+silane” group

Generally, the shrinkage vectors pointed downwards, while two shrinkage patterns were identified caused by detachment from cavity walls: in “Pattern-1” the shrinkage vectors in the upper one-third of the restoration were directed downwards, then deviated to one side of the restoration. “Pattern-2” displayed shrinkage vectors in the upper one-third moving downwards, as in “Pattern-1”, then a horizontal swirling movement in the whole lower two-third of the restoration became obvious (Figure 35). The SEM images showed an intact bond at all interfaces (Figure 37).

4.5.1.2 The displacement vector field in the “ceramic+HF+silane+DBA” group

Large shrinkage vectors in the upper part of the restoration were directed downwards, then deviated to one side of the restoration in the lower part. The vectors there were smaller than in Pattern-1 of group “ceramic+HF+silane” (Figure 38). This shrinkage pattern was similar to “Pattern-1” in the “ceramic+HF+silane” group. SEM images showed intact bond with all interfaces (Figure 39).

(A)



(B)

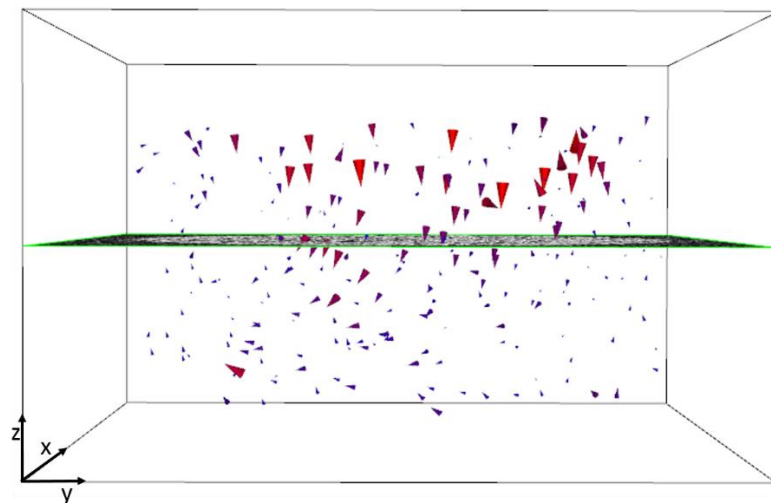


Figure 35 The displacement vector field in the “ceramic+HF+silane” group with “Shrinkage Pattern-1”: downward shrinkage at the upper part of the restoration and deviation of the shrinkage vectors toward one side at the lower part, with the y-plane (A) and the z-plane (B) of the micro-CT scan in the background. Glyphs were scaled by a factor of 5 to enhance visibility.

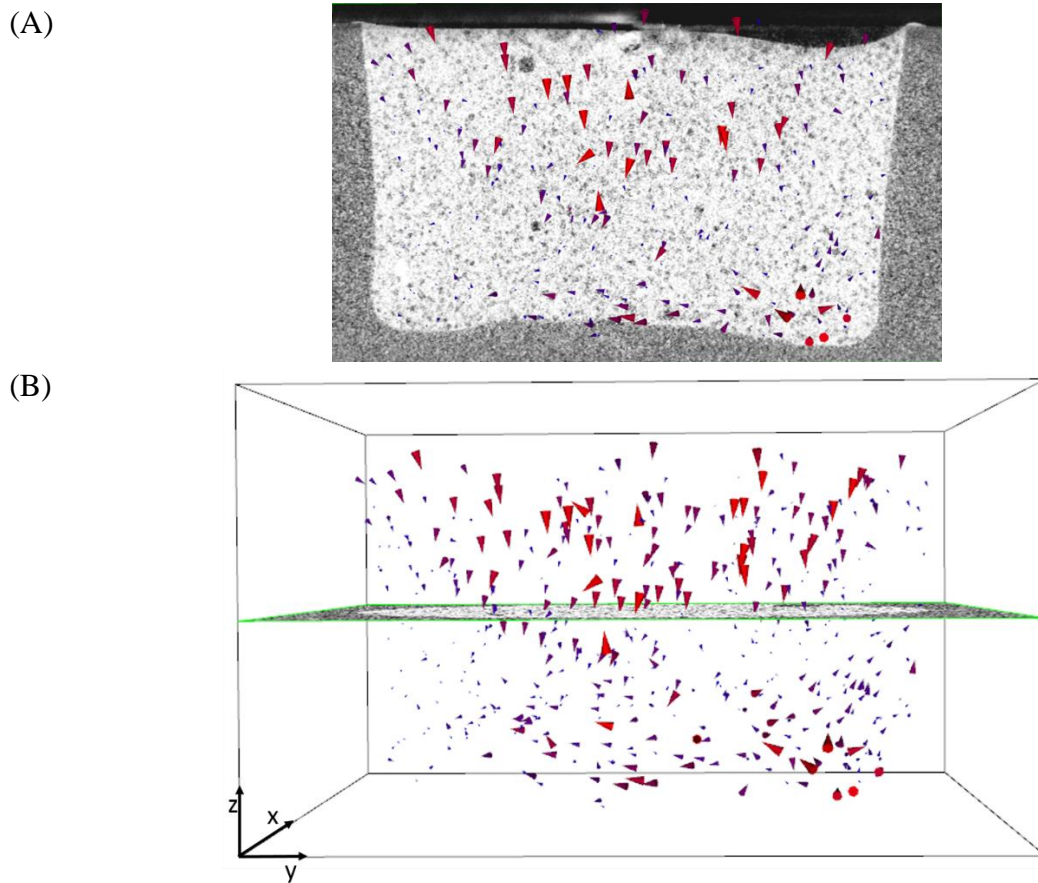


Figure 36 The displacement vector field in the “ceramic+HF+silane” group exhibited “Shrinkage Pattern-2”: downward shrinkage in the upper part of the restoration, while the lower part exhibited horizontal swirling, with the y-plane (A) and the z-plane (B) of the micro-CT scan in the background. Glyphs were scaled by a factor of 5 to enhance visibility.

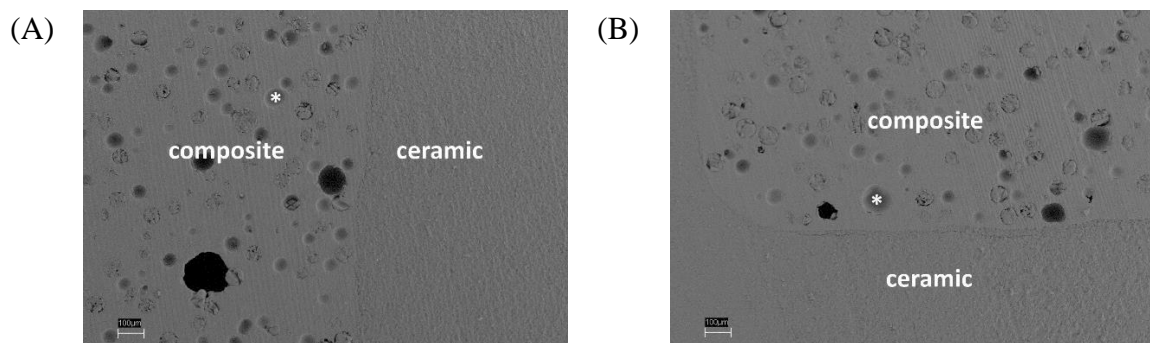


Figure 37 SEM images (x200) of the “ceramic+HF+silane” group of the restoration margin (A) and the floor (B) showing close adaptation. One traceable glass filler is marked by the star *.

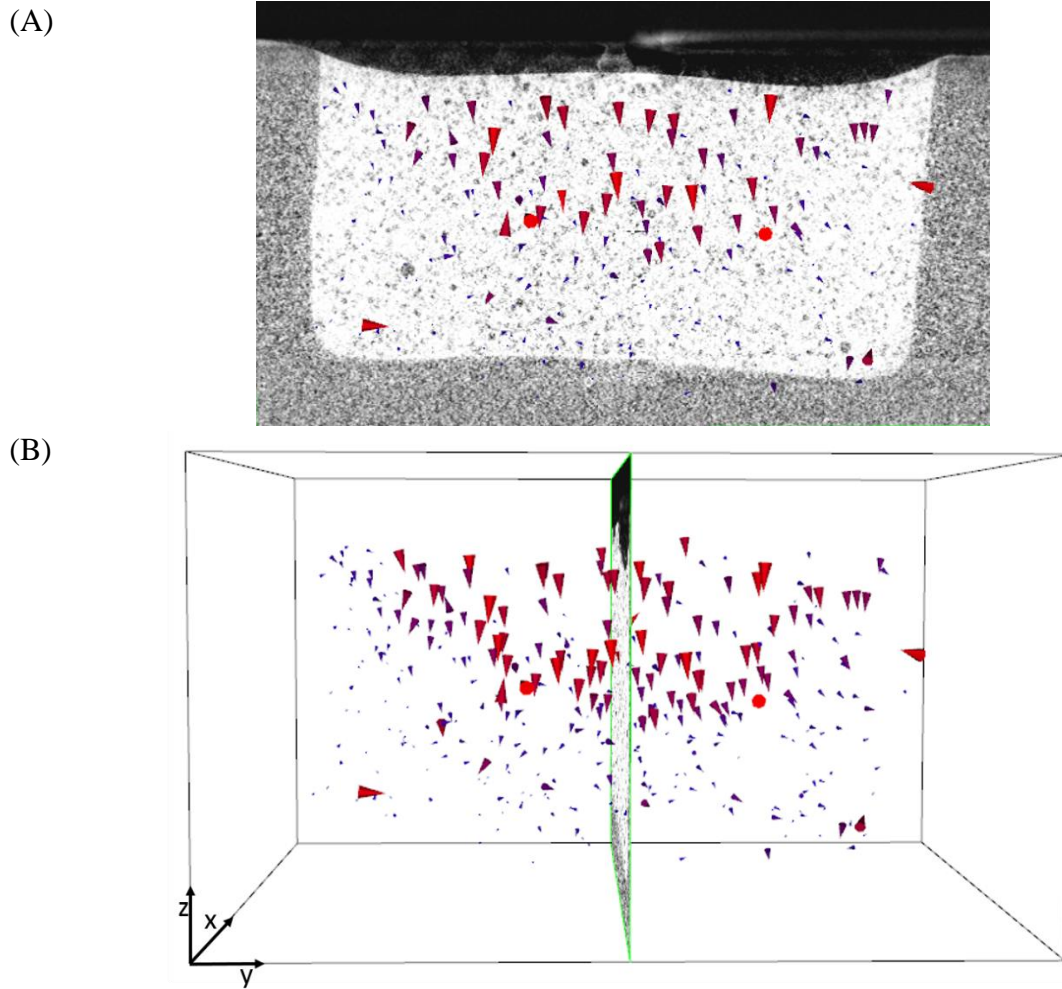


Figure 38 The displacement vector field in the “ceramic+HF+silane+DBA” group with downward shrinkage at the upper part of the restoration and deviation of the shrinkage vectors toward one side at the lower part, same as “Shrinkage Pattern-1” in the “ceramic+HF+silane” group, with the y-plane (A) and the z-plane (B) of the micro-CT scan in the background. Glyphs were scaled by a factor of 5 to enhance visibility.

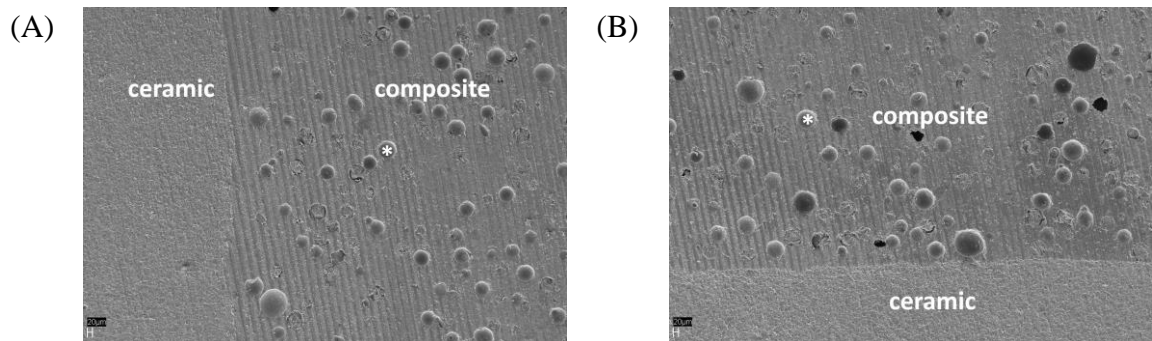


Figure 39 SEM images (x200) of the “ceramic+HF+silane+DBA” group of the restoration margin (A) and floor (B) showing close adaptation. One traceable glass filler is marked by the star *.

4.5.2 Quantitative presentation of polymerization shrinkage: values of shrinkage vectors and statistical analysis

4.5.2.1 Quantitative non-directional analysis: Probability density function of the vector length values

Mean vector lengths were computed irrespective of their direction, where the “ceramic+HF+silane+DBA” group showed higher vector lengths values ($41.6 \pm 18.9 \mu\text{m}$) than the “ceramic+HF+silane” group ($30.5 \pm 14.4 \mu\text{m}$), (Table 7). Independent samples Test was used for statistical analysis and the two groups differed significantly ($t=-14.139$; $df=1558.861$; $p<0.001$).

In the “ceramic+HF+silane” group, the greatest frequency of vectors was seen in the range of smaller values, while for the “ceramic+HF+silane+DBA” group, larger values were more frequent (Figure 40).

Table 7 Mean vector length values and mean filler movement in the z-direction of the “ceramic+HF+silane” and “ceramic+HF+silane+DBA” groups

Group	Vector length (μm)	Filler movement in the z-direction (μm)
“ceramic+HF+silane”	30.5 ± 14.4	8.4 ± 15.6
“ceramic+HF+silane+DBA”	41.6 ± 18.9	19.2 ± 16.0

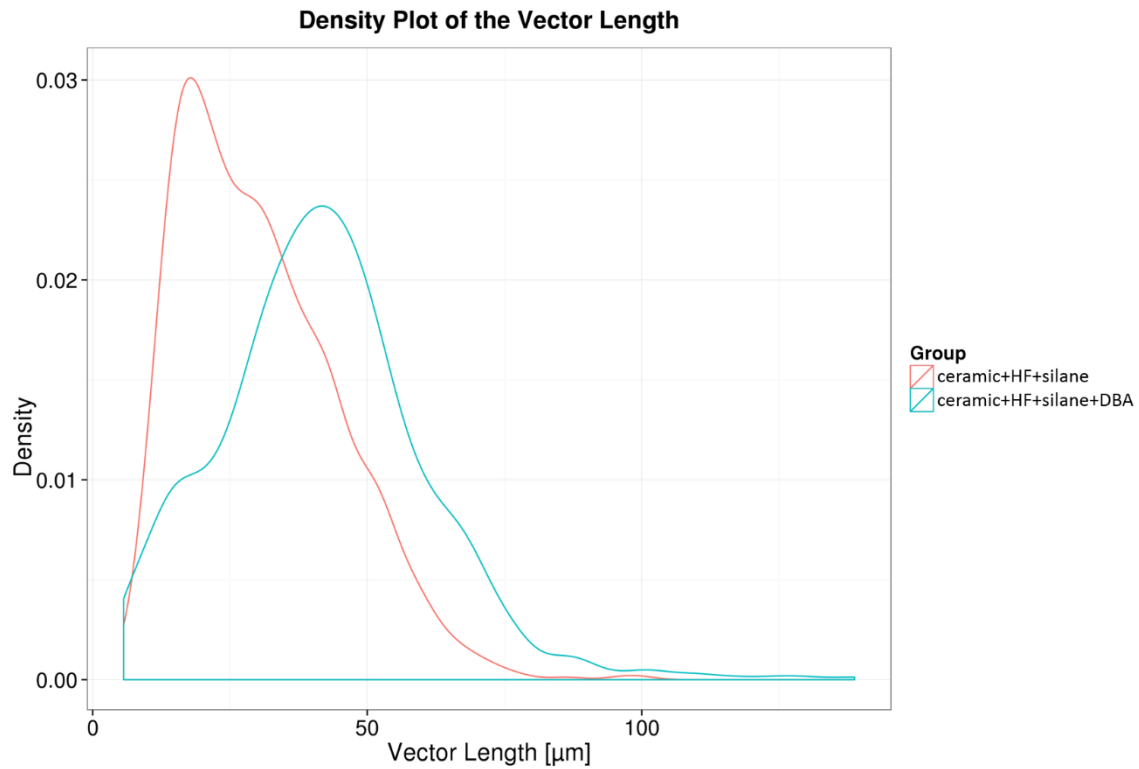


Figure 40 The probability density function of the vector lengths in the groups “ceramic+HF+silane” and “ceramic+HF+silane+DBA” shows the frequency of vector length values in the groups. In the “ceramic+HF+silane” group the maximum was located at about 20 μm which can be related to the smaller vectors located majorly in the lower part of the restoration and near the cavity walls. Yet, a considerable amount of vectors was in the range below 50 μm which can be associated with the larger vectors directing downwards in the upper part of the cavity. In the “ceramic+HF+silane+DBA” group the distribution of vector lengths values was over a larger range than in the first group. The first maximum at 20 μm could be related to small vectors of the lower third of the restoration near the cavity floor. The second maximum had most vectors at about 45 μm that were attributed to the large downward movement at the free surface.

4.5.2.2 Quantitative directional analysis: Probability density function of the vector z-component (Filler Movement in z-direction):

For analysis of the axial shrinkage, the z-component of the vectors was analyzed, as it denotes the filler movement in the z-direction. Both groups shrank downwards and away from the light source.

The axial movement in the “ceramic+HF+silane+DBA” group displayed larger values ($19.2 \pm 16.0 \mu\text{m}$) than the “ceramic+HF+silane” group ($8.4 \pm 15.6 \mu\text{m}$) (Table 7). The two groups showed a statistically significant difference ($t=-14.762$; $df=1867$; $p<0.001$) using Independent samples Test. The frequency of filler movement in z-direction of both groups is displayed in the density plot below. Positive values were more frequent in the “ceramic+HF+silane+DBA” group (Figure 41).

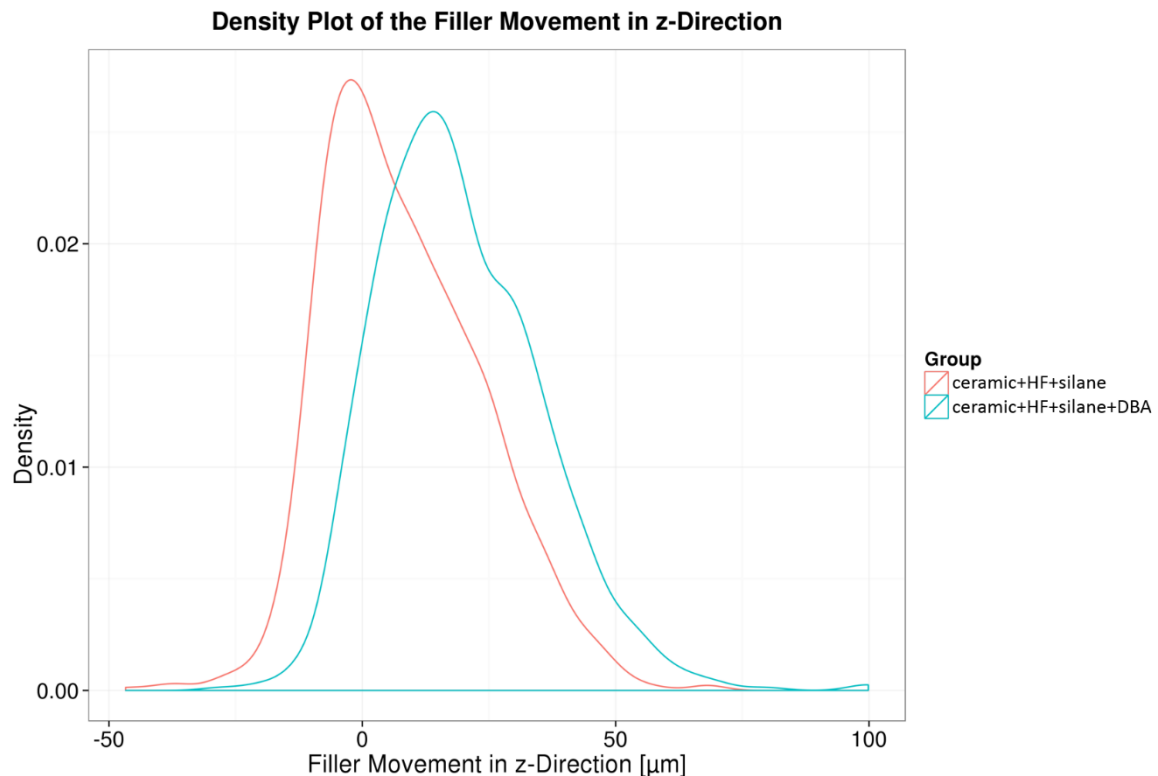


Figure 41 The probability density function of the filler movements in the z-direction in the groups “ceramic+HF+Silane” and “ceramic+HF+Silane+DBA” displays the frequency of the axial filler movement values in the groups. In the “ceramic+HF+Silane” group the maximum was located at about $-10 \mu\text{m}$ which means that the greatest frequency of axial filler movement was very small and denotes upward movement. The overall quantity of axial filler movement was in the positive range which stands for downward movement. The “ceramic+HF+silane+DBA” group displays a maximum at about $13 \mu\text{m}$ that represents a greater axial downward movement than in the “ceramic+HF+silane” group. Both curves look similar to the previous group, but the “ceramic+HF+silane+DBA” group was shifted to the right into the positive range that stands for greater downward movement.

4.6 Discussion

The ceramic material was chosen as a model cavity system for several reasons. It has a similar compliance to that of the natural tooth (Li et al., 2011) and it offers a homogenous substrate, thereby overcoming the difference in bonding between enamel and dentin. Moreover, silanes are very effective in promoting adhesion for silica-based materials, thus, provide optimal adhesion (Lung and Matinlinna, 2012). Although the cavity in a ceramic model does not represent the clinical situation, it was proposed to overcome the limitations encountered when human teeth are used as they are formed of enamel and dentin at the crown portion.

The obvious downward shrinkage movement away from the light source, was possibly due to the strong bond with silanized ceramic, and the free surface allowed the composite to bend downward. Similar observations were made by other studies as well. Cho et al., 2002, measured earlier the free surface depression by a profilometer and the interfacial gap by a scanning electron microscope in order to relate the shrinkage direction to the interfacial bond quality. They found that smaller interfacial gaps related to a greater free surface depression concluding that the establishment of a good bond could direct the shrinkage close to the bonded surface (Cho et al., 2002). Suh and Wang, 2001, investigated the direction of shrinkage through changes of the surface contours for different bonding configurations in a glass model. In the case where composite in a class I cavity was bonded, a great downward shrinkage was obvious at the free surface, similar in appearance to our results (Suh and Wang, 2001). Although their results were related to the outer surface only, they confirmed the findings of the current study. The advantage of the present method was the actual tracing of the internal movement of the embedded glass fillers, thereby, presenting the actual shrinkage vectors.

Hydrofluoric acid etching and silanisation provided optimal bonding conditions that cannot be obtained in natural teeth due to the compositional differences and surface properties of the bonding substrates. Nevertheless, even hydrofluoric acid etching and silane could not resist the contraction forces of the low modulus flowable, as the curing contraction caused disruption of the adhesion to the cavity walls and floor. This was seen by small vectors in the displacement vector fields near the cavity floor and walls. Furthermore, it was also shown in the density plot of the filler movement in the z-direction that was denoted by the negative values which were attributed to the upward movement. Unfortunately, it was not possible to identify the disruption in the micro-CT scans due to limitations of the resolution ($8^3 \mu\text{m}^3$),

and in the SEM images no detachments were seen in the cut-planes. Nonetheless, they could be situated at other locations within the cavity.

If detachment happened in a perfect cavity regarding the design and the adhesion, it is likely to occur in bulk-filled cavities in teeth as well. Nevertheless, bulk-fill materials differ in their composition and properties from a traditional composite. There are various bulk-fill composite systems and to ensure sufficient cure at full depth (4 mm), either an increased amount of initiator or a more reactive initiator is added. High polymerization shrinkage stresses that develop could be decreased in some bulk-fill materials by adding a polymerization modulator. Some manufacturers of the bulk-fill composites claim that the modified methacrylate-resin has a slow polymerization rate through the use of a polymerization modulator, which can possibly render a more favorable polymerization shrinkage (Cramer et al., 2011; Moorthy et al., 2012). At the time the current study has been started, there were no bulk-fill materials available. Still, these experiments can be repeated with bulk-fill composites in order to visualize their shrinkage patterns. On the other hand, the results can be compared to previous studies from Chiang et al., 2009, and Versluis et al., 1998 because the same experimental composite and cavity dimensions were used (Chiang et al., 2009; Chiang et al., 2010; Versluis et al., 1998)

The occurrence of two shrinkage patterns in the “Ceramic+HF+silane” group could be attributed to different methods or types of detachments from the cavity walls: in “Pattern-1” the shrinkage in lateral direction was greater at one side which is possibly the site of least resistance; here, the composite must have predominantly detached in the form of a large patch. On the other hand, in “Pattern-2” the horizontal swirling was probably caused by mainly detaching at many separate small sites or spots at the cavity bottom and lower part of walls. The SEM images did not display any bond discontinuity in neither shrinkage patterns, where the cut-planes were arbitrarily selected. The gap or detachment might have been at any other location within the restoration. The variation of shrinkage patterns could be in part related to the inhomogeneity of the curing light, as stated by the beam profile analysis (Price et al., 2011), although for all experiments, the same light-curing unit has been used. Another reason could be the distraction of the light by the embedded glass beads. Likewise, it is difficult to explain why two shrinkage patterns have formed within the “Ceramic+HF+silane” group. On the other hand, it points out the advantage of using micro-CT scans and the current shrinkage vector evaluation method. Such fine differences in results could not be explored with FEA because it is based on idealized conditions and does not include the possible variations of outcome.

Previous studies used micro-CT scans of uncured and cured composite for volumetric shrinkage and leakage analysis. They showed that debonding or leakage occurred in the form of a large area or patch that showed at its peripheries many separate small spots that passed into the non-detached areas (Sun et al., 2009a; Sun et al., 2009b; Zeiger et al., 2009). Although they calculated the volumetric shrinkage by subtracting the pre-cure from the after-cure volume and detected the sites of potential leakage, they neither calculated shrinkage vectors nor visualized internal movements or displacement vector fields.

The layer of the bonding agent produced a more uniform and reproducible shrinkage pattern in the “ceramic+HF+silane+DBA” group because all displacement vector fields exhibited only “Pattern-1” and no swirl could be detected. The presence of the bonding agent rendered greater vector length values and allowed greater axial movement in comparison to the “ceramic+HF+silane” group which might lead to a decrease in the shrinkage stresses. A previous study concluded that an unfilled adhesive applied in thick layers (Kemp-Scholte and Davidson, 1990) or an intermediate layer of flowable under composite could reduce stress significantly (Cara et al., 2007). Results from a FEA study on the adhesive layer properties showed that its thickness and rigidity are important factors regarding the mechanical behavior on the restored tooth playing an important role in attenuation of the polymerization and occlusal loading stresses (Ausiello et al., 2002). Another study pointed out that with increasing adhesive layer thickness contraction stresses and microleakage decreased (Choi et al., 2000). However, the adhesive layer could neither be identified in the micro-CT scans nor in the SEM images, assuming that it was very thin and its role of reducing stresses unknown.

The displacement vector fields in “Pattern-1” in the “ceramic+HF+silane” group and “ceramic+HF+silane+DBA” group are in agreement with the FEA results reported by Versluis et al., 1998, for the situation with perfect bond to both enamel and dentin. They provided more information on pre-gel and post-gel shrinkage separately which could not be seen in our evaluation due to 1.5 h scanning time per scan (Versluis et al., 1998). These findings were opposed by Chiang’s findings where in a heterogenous cavity the shrinkage was governed by the presence of enamel and dentin and their bonding properties (Chiang et al., 2009; Chiang et al., 2010). Thus, in a heterogenous cavity, as in human teeth, shrinkage is directed toward the part providing better bonding and being present in greater quantity, while in a homogenous cavity, the adhesive is more important, that is to say, it is the decisive factor. Boundary conditions, in this case, the bonding substrate and adhesion or the bond quality to it, seem to play an important role in the behavior of polymerization shrinkage.

Conclusions

Within the limitations of this study, the following can be concluded:

1. The ceramic model did provide optimal bonding conditions that could not be obtained with natural teeth due to their heterogeneity.
2. The shrinkage movement was directed downwards and away from the light source which was attributed to the strong bond with the etched and silanized ceramic cavity model.
3. Nevertheless, detachment happened either in form of a large area when composite deviated towards one side or in the form of many small patches when swirling of shrinkage vectors was detected at the lower restoration part.
4. SEM images could not show any detachments or defects at the restoration-ceramic-interface.
5. The direction of shrinkage vectors mainly relates to the bonding condition which depends to a large extent on the bonding substrate itself.

5 Composite Shrinkage Vector Patterns In Non-Adhesive Teflon Cavities

5.1 Abstract

Objectives: Shrinkage vectors of self-cured composites are supposed to be directed toward the center of the mass, while light-cured composites are believed to shrink toward the light source. The aim of this study is to visualize the polymerization shrinkage of a light-initiated flowable resin composite in form of displacement vector fields and to detect the shrinkage direction in a non-adhesive cavity in relation to the light-source. This bonding condition was chosen to investigate the effect of cavity geometry without adhesion on the shrinkage direction.

Methods: A cylindrical cavity (diameter 6 mm, depth 3 mm, n=9) was prepared into a Teflon block and filled with a model resin composite (Tetric EvoFlow, Ivoclar Vivadent) to which 2 wt% traceable glassbeads were added. Two micro-CT scans were performed of each specimen (uncured, cured), subjected to image segmentation for extraction of glass beads and followed by registration based on a block-matching algorithm. The displacement vector fields exhibited the distribution of shrinkage vectors three-dimensionally. Additionally, shrinkage vectors were analyzed in the vertical dimension.

Results: The mean vector lengths ($23.5 \pm 5.3 \mu\text{m}$) were computed irrespective of their direction. To analyze the shrinkage direction in relation to the light-source, the filler movement was investigated in the z-direction only, where negative values denoted an upward movement towards the light-source and positive ones meant downward shrinkage. The mean filler movement ($-0.5 \pm 10.9 \mu\text{m}$) moved minimally upward. The displacement vector field clearly showed shrinkage to the center, while the lateral movement was slightly deviated toward one side.

Conclusion: The composite shrank centrally, although it was a light-cured type, concluding that this pattern was related to the fact that it was unbonded. Shrinkage in lateral direction was greater at one side, which is possibly the site of least resistance to adaptation and first detachment due to shrinkage. Shrinkage pattern is related to bonding conditions and not type of activation.

5.2 Introduction

The general belief in dentistry is that self-cured resin-based composites shrink toward the center of the mass, while light-cured composites shrink toward the light source. Studies on the boundary conditions influencing the shrinkage direction of composite restorations have questioned this (Chiang et al., 2009; Cho et al., 2011; Suh and Wang, 2001; Versluis et al., 1998).

Chiang et al., 2009, 2010, found out that the thickness of enamel margins did influence the shrinkage direction of composite: it detached from thin enamel margins and moved toward the thicker ones (Chiang et al., 2009; Chiang et al., 2010; Rösch et al., 2009). In the previous chapter, the shrinkage vectors were analyzed in a ceramic cavity with optimal adhesion to eliminate any inhomogeneity of the bonding substrate, as it is the case in human teeth due to the presence of enamel and dentin. Asmussen and Jorgensen, referred to the shrinkage inside a cavity as the “effective shrinkage” while shrinkage per se is the “net shrinkage” or the “free shrinkage” (Hansen, 1982a; b). The “effective shrinkage” is related to the cavity boundary which implies that the composite adapts to the cavity walls even without the use of a bonding agent (Asmussen and Jorgensen, 1972). Cavity boundaries are related to the cavity outlines on one hand and the bonding substrates with associated bonding conditions on the other hand.

The unbonded condition of composite inside a prepared cavity can be presented in different ways: when human teeth are used, the composite is directly applied without prior surface treatment of the cavity nor the application of an adhesive (Chiang et al., 2010; Takahashi et al., 2010). If the cavity is prepared in an artificial model such as composite or glass, then either no bonding agent is applied or a layer Vaseline is used as a separating agent (Cho et al., 2011).

An excellent non-adhesive substrate is Teflon (polytetrafluoroethylene). Teflon is slippery, thus, rendering it the non-adhesive property, in addition, it has high temperature resistance, little reaction to most chemicals, and reduced stress cracking and corrosion. Therefore, Teflon has important applications in cookware, and in the chemical and steel industries, just to mention some (Toefco Engineered Coating Systems, 2013).

In dentistry, Teflon is not being used in dental applications, neither by the dentist, nor by the dental lab technician, although in research, it is commonly used as an adjunctive material in form of Teflon tape where non-bonded contact is desirable (Cheetham et al., 2014; Dionysopoulos et al., 2013; Lee et al., 2012; Tornavoi et al., 2013), as well as Teflon molds

for the fabrication of specimen discs of composites (Badole et al., 2013; de Melo Monteiro et al., 2011; Guven et al., 2013; Miletic et al., 2011; Mungara et al., 2013). Teflon is also used in machines as a Teflon spacer (Davidson et al., 1984) or as a pedestal in the AcuVol machine for volumetric polymerization shrinkage measurements (Labella et al., 1999). In the periodontal and bone research Teflon is now used as coating, scaffold material or membrane, in addition to its use in bacterial research (Cheng et al., 2013; Hayashi et al., 2013; Kapferer et al., 2013; Lopes et al., 2013; Schweikl et al., 2013; Suzuki et al., 2014).

Cavities prepared in Teflon blocks were used for testing bulk-fill composites for their temperature changes (Chang et al., 2013). Recent studies employed Teflon molds for gap analysis (Pereira et al., 2008; Takahashi et al., 2010), volumetric analysis (de Melo Monteiro et al., 2011) and image analysis of composites to detect discrepancies due to shrinkage (Miletic et al., 2011). The unbonded situation in a non-adhesive Teflon cavity is just one of many possibilities of a non-adhesive situation.

5.3 Aim of the study

The aim of this study was to visualize the polymerization shrinkage vectors of a light-cured composite three-dimensionally and axially when applied in a non-adhesive Teflon mold in order to observe the effect of a nonbonded boundary condition on the shrinkage pattern.

5.4 Materials and Methods

The composition of the experimental composite was listed in Table 4, p.39.

5.4.1 Specimen preparation

A Teflon cylinder (diameter 11 mm, height 15 mm) was cut from a block of Teflon, into which a cylindrical cavity (diameter 6 mm, depth 3 mm, n=9) was prepared (Chiang et al., 2009; Chiang et al., 2010; Versluis et al., 1998). Flowable composite was applied to the outer surface of the Teflon cylinder and light cured all around to obtain a reference mark that simulates enamel (Figure 42). This procedure was significant for the process of rigid registration (overlay of both micro-CT-scans) at a later step. Identification of different substrates depends on the corresponding greyvalue. The specimen was fixed into the sample holder with composite to avoid its movement during scanning. The experimental composite was applied into the prepared cavity of the Teflon model without the use of any adhesive. Attachment to cavity walls was through secondary van der Waals forces only.

When the pilot studies have been conducted, one composite sample (n=1) was scanned on a flat Teflon disc with the aim of visualizing shrinkage vectors upon polymerization when in contact with just one surface.

The steps for the preparation of the experimental composite, the micro-CT measurements, the data processing and the polymerization shrinkage evaluation were described in Chapter 3. After the first scan of uncured material, the composite was light-cured for 40 s perpendicular to the long axis of the tooth.



Figure 42 The Teflon cylinder serving as a cavity model. Flowable composite was applied to the outer contour simulating enamel in order to serve as a reference point for the rigid registration.

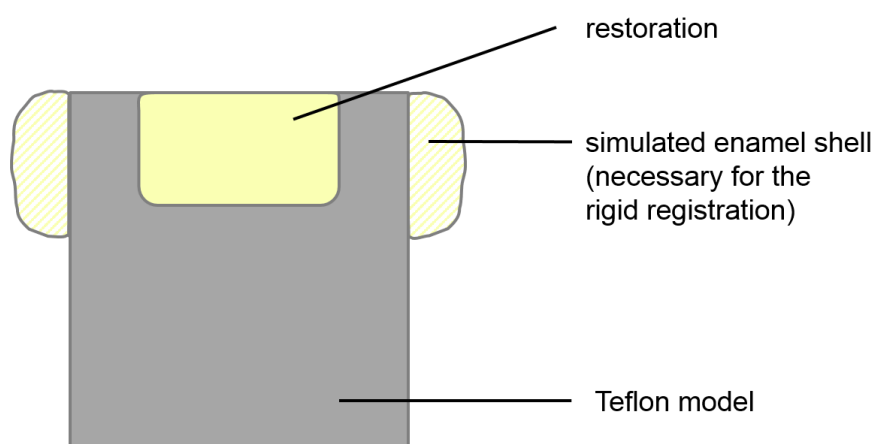


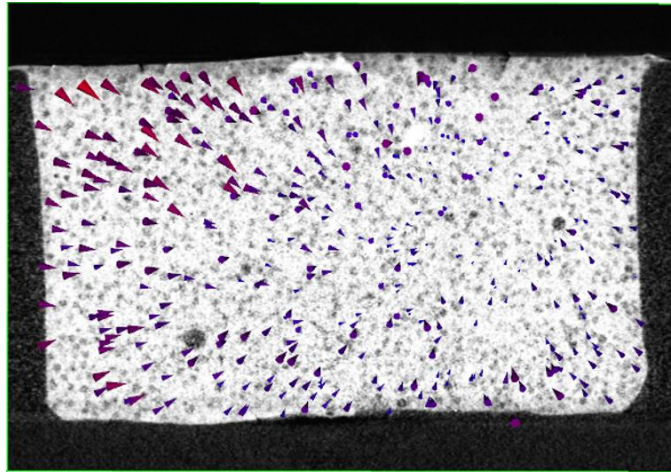
Figure 43 Schematic drawing of the Teflon model.

5.5 Results

5.5.1 Qualitative presentation of polymerization shrinkage: Visualization of shrinkage vectors in the displacement vector field

The qualitative presentation of the polymerization shrinkage was in form of displacement vector fields which clearly showed shrinkage to the center of the restoration three-dimensionally. All samples exhibited the same shrinkage pattern through detachment from all cavity walls and the cavity floor as well. Lateral movement was slightly deviated toward one side due to detachment from the site of least resistance (Figure 44).

(A)



(B)

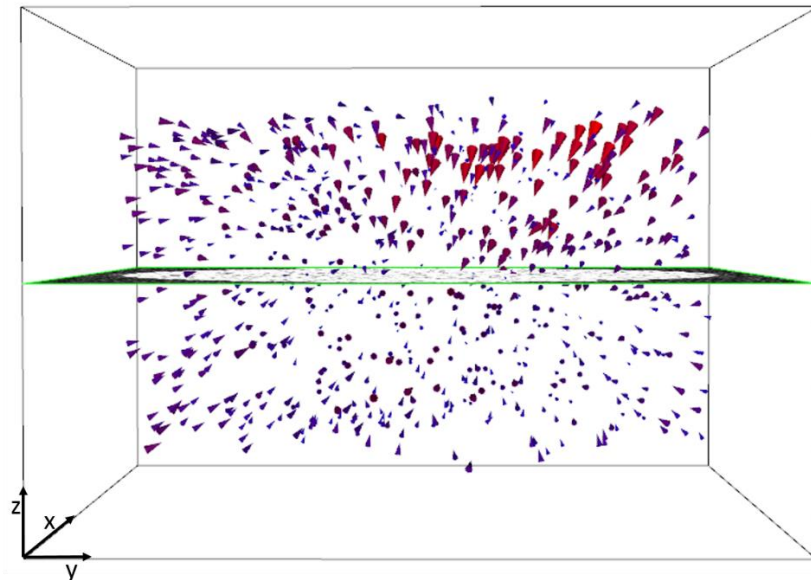


Figure 44 The displacement vector field in a non-adhesive “Teflon” cavity with the x-plane of the micro-CT scan in the background with two different views (A) and (B). Glyphs were scaled by a factor of 5 to enhance visibility. Polymerization shrinkage vectors pointed to the center, with lateral movement greater at one side denoting the site of first detachment from the cavity walls.

5.5.2 Quantitative presentation of polymerization shrinkage: values of shrinkage vectors and statistical analysis

5.5.2.1 Quantitative non-directional analysis: Probability density function of the vector length values

Vectors were computed 3-dimensionally and the mean vector length was $23.5 \pm 5.3 \mu\text{m}$ irrespective of the direction (Figure 45, Table 8).

Table 8 Mean vector length values and mean filler movement in the z-direction of the “Teflon” group

Group	Vector length (μm)	Filler movement in the z-direction (μm)
“Teflon”	23.5 ± 5.3	-0.5 ± 10.9

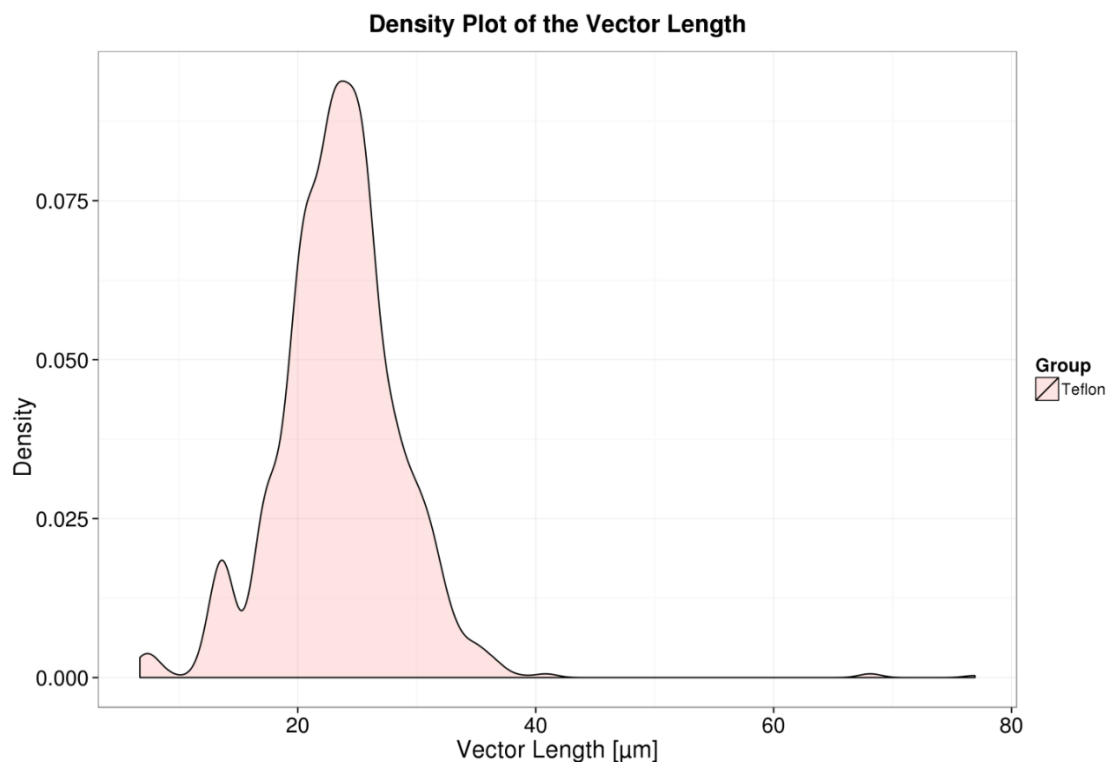


Figure 45 The probability density function of the vector lengths in the “Teflon” group shows a multimodal distribution of the values. The first peak relates to the very small vectors that can be found close to the center of the restoration, the second peak can be linked to the small vectors at the restoration side with less movement, while the third peak stands for the main quantity of shrinkage vectors in the “Teflon” group that are directed towards the center of the restoration.

5.5.2.2 Quantitative directional analysis: Probability density function of the vector z-component (Filler Movement in the z-direction):

The mean filler movement in the z-direction was $-0.5 \pm 10.9 \mu\text{m}$ which related to minimal upward movement toward the light source (Figure 46, Table 8).

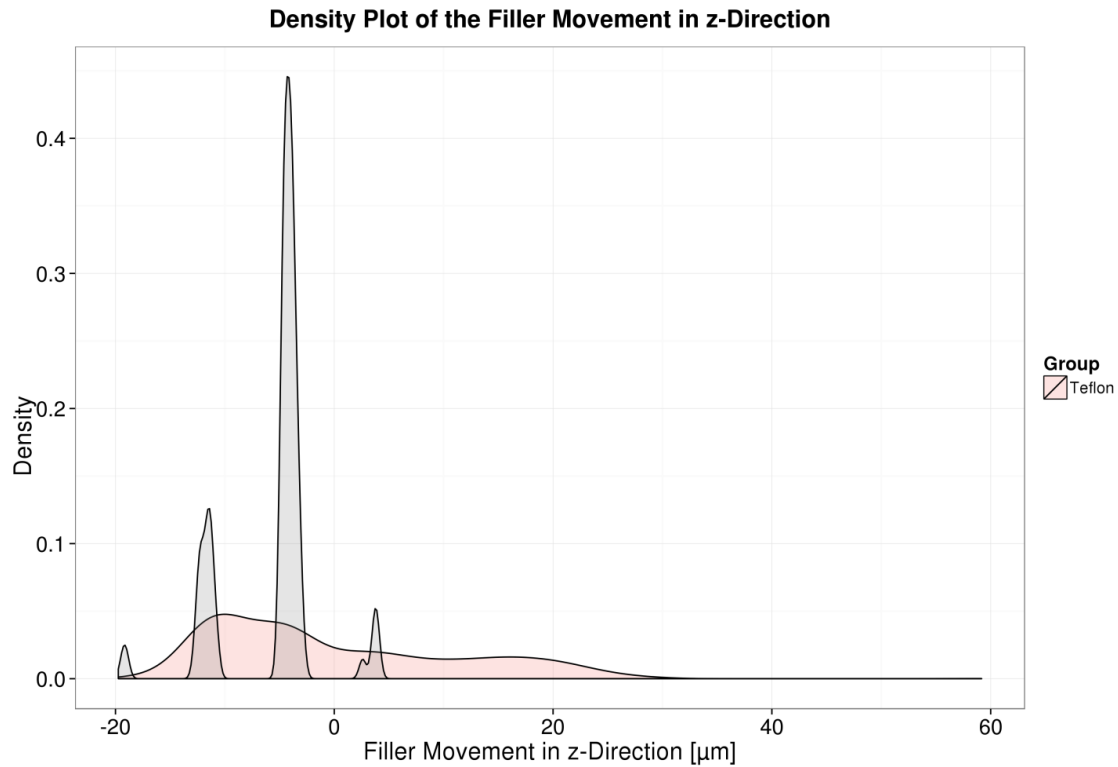


Figure 46 The probability density function of the filler movements in the z-direction in the “Teflon” group shows a multimodal distribution with 4 peaks (grey color). The areas below the separate peaks are joined into one area (pink color). The first and second peaks conform to upward shrinkage movement that was found at the cavity floor and the lower restoration part. The third peak constitutes the large quantity of small axial movement with slight downward shrinkage which can be related to the middle part of the restoration where the glass beads moved mainly in horizontal direction toward the restoration center. The last peak can be linked to the downward movement of glass beads at the free surface of the restoration.

5.6 Discussion

The Teflon block did provide a satisfactory model for the cavity without problems neither with the composite application, nor the micro-CT scanning procedure, nor in the evaluation phase. As an inherently non-adhesive substrate it is superior to the use of a separating agent as seen in other studies (Cho et al., 2011). The limitation of this cavity model with regards clinical application is the fact that Teflon as a bonding substrate is not comparable to the natural tooth structure, but it was the purpose of this study to obtain the ultimate nonbonded condition.

The three-dimensional shrinkage toward the center of the restoration stands in contrast to the longlasting belief that light-cured composites shrink toward the light. Shrinkage in the lateral direction was greater at one side, which was possibly the site of least resistance to adaptation and first detachment due to shrinkage; this finding is in agreement with (Asmussen and Jorgensen, 1972). Resin composites can adapt to cavity walls due to weak secondary forces even if no bonding agent is applied. Therefore, it was concluded that this specific three-dimensional shrinkage pattern was related to the unbonded boundary condition rather than the type of activation. Similar findings were previously reported when a nonbonded composite was investigated for its surface depression and marginal gaps (Suh and Wang, 2001).

An earlier study employing micro-CT scans for the volumetric analysis of polymerization shrinkage showed volume loss at one side of the cylindrical cavity, although data on the internal contraction behaviour were not available (Sun et al., 2009b). Interestingly, their observation can be related to the lateral movement by the shrinkage vectors. Our results also coincided with the FEA simulation regarding the unbonded condition (Versluis et al., 1998), which confirmed the presence of uniform boundary conditions in our case. On the other hand, our results varied from those reported by Chiang et al., 2010, in their unbonded condition in teeth where shrinkage vectors pointed toward one side of the cavity (Chiang et al., 2009; Chiang et al., 2010) and the unbonded condition in a composite model reported by Cho et al., that showed upward movement of the shrinkage vectors (Cho et al., 2011).

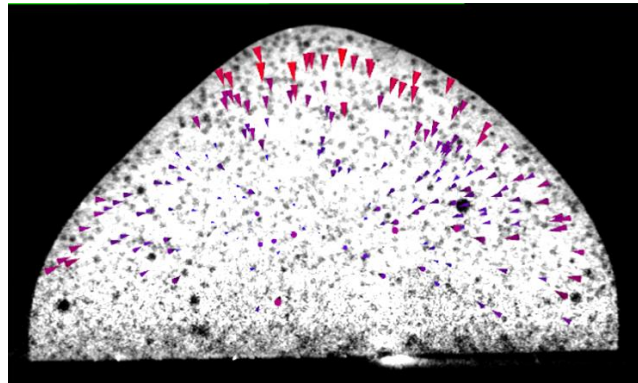
The mean axial movement was almost zero micrometer due to negation of upward and downward movements. The downward contraction can be explained by the composite's free surface and the upward shrinkage by the detachment from the non-adhesive interface with Teflon. This shrinkage pattern is in clear contrast to that seen in the ceramic cavities that were perfectly bonded and showed downward movement toward the floor due to the strong

bond by the silane coupling agent. The axial movement was similar to that observed in the “cylindrical cavity” in the Chapter 3, though in the Teflon group a greater horizontal movement was detected due to lack of bonding to the cavity walls. Cho’s unbonded condition in a composite mold differed from our results in the Teflon mold by displaying only upward movement and no movement toward the center. On the other hand, their bonded condition was in agreement with those of the “cylindrical cavity” in teeth where downward shrinkage from the free surface met the upward shrinkage from the lower part in a fictional zero-line, a line where no axial movement was spotted (Cho et al., 2011).

How would a light-cured composite shrink if simply laid down on a Teflon disc without any constraining cavity walls? If the surface was absolutely smooth, it would have shrunk from all free surfaces, even at the margins between the composite and the flat surface. In the “free shrinkage” it shrank toward the center from all contactfree sides, but in the lower part in contact with the Teflon disc (0.5 mm) almost no shrinkage was detectable with the sample being light-cured from above (Figure 47). Therefore, the Teflon surface is assumed to be incompletely smooth with some degree of roughness or physical adhesion unlike the dental adhesion. Certainly, such contraction movement is related to its boundary condition, because there is just a flat surface and no cavity walls to detach from. This leads to the need to investigate polymerization shrinkage, not only under different boundary conditions in terms of the bonding situation, but also in cavities with different C-factors and classes.

Teflon represents the most extreme unbonded condition that cannot be surpassed. The current results give an insight into the shrinkage behavior under such condition which leads to a basic understanding on how boundary conditions affect the shrinkage pattern. Human tooth structures and bonding agents offer many factors resulting in variations in bonding quality which in turn affect the shrinkage vectors’ direction and magnitude. The wide variety of dentin-bonding agents, both self-etch and total-etch systems, have great differences in their bond strength values. This topic needs further research that will be addressed in the next chapter.

(A)



(B)

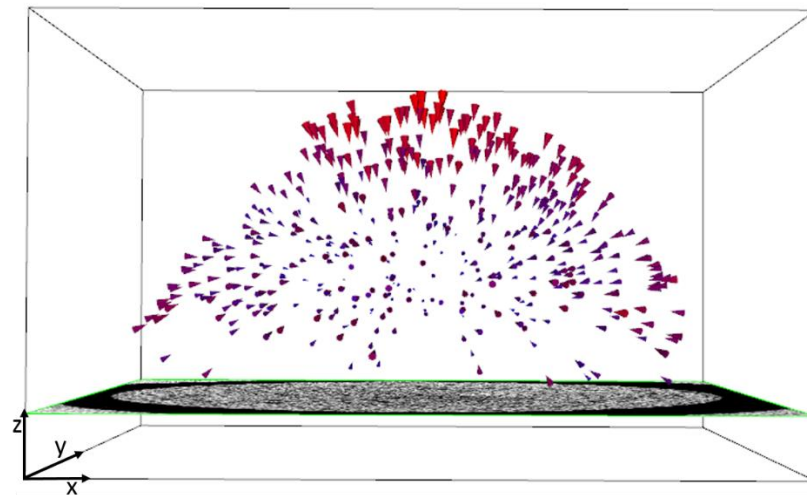


Figure 47 The experimental composite was placed on a Teflon disc and exhibited the “free shrinkage” and light was applied from above. Shrinkage vectors pointed toward the center of the composite and the y-plane (A) and z-plane (B) of the micro-CT scan were seen in the background. The composite in contact with the Teflon disc displayed almost no shrinkage vectors. Glyphs were scaled by a factor of 5 to enhance visibility.

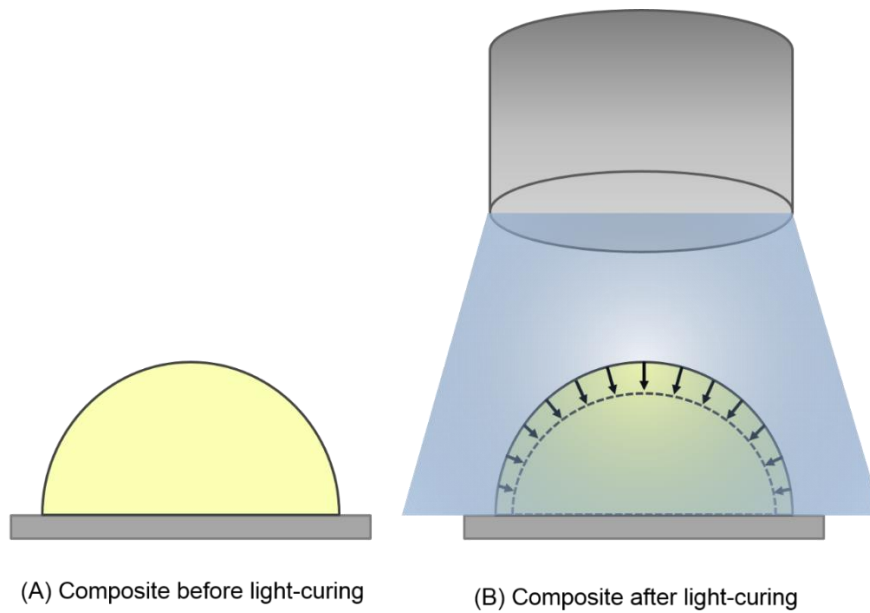


Figure 48 Schematic drawing of composite before (A) and after (B) light-curing on the Teflon disc. A completely smooth surface would even allow for shrinkage movement on the Teflon disc surface toward the center.

Conclusions

Within the limitations of this study the following can be concluded:

1. The Teflon cavity model served well as a non-adhesive cavity.
2. The composite shrank toward the center, although it was a light-cured type.
3. It can be concluded that this shrinkage pattern was related to the fact that composite was unbonded.
4. Shrinkage in lateral direction was greater at one side, which is possibly the site of least resistance to adaptation and first detachment due to shrinkage.
5. The shrinkage pattern is related to the bonding conditions and not the type of activation.
6. The results of this study can be transferred to weak bonding agents or dental substrates with unfavorable bonding properties.

6 Shrinkage Vectors in an Experimental Cavity with Enamel Floor

6.1 Abstract

Objectives: As bonding to enamel is stronger than bonding to dentin, the aim of this study was to determine the role of enamel or its influence on the direction of shrinkage vectors.

Methods: 36 human teeth were divided into 4 groups (n=9); first, according to the cavity form into “experimental” and “cylindrical” groups, then subdivided according to the bonding agent into “self-etch” and “total-etch” groups. In the “experimental” group teeth were embedded upside down in the acrylic resin, the roots removed and cylindrical class I cavities were prepared (6 mm diameter, 3 mm deep) into dentin with enamel at the cavity floor with the purpose to evaluate enamel’s influence on the shrinkage direction. In the “cylindrical” group teeth were embedded with their roots in the acrylic resin followed by the cylindrical cavity preparation. Then 2 wt% traceable glass beads were added to the composite (Tetric EvoFlow, Ivoclar Vivadent) and bonded with self-etch-adhesive (Adper Easy Bond, 3M ESPE) or a total-etch-adhesive (OptiBond FL, Kerr). Two micro-CT scans were performed of each specimen (uncured, cured), subjected to image segmentation for extraction of glass beads and followed by registration based on a block-matching algorithm. The resulting displacement vector field showed shrinkage vectors three-dimensionally and shrinkage vectors were analyzed regarding the vertical dimension as well.

Results: Mean vector lengths were computed irrespective of their direction, where the “experimental-self-etch” showed longer vectors ($31.8 \pm 14.3 \mu\text{m}$) than “cylindrical-total-etch” ($25.8 \pm 11.0 \mu\text{m}$), “experimental-total-etch” ($25.5 \pm 14.7 \mu\text{m}$) and “cylindrical-self-etch” ($23.3 \pm 11.1 \mu\text{m}$) using one-way ANOVA ($F=100.7$, $Df=3,5960$; $p<0.001$) and post-hoc pairwise comparison using Tamhane’s T2 test showed significant differences between all groups except for “experimental-total-etch” and “cylindrical-total-etch” groups ($p=0.991$). Analyzing the glass bead movement in the z-direction only displayed downward movement in “experimental-self-etch” ($7.6 \pm 15.9 \mu\text{m}$) and “experimental-total-etch” ($4.5 \pm 13.2 \mu\text{m}$) groups, while in “cylindrical-self-etch” ($-3.7 \pm 13.6 \mu\text{m}$) and “cylindrical-total-etch” ($-5.2 \pm 13.4 \mu\text{m}$) the tracer particles moved upward. One-way ANOVA revealed significant differences ($F=271.5$, $Df=3,5982$; $p<0.001$) and the post-hoc pairwise comparison using Tamhane’s T2 test showed significant differences between all groups ($p<0.05$).

Additionally, the vector lengths were analyzed using the univariate ANOVA: the dependent variable was the vector length, the independent variables were the cavity form and the bonding agent each with 2 levels: the “experimental” and the “cylindrical” cavities, and the self-etch and the total-etch adhesives. The same investigation was applied to the filler movements in the z-direction using IBM SPSS Statistics 20. This investigation aimed at analyzing the effect of each the cavity and the bonding agent.

Conclusion: The enamel influenced the direction of the shrinkage vectors. The shrinkage vectors were always directed towards the enamel substrate. The bonding agents caused variations in the magnitude of the shrinkage vectors.

6.2 Introduction

Bonding to enamel is stronger than bonding to dentin (Swift et al., 1995). Presently, there has been little information on how enamel influences the shrinkage direction of bonded resin composites. Data on the displacement vectors in human teeth are available from Chiang et al., (Chiang et al., 2009; Chiang et al., 2010) and from the first part of this study. Chiang et al., illustrated that unequal amounts of enamel lead to changes in the displacement vector fields: in cavities with margins of unequal enamel thickness showed shrinkage towards the thick enamel margin, while in cavities (Chiang et al., 2009; Chiang et al., 2010). Different cavity configurations implied that enamel margins which were cut at various angles also resulted in alterations of the displacement vector fields.

Referring to the fact that bonding to enamel is assumed to be stronger than bonding to dentin (Van Meerbeek et al., 2003), it is possible that the adhesion to enamel pulls the bonded composite away from dentin. Thus, in a traditional class I cavity prepared for an adhesive restoration, the shrinkage vectors should point upwards towards enamel (Chapter 3). This has been interpreted earlier as “shrinkage toward the light source” (Porte et al., 1984).

The preparation of an experimental cavity with enamel at the cavity floor may clarify the influence of enamel in terms of the bonding substrate on the shrinkage direction. According to the “traditional” hypothesis in dentistry, the composite should be shrinking toward the light source. However, we hypothesize adhesion is more important than the direction of the light. Therefore, we would assume that the composite shrinkage vectors should be directed towards the enamel areas inside the cavity.

6.3 Aim of the study

How strong is the influence of enamel on the shrinkage direction? In the “experimental” group a cylindrical cavity with enamel at the cavity floor was prepared and compared to the “cylindrical” group of Chapter 3. Moreover, the cylindrical cavities can be associated with previous studies (Chiang et al., 2009; Chiang et al., 2010; Versluis et al., 1998). The aim of this study was to analyze the effect of the bonding substrates enamel and dentin and two bonding conditions on the polymerization shrinkage in form of shrinkage vectors. The results could contribute to a more profound understanding of the effect of boundary conditions on the shrinkage direction.

6.4 Materials and Methods

The compositions of the experimental composite and the self-etch adhesive were listed in Table 4, p.39, and the total-etch adhesive was listed in Table 6, p.64.

6.4.1 Specimen preparation

A total of 36 teeth were divided into 4 groups (n=9). First, teeth were divided into two groups according to the bonding substrate into “experimental” and “cylindrical”, then subdivided according to the bonding agent (bonding condition) into “self-etch” and “total-etch” groups.

In the “experimental” group, the teeth were embedded in acrylic resin (Technovit 4000, Heraeus Kulzer, Germany) upside down, with the crown inside the acrylic resin. Then the roots were removed using a slow speed water-cooled diamond saw (Isomet, Buehler, Illinois, USA), (Figure 49, Figure 67), and a cylindrical class I cavity (3 mm deep and 6 mm in diameter) was prepared from the pulpal side with cavity margins in the dentin and the floor of the cavity in enamel. This experimental cavity model was intended to analyze the effect of having a cavity floor of enamel offering stronger bonding properties than dentin. In the “cylindrical” group, teeth were embedded in acrylic resin below the cement-enamel junction and the occlusal surface flattened for easy perpendicular light application (Figure 49, Figure 68).

The “cylindrical” cavity was prepared according to Chiang et al., with cylindrical walls (Chiang et al., 2009; Chiang et al., 2010; Versluis et al., 1998). The samples were fixed to the sample holder with composite to prevent any movement during the scanning procedure.

The details of the preparation of the experimental composite, the micro-CT measurements, the data processing, polymerization shrinkage evaluation and the SEM analysis were described in Chapter 3.

Shrinkage vectors were analyzed both qualitatively in the form of displacement vector fields and quantitatively in the form of shrinkage vector values. These were analyzed non-directional by evaluating the 3-dimensional vector length values irrespective of their direction and directional by analyzing the movement of the glass beads in the axial direction only.

6.4.2 Statistical analysis

The mean vector lengths were computed and subjected to one-way ANOVA with post-hoc pairwise comparisons using Tamhane's T2 to detect significant differences between the four groups (using IBM SPSS Statistics 20). In addition, the vector lengths were analyzed using the univariate ANOVA: the dependent variable was the vector length, the independent variables were the cavity form and the bonding agent each with 2 levels: the "experimental" and the "cylindrical" cavities, and the self-etch and the total-etch adhesives. The same investigation was applied to the filler movements in the z-direction using IBM SPSS Statistics 20. This investigation aimed at analyzing the effect of each the cavity and the bonding agent.

6.4.3 Scanning electron microscopy

One sample per group was critically point dried in alcohol, sectioned longitudinally and examined for marginal adaptation with a scanning electron microscope (ZEISS GEMINI® FESEM, SUPRA™ 55VP, Carl Zeiss SMT AG, Oberkochen, Germany) at x200 magnification after sputter coating.

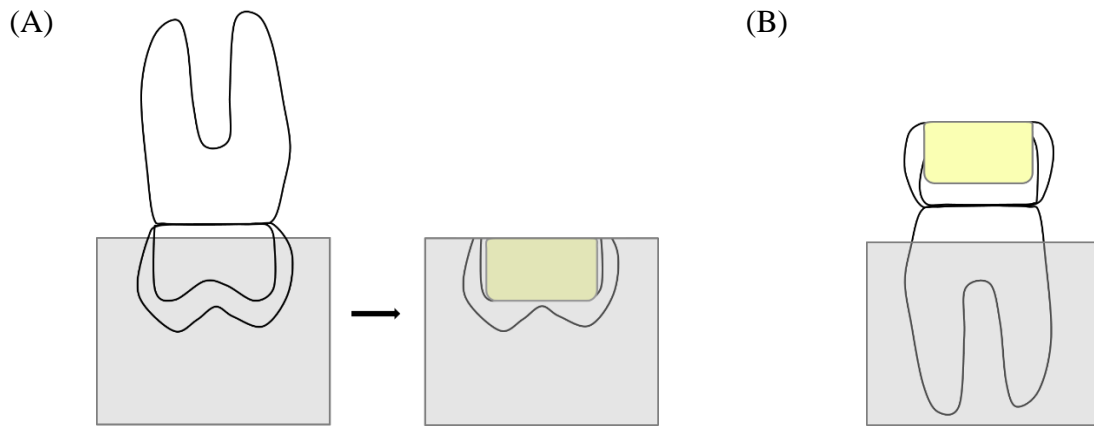


Figure 49 Diagrammatic presentation of the “experimental” cavity with enamel at the cavity floor and dentin margins to study the effect of the bonding substrate on the shrinkage direction (A) and the “cylindrical” cavity that represents a cylindrical class I cavity (B).

6.5 Results

6.5.1 Qualitative presentation of polymerization shrinkage: Visualization of shrinkage vectors in the displacement vector field and SEM

6.5.1.1 Displacement vector field in the “experimental-self-etch” cavity

The displacement vector field in the “experimental-self-etch” group showed great downward shrinkage in the upper half of the restoration. In the lower one third of the restoration, vectors were small and indicated upward shrinkage. Many small vectors were found along the dentin walls resulting in the general tendency of shrinkage direction toward the center (Figure 50). The SEM images showed a defective bond at the dentin margin, but an intact bond at the enamel floor (Figure 51).

6.5.1.2 Displacement vector field in the “experimental-total-etch” cavity

In the “experimental-total-etch” group the displacement vector field showed great downward shrinkage in the upper half, then deviated toward one side with smaller vectors which met small vectors that pointed from the floor upward in the lower one fourth. Almost no shrinkage vectors were detected near the dentin walls (Figure 52). The SEM images showed an intact bond along cavity margins and the enamel floor (Figure 53).

6.5.1.3 Displacement vector field in the “cylindrical-self-etch” cavity

The displacement vector field of the “cylindrical-self-etch” group showed downward shrinkage in the upper half of the restoration, while in the lower part the vectors pointed upward (Figure 24, p.44). In the SEM images one cavity margin was intact, while the other cavity margin and the floor were defective (Figure 25, p.45).

6.5.1.4 Displacement vector field in the “cylindrical-total-etch” cavity

In the “cylindrical-total-etch” group the displacement vector field displayed was similar to that in the “cylindrical-self-etch” group (Figure 54). Here, in contrast to the previous group, cavity margins were intact, but the floor presented a defective bond (Figure 55).

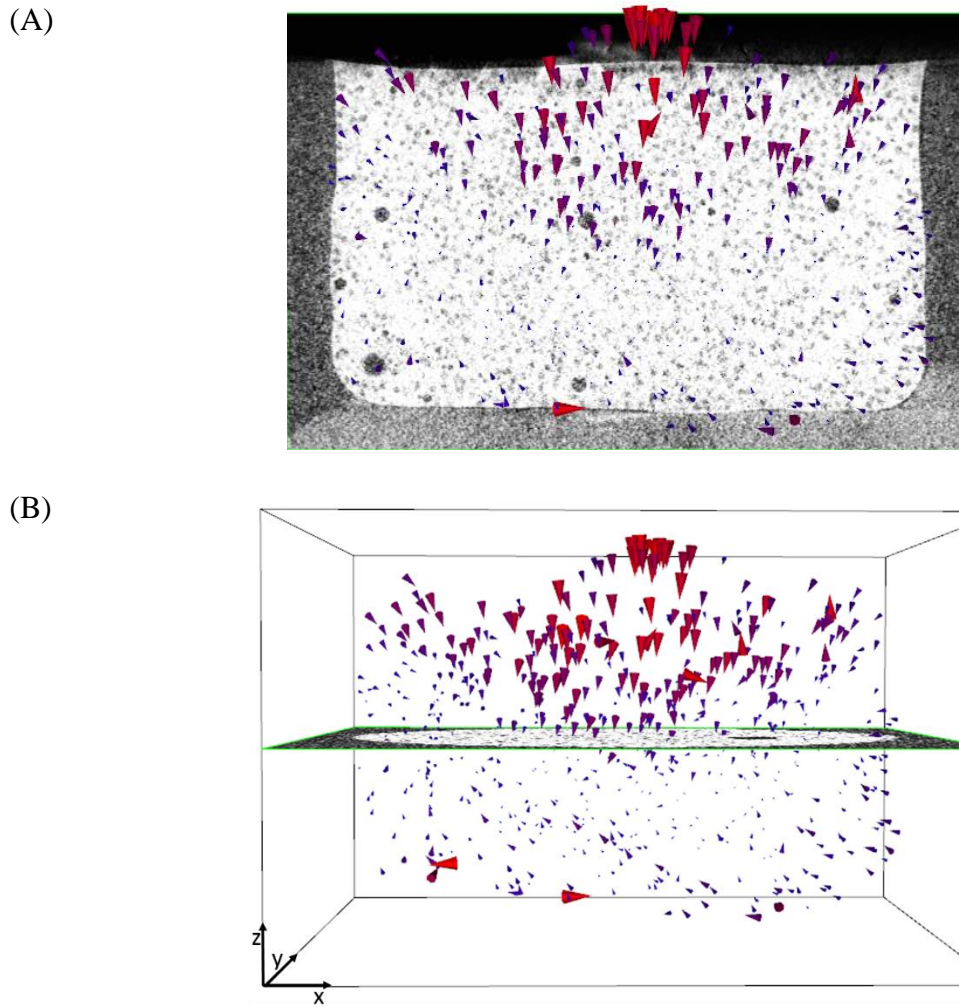


Figure 50 The displacement vector field of the “experimental-self-etch” cavity, with the x-plane (A) and the z-plane (B) of the micro-CT scan in the background. Glyphs were scaled by a factor of 5 to enhance visibility. Large shrinkage vectors were detected in the upper restoration part and small vectors pointed away from cavity walls.

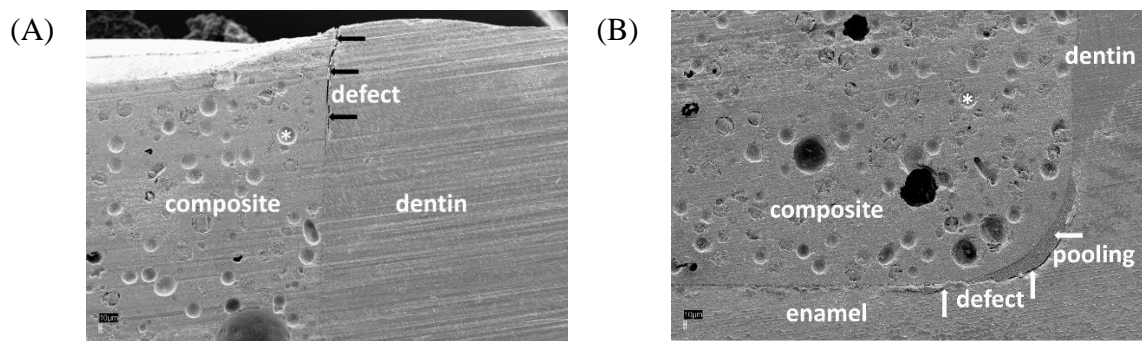
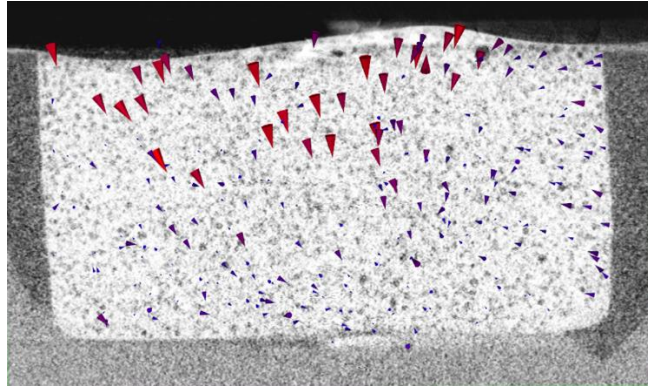


Figure 51 SEM images (x200) of the “experimental-self-etch” group with a defective dentin margin (A) and an intact bond at the enamel floor (B). One traceable glass filler is marked by the star *.

(A)



(B)

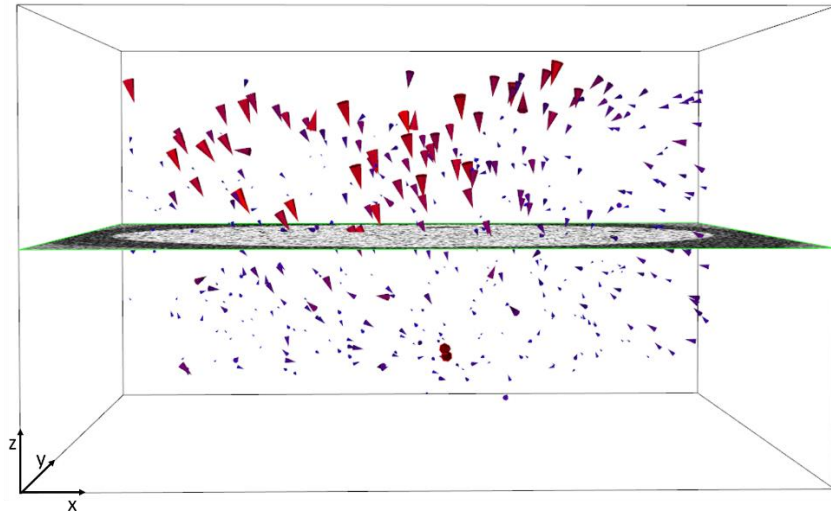
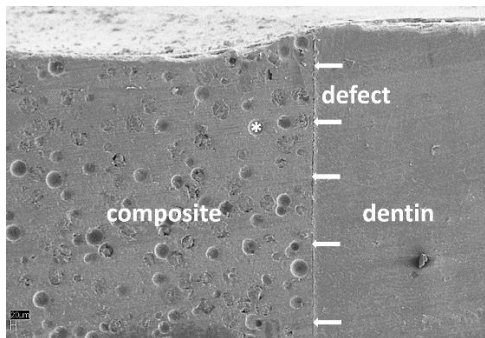


Figure 52 The displacement vector field of the “experimental-total-etch” cavity with the x-plane (A) and the z-plane (B) of the micro-CT scan in the background. It showed downward shrinkage at the upper part of the restoration and deviation of the shrinkage vectors toward one side; at the lower part (quarter) small vectors pointed upward. Glyphs were scaled by a factor of 5 to enhance visibility.

(A)



(B)

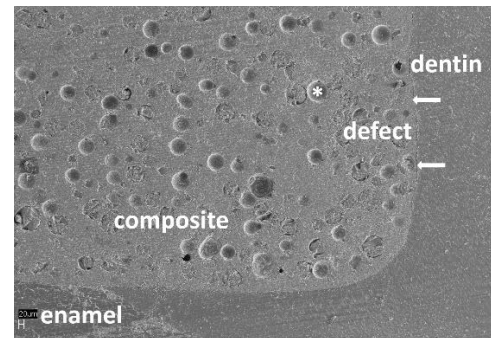


Figure 53 SEM images (x200) of the “experimental-total-etch” group with both an intact dentin margin (A) and an intact bond at the enamel floor (B). One traceable glass filler is marked by the star *.

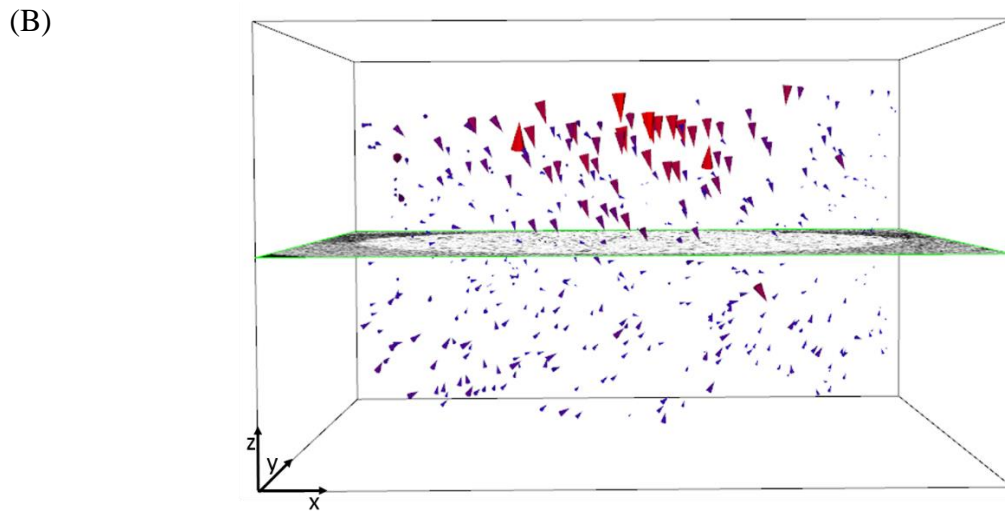
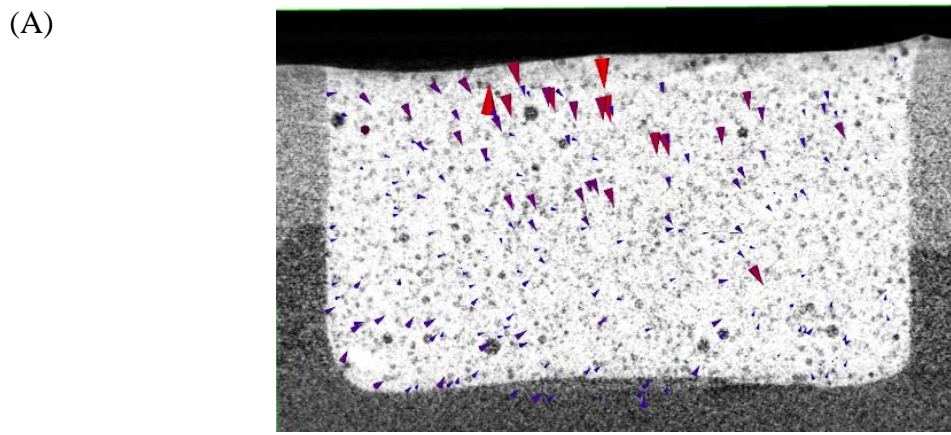


Figure 54 The displacement vector field of the “cylindrical-total-etch” cavity, with the x-plane (A) and the z-plane (B) of the micro-CT scan in the background. Glyphs were scaled by a factor of 5 to enhance visibility. Downward shrinkage at the upper restoration part and smaller shrinkage upward pointing upward at the cavity floor.

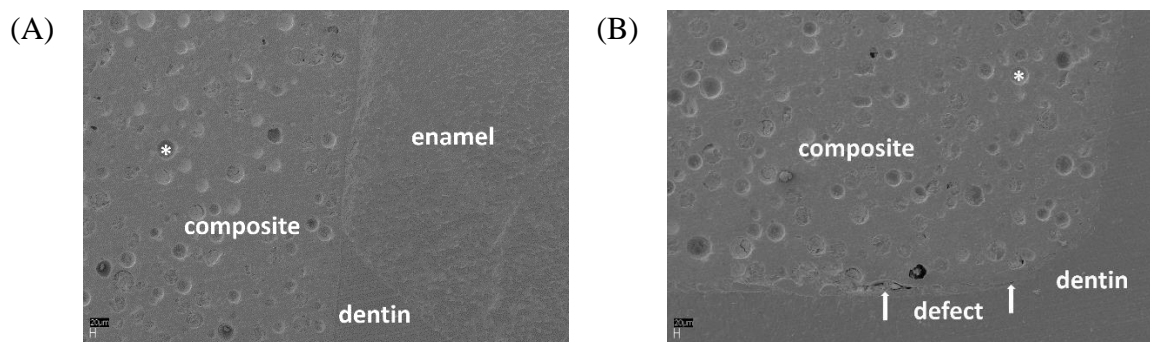


Figure 55 SEM images (x200) of the “cylindrical-total-etch” cavity displaying an intact bond at the enamel margin (A), while the bond with the dentin floor was defective (B). One traceable glass filler is marked by the star *.

6.5.2 Quantitative presentation of polymerization shrinkage: values of shrinkage vectors and statistical analysis

5.6.1.1 Quantitative non-directional analysis: Probability density function of the vector length values

The longest shrinkage vectors were found in the “experimental-self-etch” group ($31.8 \pm 14.3 \mu\text{m}$), followed by the “cylindrical-total-etch” group ($25.8 \pm 11.0 \mu\text{m}$), the “experimental-total-etch” group ($25.5 \pm 14.7 \mu\text{m}$) and least in the “cylindrical-self-etch” group ($23.3 \pm 11.1 \mu\text{m}$) (Table 9, Figure 56).

One-way ANOVA revealed significant differences ($F=100.7$, $Df=3,5960$; $p<0.001$) and the post-hoc pairwise comparison using Tamhane’s T2 test showed significant differences between all groups except for “experimental-total-etch” and “cylindrical -total-etch” groups ($p=0.991$).

The univariate ANOVA revealed that the cavity forms had highly significant differences ($F=138.531$; $df=1, 5960$; $p<0.001$) and the bonding agent as well ($F=31.181$; $df=1, 5960$; $p<0.001$). The interaction between the cavity form and the bonding agent was also significant ($F=157.793$; $df=1, 5960$; $p<0.001$). The R-squared is 0.048 implying that 4.8% of the observed variance of the vector lengths can be explained by the 2 factor model, that is cavity and bonding agent.

Table 9 Mean vector length values and mean filler movement in the z-direction of the in the 4 study groups

Group	Mean vector length (μm)	Filler movement in the z-direction (μm)
“experimental-self-etch”	31.8 ± 14.3	7.6 ± 15.9
“experimental-total-etch”	25.5 ± 14.7	4.5 ± 13.2
“cylindrical-self-etch”	23.3 ± 11.1	-3.7 ± 13.6
“cylindrical-total-etch”	25.8 ± 11.0	-5.2 ± 13.4

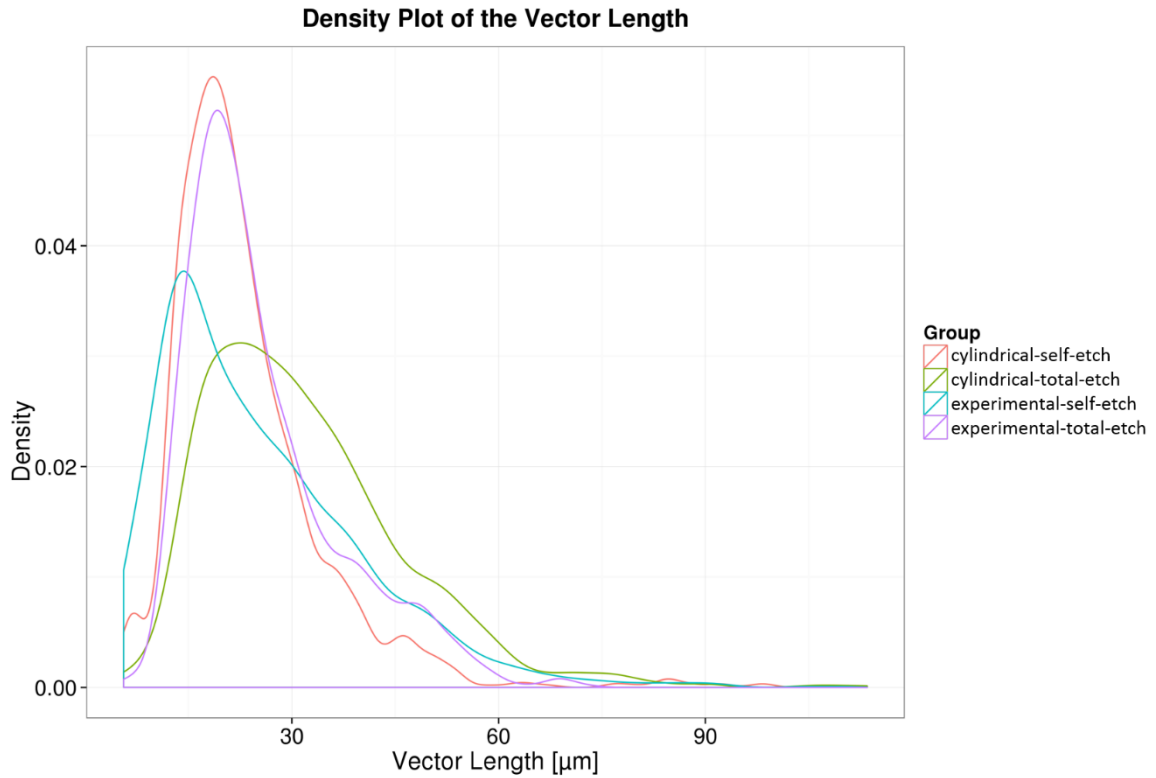


Figure 56 The probability density function of the vector lengths in the four groups. The peaks of the vector length values of all groups are located in the range below 30 μm. The “experimental-total-etch” (lila) and the “cylindrical-self-etch” (orange) groups have a similar curve with greatest frequency of vectors at about 20 μm. The “cylindrical-total-etch” (green) has its peak at a lower level, but with more vectors and larger vector length values. The “experimental-self-etch” (turquoise) has the peak at about 15 μm and large vectors also in a similar distribution as in the other groups.

6.5.2.1 Quantitative directional analysis: Probability density function of the vector z-component (Filler Movement in the z-direction):

In the “experimental” group tracer beads generally moved downward and away from the light source. The movement in the “experimental-self-etch” group was greater ($7.6 \pm 15.9 \mu\text{m}$) than in the “experimental-total-etch” group ($4.5 \pm 13.2 \mu\text{m}$). On the contrary, in the “cylindrical” groups the tracers moved upward and toward the light source with greater values in the “cylindrical-total-etch” group ($-5.2 \pm 13.4 \mu\text{m}$) than in “cylindrical-self-etch” group ($-3.7 \pm 13.6 \mu\text{m}$) (Table 9, Figure 57).

One-way ANOVA revealed significant differences ($F=271.5$, $Df=3,5982$; $p<0.001$) and the post-hoc pairwise comparison using Tamhane’s T2 test showed significant differences between all groups ($p<0.05$).

The univariate ANOVA revealed that the cavity forms had highly significant differences ($F=810.167$; $df=1, 5982$; $p<0.001$) and the bonding agent as well ($F=39.535$; $df=1, 5982$; $p<0.001$). The interaction between cavity and the bonding agent was also significant ($F=4.420$; $df=1, 5982$; $p<0.001$). The R-squared is 0.12 implying that 12% of the observed variance of the filler movement in the z-direction can be explained by the 2 factor model, that is the cavity and the bonding agent.

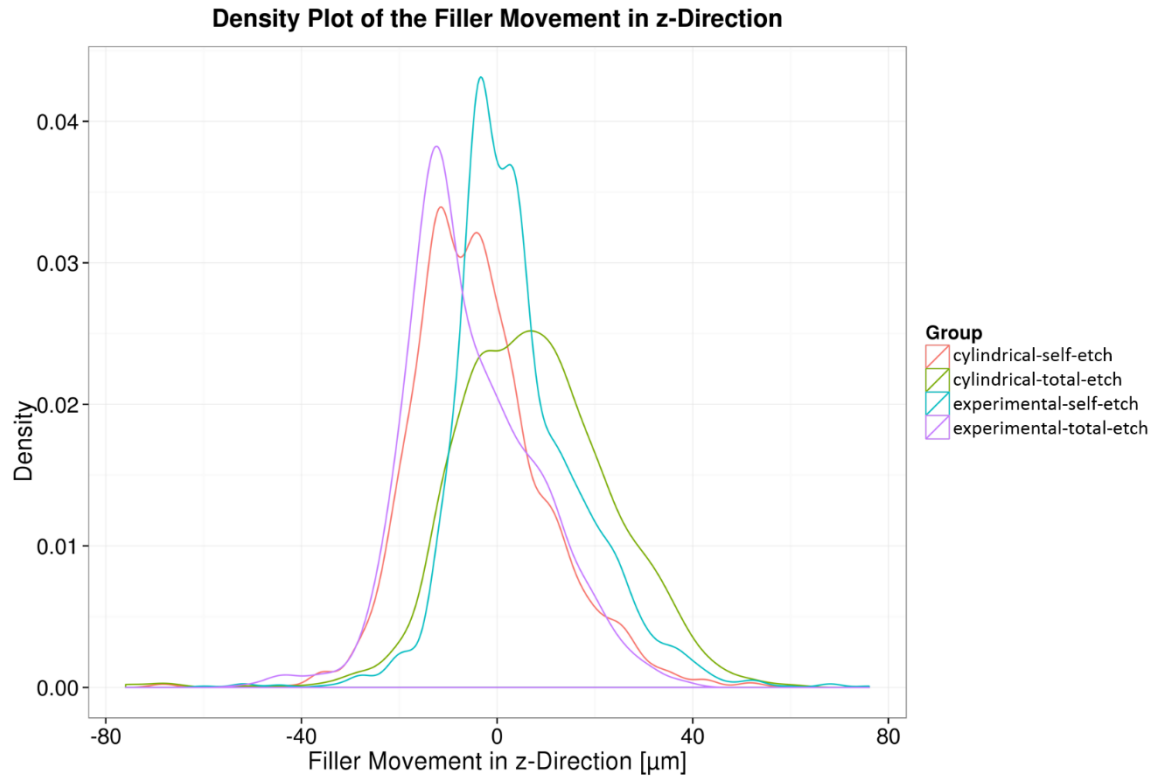


Figure 57 The probability density function of the filler movements in the z-direction in the four groups. 3 Groups have a multimodal distribution of the axial filler movement values. The “experimental-self-etch” group (turquoise) has the first peak in the negative range of small movements related to upward shrinkage found at the cavity floor, while the second peak is located in the positive range that can be attributed to the downward shrinkage of the free surface. The “experimental-total-etch” group (lila) has only one peak that is located in the negative range at about $-15 \mu\text{m}$ which relates to the upward shrinkage; yet, another large portion of the values are in the positive range that conforms to the downward movement of the free restoration surface. In the “cylindrical-self-etch” group (orange) the two peaks are situated in the negative range denoting upward shrinkage. In the “cylindrical-total-etch” group (green) one peak was located in the negative values but the majority of vectors are in the positive range which indicate downward shrinkage.

6.6 Discussion

This study demonstrated that the bonding substrate significantly influenced the polymerization shrinkage direction. The filler movement in the z-direction showed marked differences between the “experimental” and the “cylindrical” groups. On the other hand, varying the bonding condition (self-etch versus total-etch) did not affect the shrinkage direction, but rather produced alterations in the magnitude of the vector lengths. The self-etch adhesive was more prone to variations and vector lengths differed significantly between the “experimental-self-etch” and “cylindrical-self-etch” groups. The vector lengths in the “total-etch” groups showed no significant difference. Equal vector length values could be related to the increased film thickness of the total-etch adhesive which balances local variations, thus, decreases detachment from the cavity walls.

The fictional zero-line was a plane where shrinkage vectors of opposite directions met; shrinkage vectors from the free surface moved downward, while shrinkage vectors from the lower restoration part moved upward to join in a region of no horizontal movement. In all groups, except for the “experimental-total-etch”, the fictional zero-line was located midway between the cavity floor and the free surface. However, the net axial shrinkage direction differed depending on the bonding substrate. Yet, in the “experimental-total-etch” group, the fictional zero-line was located at the lower quarter. Moreover, the displacement vector field of the “experimental-total-etch” group resembled that of the ceramic cavities with optimal adhesion (Chapter 4). For this reason, it can be assumed that the bond between the composite and specially the cavity floor was stronger than in the other groups. This strong bond could be attributed to both the presence of enamel at the cavity floor, acid etched enamel and the use of the total-etch adhesive.

The cylindrical cavity with parallel walls was the cavity configuration of choice as it was free of any configurational variations. In addition, it can be compared to previous studies (Chiang et al., 2009; Versluis et al., 1998) and the results presented in Chapter 3-5 as well. On the other hand, the C-factor of the cylindrical class I cavities was the most unfavorable resulting in greater shrinkage stresses that can lead to subsequent debonding or detachment from the cavity floor and/or margins. Detachments were seen in the “experimental” group at dentin cavity margins, maybe due to greater downward shrinkage of the free surface or because the bond with the dentin margin was weaker than the bond with the enamel margin. Or in other words, debonding of the composite from the dentin cavity margins occurred and in turn composite could move downward. On the contrary, detachments in the “cylindrical”

groups were rather seen at the cavity floor that consisted of dentin as in the clinical situation. The detachments were in agreement with the larger shrinkage vectors: in the “experimental” large vectors were seen in the upper restoration part near the free surface, while in the “cylindrical” cavities the large shrinkage vectors were located at the lower restoration part.

However, information on the topic of shrinkage vectors is scarce. The results of this study varied from findings of Chiang et al., 2009, with regards to the displacement vector field. This could be related to the quantity of enamel at the margins as well as the applied bonding agent which was in their case a weak self-etch adhesive. Shrinkage vectors point upward in a cavity with equal enamel margins and point toward one side in a cavity with unequal enamel margins (Chiang et al., 2009; Chiang et al., 2010). The self-etch adhesive of the current study was stronger and the cavities did not show noticeable variations in the amount of enamel at the cavity margins. Consequently, the displacement vector fields were similar even with the use of self-etch and total-etch adhesives.

The “experimental” cavity with the enamel floor is clinically not relevant or possible, but the results are useful for learning more about the effect of the bonding substrates on the shrinkage direction. It highlighted that the location of enamel is able to change the direction of shrinkage vectors when all other boundary conditions are constant. This is in agreement with findings of Chiang et al., 2009, that showed that variation of enamel margin’s thickness led to change in direction of shrinkage vectors (Chiang et al., 2009; Chiang et al., 2010), though in the current study the enamel was located at the cavity floor. Moreover, the “cylindrical” group did not have these variations of enamel margin thickness. In the “experimental” group the cavity floor was not always completely located in enamel because the presence and amount of enamel is related to the shape of the dentin-enamel junction and the enamel cap. Accordingly, some cavities had a cavity floor with only a central area of enamel surrounded by dentin, while other cavity floors were completely formed of enamel. Nevertheless, the enamel floor pulled the composite, especially in the “total-etch” group. In the “self-etch” group, this effect was less pronounced which may be attributed to the lower bond strength values of self-etch adhesives compared with total-etch adhesives (Goracci et al., 2004; Inoue et al., 2001), even more, when bonding to enamel without previous acid etching. Indeed, it proved in a tooth model that shrinkage was related to the bonding substrate and not the light source.

Another study investigating shrinkage vectors used an artificial mold of composite instead of human teeth (Cho et al., 2011), likewise a glass model cavity was used for shrinkage stress assessment (Li et al., 2011). Other studies used Teflon molds for gap analysis (Pereira et al.,

2008; Takahashi et al., 2010), volumetric analysis (de Melo Monteiro et al., 2011) and composite shrinkage by image analysis (Miletic et al., 2011). As the results from this study and Chapter 4-5 show, the boundary conditions do have a great influence on the shrinkage direction and the resulting displacement vector fields. Therefore, the comparison of displacement vector fields of restorations applied into artificial molds should be viewed cautiously, as they do not perfectly mimic the clinical situation. Nevertheless, they do contribute valuable information for the understanding of the shrinkage patterns with boundary conditions other than in the human teeth. In the etched and silanized ceramic cavities of Chapter 4, an optimal bond was obtained and shrinkage vectors were directed downward. In the ceramic cavities, where a layer of bonding agent was applied, the shrinkage pattern was more uniform and reproducible. This is in agreement with the shrinkage pattern of the “experimental-total-etch” group. On the contrary, non-adhesive Teflon cavities in Chapter 5 presented a displacement vector field with different shrinkage pattern: shrinkage vectors from the free surface, the cavity walls and the cavity floor were all directed toward the center of the restoration. Even though ceramic and Teflon model cavities do not relate to the clinical situation, the results emphasized on the importance of the bonding substrate and related bonding conditions.

The inherent uncontrollable variable when using human teeth is the variation in quality and quantity of enamel and dentin within a single tooth and among teeth in general. In addition, the cavity preparation depends on factors including the caries extension into hard dental tissues, or replacing an old restoration, while the choice of the bonding agent varies from one clinical situation to another, even the type of cavity preparation, bevel and bevel length, instrumentation, cooling and preparation at high or low speed.

The shrinkage vectors were obtained in the form of 3D displacement vector fields that could be evaluated, rotated, zoomed in and out on the computer screen, but only 2D images can be presented here. Furthermore, the coordinate numbers denoting the position of the glass beads were available from the output file of the evaluation process from which the vectors were computed. Hence, two types of data analyses were performed. First, the qualitative analysis by the visualization of the displacement vector fields, and second, the quantitative analysis which is two-fold; non-directional and directional. The non-directional analysis evaluated vector length values independent of their direction, while the directional analysis investigated the movement of the glass beads in the z-direction only in order to relate to the hypothesis whether composites shrink towards light or not. This evaluation was confirmed by the statistical analysis using the univariate ANOVA that analyzed the effect of the cavity

independent of the effect of the bonding agent and hereby confirmed the qualitative shrinkage vector analysis of the displacement vector fields. The qualitative and quantitative evaluations complement each other and are well supported by the SEM images.

Therefore, the specific displacement vector field for each restoration cannot be fully predicted. However, the pieces of information gained through this study can be considered when restoring a tooth defect. The detrimental fact about the polymerization shrinkage is the generation of shrinkage stresses that lead to detachment of the composite restoration from the tooth structure. Once debonding occurred, shrinkage is directed away from the detached part. The critical question is how to manage the detachment at the cavity floor and how to manage gap formation at the cavity margin. Taking into consideration that the experimental resin composite, Tetric EvoFlow with added glass beads, is not recommended for application in bulk, more investigations are needed with bulk-fill composites. The used composite was fair enough for the evaluation procedure and bulk-fill composites were available only after the start of the experiments. The composite was sufficiently cured even at a depth of 3 mm (Lindberg et al., 2004).

Scientists need to reevaluate current restorative techniques and adapt them in the light of these results. It was suggested that the filling technique and the composite type might have a strong influence on the adhesion of composite, especially with high C-factor (Van Ende et al., 2013). More information is needed on the traditional layering technique and its effect on the direction of shrinkage vectors. Also, reducing the C-factor could help in preserving a stable bond. In cavities with a high C-factor, oblique composite application could reduce the C-factor, and perhaps lead to better marginal integrity. Finally, shrinkage vectors can give answers to these questions.

Conclusions

From the results of this study, the following can be concluded:

1. The knowledge gained from this study confirmed that the strong bond to enamel was the decisive factor in pulling the composite. Thereby, the general assumption that composites shrink toward light can be disproved.
2. In the “experimental” group with enamel at the cavity floor, detachment occurred with both the self-etch and the total-etch adhesives at the dentin margin, and no detachment at the cavity floor.
3. In the “cylindrical” cavities detachment always occurred at the cavity floor, whether self-etch or total-etch adhesives were used.
4. It can be concluded that shallow cavities in dentin that reach only beyond the dentin-enamel junction will have a good bond with the cavity floor and margins, especially when a total-etch adhesive is used.
5. In deep cavities of 3 mm depth usually debonding happens at the cavity floor and sometimes at the margin, with both self-etch and total-etch adhesives. Therefore, composite should preferably not be applied in bulk unless it is a bulk-fill material. Still, no information on the shrinkage patterns of bulk-fill materials and incrementally applied composites is available.

7 Summary

Tooth-colored resin composite restorations are nowadays the material of choice for filling tooth-defects. Unfortunately, polymerization is accompanied by volumetric shrinkage leading to marginal gaps at the tooth-restoration interface. In dentistry, it is assumed that light-cured composites shrink toward the light source. However, this hypothesis lacks scientific proof. Recently, research groups in Munich and Tokyo have developed methods employing micro-CT scans of the uncured and cured composite restorations with embedded tracer fillers. The current method employed sphere registration and segmentation based on a block-matching algorithm (Chiang et al., 2009; Chiang et al., 2010; Rösch et al., 2009). The glass beads were traced and shrinkage vectors were computed.

This study investigated the effect of boundary conditions on the polymerization shrinkage vectors of light-initiated dental resin composites. Boundary conditions include cavity configurations, bonding conditions (DBA) and bonding substrates.

The first part of this study (Chapter 3) investigated the effect of different cavity configurations on the shrinkage vectors. In the “adhesive” cavity (beveled margin, undermining preparation) which is proposed for composite restorations shrinkage vectors pointed upward, but it had a tight marginal seal. In our samples, detachment was detected at the cavity floor, which can cause postoperative pain due to a pumping effect on dentinal fluid. In contrast, the “diverging” cavity displayed great downward shrinkage, while the „cylindrical” cavity had smallest vectors that moved toward the center. Shrinkage vectors in the “adhesive” cavity matched the assumption, that is not because composites shrink toward the light, but rather due to the strong bond to enamel. The shrinkage patterns of the “diverging” and „cylindrical” cavities proved that shrinkage was not related to the light source, but to the cavity configurations.

In the clinical situation, the “adhesive” cavity design should only be applied to remove carious tissue, otherwise, undercuts should not be prepared on purpose. An enamel bevel cut perpendicular to the enamel prisms can enhance the marginal integrity but also influence the shrinkage direction. The “adhesive” cavity can clinically be prepared in rather small to medium sized cavities, but not in very large ones, therefore, the correct bevel preparation is not always granted. Further investigations are needed to find out how to manage or avoid

the gap formation by an incremental application technique and the use of dentin bonding agents.

In the following study parts (Chapter 4-6) the effect of other boundary conditions were investigated. As the bonding condition is related to a great extent to the bonding substrate, specific aspects were addressed. In the second part (Chapter 4), shrinkage vectors in ceramic cavities with different boundary conditions were analyzed. The etched and silanized surface provided optimal adhesion. Furthermore, the ceramic served as a homogenous cavity model in contrast to the heterogenous tooth structure. This validated our assumption that enamel influences the direction of the shrinkage vectors and that it is not only a possible detachment of the composite from the dentin due to a weak bonding agent. The displacement vector field demonstrated a clear downward shrinkage in the whole restoration that was attributed to the strong bond. However, in the lower two third of the restoration two shrinkage patterns could be distinguished: pattern-1 showed a deviation of shrinkage vectors toward one side, while pattern-2 displayed swirling of vectors in the whole lower restoration part. The use of an intermediate bonding agent in the ceramic cavities resulted in a more uniform and reproducible shrinkage pattern. Nevertheless, the two shrinkage patterns generally indicate that detachment has occurred, but the area of detachment was rather by coincidence. It is not clear, if this can be related to the unfavourable C-factor or the application of composite in bulk. The use of a bulk-fill material has greater modulus of elasticity than the flowable which can lead to greater shrinkage stresses at the tooth-restoration interface.

In contrast to the optimal bonding condition, a non-adhesive Teflon cavity was used in the third study part (Chapter 5) with only the influence of cavity geometry on the shrinkage. Shrinkage vectors pointed toward the center of the restoration, although the contraction movement was greater at one side. The region with larger vectors was thought to be the site of first detachment.

To investigate the influence of enamel as a bonding substrate on the shrinkage direction, an “experimental” cavity with an enamel floor was proposed (Chapter 6) and compared to the “cylindrical” cavity from the first part (Chapter 3). In the “experimental” cavity, enamel at the cavity floor pulled the composite and shrinkage was directed downward, similar to the shrinkage pattern found in the “ceramic” cavities. On the other hand, in the “cylindrical” cavity the composite shrank toward the midplane of the restoration. Variation of the bonding condition was achieved by the use of a self-etch versus a total-etch adhesive. This resulted only in small variations in magnitude. It can be concluded that the bonding substrate plays a

major role in determining the shrinkage direction, while the bonding condition plays a minor role. Nevertheless, the bonding condition depends on the bonding substrate to a great degree.

Although the basic investigations of Chapter 4-6 cannot be applied in the clinical situation, they were important to identify each factor's role with regard to the polymerization shrinkage direction. More studies are needed to investigate the effect of the C-factor on the shrinkage direction, as well as analyzing shrinkage patterns in incrementally applied and bulk-fill composite restorations. Additionally, more realistic cavity designs instead of cylindrical class I cavities need to be prepared, as well as class II cavities. More investigations are needed on the effect of the curing-light source on the shrinkage vectors.

Finally, the results of this study enable researchers to understand some factors affecting polymerization shrinkage and utilize this knowledge to reevaluate current application techniques and to suggest adjustments for common drawbacks. For these reasons, every patient receiving a composite restoration will benefit from this research.

Conclusions

Within the limitations of the current study, the following can be concluded regarding the effect of the boundary conditions on the polymerization shrinkage vectors of light-cured dental resin composites:

1. The shrinkage amount and direction varied according to the cavity configuration, with greatest shrinkage vectors in the “adhesive” cavity, followed by the “diverging” and it was least in the “cylindrical”.
2. The “adhesive” versus the “cylindrical” cavity showed that the cavity margin influenced the shrinkage direction and the gap formation.
3. In the ceramic model the dentin bonding agent acted as a stress breaker that allowed for more movement, therefore, the mechanical properties of bonding agents are important as they influence the polymerization shrinkage direction.
4. In the Teflon group shrinkage in lateral direction was greater at one side, which is possibly the site of least resistance to adaptation and first detachment due to shrinkage.
5. The knowledge gained from the study with the “experimental” and “cylindrical” cavities confirmed that the boundary conditions influenced the shrinkage direction of light-cured dental resin composites.
6. The claim that composites shrink toward the light source is disproved.

Recommendations for future research

1. Further studies are needed to evaluate different types of self-etch and total-etch adhesives and investigate the relation between bond strength values and the shrinkage direction.
2. More clinically relevant cavity designs are also needed to relate to the clinical situation such as the classical cross-shaped occlusal cavity, MO/MOD-cavities, cervical cavities and others.
3. Moreover, more types of restorative materials should be investigated to explore the shrinkage patterns in incrementally applied and bulk-fill composites, in order to give insight into more clinically relevant information.

8 Zusammenfassung

Kompositfüllungen werden heutzutage routinemäßig gelegt, um Zahndefekte zu beheben. Der große Nachteil der Kompositfüllungen ist deren Schrumpfung, welche zum Randspalt führen kann. In der Zahnmedizin wird angenommen, dass lichthärtende Komposite zur Lichtquelle hin schrumpfen, wobei es für diese Hypothese aber keinen wissenschaftlichen Beweis gibt. Erst in den letzten Jahren ist es Forschungsgruppen aus Tokio und München gelungen, eine Methode zu entwickeln, die Micro-CT-scans von ungehärtetem und lichtgehärtetem Komposit mit eingebetteten Glasfüllkörpern verwenden, um Schrumpfungsvektoren darzustellen. Die in der vorliegenden Studie angewendete Methode basiert auf der Sphärenregistrierung und –segmentierung durch einen Block-matching Algorithmus (Chiang et al., 2009; Chiang et al., 2010; Rösch et al., 2009). Die Füllkörper wurden in beiden Scans verfolgt und die Schrumpfungsvektoren berechnet und graphisch dargestellt.

Diese Studie untersuchte den Einfluss der Rahmenbedingungen auf die Schrumpfungsvektoren in lichthärtenden dentalen Kompositen. Die Rahmenbedingungen beinhalten die Kavitätskonfigurationen, Haftungsbedingungen und Haftsubstanzen.

Im ersten Teil dieser Studie (Kapitel 3) wurde der Einfluss der Kavitätskonfigurationen auf die Schrumpfungsvektoren untersucht. In der „adhäsiven“ Kavität, die für adhäsive Füllungen indiziert ist, haben die Vektoren nach oben, in Richtung der Lichtquelle gezeigt. Im Gegensatz dazu, zeigten die Schrumpfungsvektoren der „divergierenden“ Kavität nach unten, wobei sie in der „zylindrischen“ Kavität insgesamt am kleinsten waren und zur Mitte zeigten. Die Vektoren der „adhäsiven“ Kavität bestätigten die Annahme; dabei geschah dies nicht, weil Komposit zur Lichtquelle hin schrumpft, sondern wegen seiner starken Haftung am Schmelz. Die Schrumpfungsmuster der „divergierenden“ und „zylindrischen“ Kavitäten bewiesen, dass die Schrumpfung nicht von der Lichtquelle abhängig war, sondern von der Kavitätskonfiguration. In der Praxis sollte die „adhäsive“ Kavität nur präpariert werden, um kariöse Zahnschmelzsubstanz zu entfernen, aber Unterschnitte sollten nicht absichtlich präpariert werden. Eine Schmelzanschrägung sollte senkrecht auf die Schmelzprismen erfolgen, um die Randintegrität zu fördern, die jedoch auch die Schrumpfrichtung beeinflussen.

In den übrigen Abschnitten (Kapitel 4-6) wurden die Einflüsse der weiteren Rahmenbedingungen untersucht. Da die Haftungsbedingungen zum großen Teil von den

Haftsubstanzen abhängen, wurden bestimmte Aspekte untersucht. Im zweiten Teil (Kapitel 4) wurden die Schrumpfungsvektoren in Keramikkavitäten mit unterschiedlichen Rahmenbedingungen untersucht. Die geätzte und silanisierte Keramikoberfläche stellte optimale Haftungsbedingungen dar. Außerdem funktionierte die Keramik als homogenes Material für das Kavitätenmodell im Gegensatz zum heterogenen natürlichen Zahn. Das Vektorenfeld zeigte eine klare Schrumpfung nach unten, die der starken Haftung zu Grunde lag. Andererseits konnten zwei unterschiedliche Schrumpfungsmuster im unteren Teil der Füllung erkannt werden: in Muster-1 schrumpften die Vektoren zu einer Seite hin, wobei sie in Muster-2 quer durcheinanderwirbelten. Die Anwendung eines Dentinadhäsivs führte zu einem ebenmäßigeren Erscheinungsbild der Vektoren.

Im dritten Teil der vorliegenden Arbeit (Kapitel 5) wurde nun im Kontrast zur optimalen Haftung eine nicht-haftende Teflon-Kavität verarbeitet. Die Schrumpfungsvektoren zeigten zur Mitte der Füllung, auch wenn die Vektoren auf der einen Seite grösser waren. Dies scheint der Bereich zu sein, von dem sich das Material als erstes von der Wand ablöst.

Wie stark beeinflusst der Schmelz als Haftsubstanz die Schrumpfungsrichtung? Um dies herauszufinden, wurde eine Kavität mit einem Schmelzboden improvisiert (Kapitel 6) und mit der „zylindrischen“ Kavität verglichen (Kapitel 3). In der improvisierten Kavität hat der Schmelz das Komposit nach unten gezogen, ähnlich wie bei der Keramikkavität. Andererseits schrumpfte das Komposit in der „zylindrischen“ Kavität zur Mitte der Restauration.

Variationen der Haftbedingungen wurden durch die Anwendung von einem Self-etch- und einem Total-etch-Adhäsiv erzielt. Dies führte nur zu kleinen Unterschieden in der Länge der Vektoren, beeinflusste aber nicht die Schrumpfungsrichtung. Daraus kann man schließen, dass die Haftsubstanz eine große Rolle bezüglich der Schrumpfungsrichtung spielt, die Haftungsbedingungen jedoch nur eine kleine, wobei diese jedoch weitgehend vom Haftungssubstrat abhängig sind.

Obwohl die Untersuchungen aus den vorherigen Kapiteln 4-6 nicht in der Praxis angewendet werden können, waren sie wichtig, um zu erkennen, welche Rolle jeder Faktor bezüglich der Schrumpfungsrichtung spielt. Es werden noch weitere Studien benötigt, um sowohl den Einfluss des C-Faktors zu untersuchen, als auch die Schrumpfungsmuster in schichtgelegten Füllungen und in Bulk-fill-Kompositen. Zusätzlich dazu müssten realistischere Kavitätsformen und Klasse II Kavitäten untersucht werden anstelle der hier untersuchten

zylindrischen Klasse I Kavitäten. Außerdem könnte der Einfluss der Lichtquelle auf die Schrumpfrichtung noch erforscht werden.

Somit führen die Ergebnisse dieser Studie zum Verständnis einiger Faktoren, welche die Schrumpfung beeinflussen. Dieses Wissen kann wiederum angewendet werden, um gängige Anwendungsmethoden zu beurteilen und Verbesserungen vorzuschlagen. Aus diesen Gründen profitiert jeder Patient, der eine Kompositfüllung erhält, von dieser Forschungsarbeit.

5 List of tables

Table 1 Classification of composites according to the functional group determining their cure (Kunzelmann, 2008)	3
Table 2 Kunzelmann’s classification of composites according to filler system (Kunzelmann, 2008).....	4
Table 3 Traditional classification of resin composites (Sakaguchi and Powers, 2012)	5
Table 4 Composition of the experimental resin composite and the self-etch adhesive.....	39
Table 5 Mean vector length values and mean filler movement in the z-direction in the different cavity configurations.....	46
Table 6 Composition of the ceramic block, hydrofluoric acid, silane coupling agent and the total-etch adhesive	64
Table 7 Mean vector length values and mean filler movement in the z-direction of the “ceramic+HF+silane” and “ceramic+HF+silane+DBA” groups	69
Table 8 Mean vector length values and mean filler movement in the z-direction of the “Teflon” group.....	81
Table 9 Mean vector length values and mean filler movement in the z-direction of the in the 4 study groups.....	97

6 List of figures

Figure 1 The chemical structure of Bis-GMA (A), UDMA (B), TEGDMA (C) and Bis-EMA6 (D).....	2
Figure 2 The silane coupling agent.....	6
Figure 3 Failures that may occur after application of a composite restoration, modified after Tantbirojn et al., 2004 (Tantbirojn et al., 2004)	8
Figure 4 stress-strain analyzer machine designed by Dullin, modified after Chen et al., 2001 (Chen et al., 2001; Chen et al., 2003; Dullin, 1998).....	10
Figure 5 The Bioman shrinkage-stress instrument, modified after Watts et al., 2003 (Watts et al., 2003).	11
Figure 6 Overview of the methods for measuring the polymerization shrinkage strain.	13
Figure 7 Measurement of the linear polymerization shrinkage of a composite cylinder. ...	15
Figure 8 The bonded-disc method for measurement of the linear polymerization shrinkage, also referred to as “Watts method”, modified after Watts and Cash, 1991 (Watts and Cash, 1991).....	16
Figure 9 Linometer for the measurement of linear polymerization shrinkage, modified after de Gee et al., 1993 (de Gee et al., 1993).....	17
Figure 10 The image processing of the 2D shrinkage vector evaluation : (A) the original source image of the uncured resin composite with the deformation grid. (B) The displacement field obtained from the elastic registration is superimposed to the output source-target image of the registered target image. The vector field displays the deformation due to the mass movement of the polymerization shrinkage and the dotted line marks the deformed shape after light-curing of the composite (Chiang et al., 2009). Reuse of the images is with written permission by Dr Yu-Chih Chiang (2014).	23
Figure 11 The 3D deformation field by Chiang et al., 2009 (Chiang et al., 2009). Reuse of the images is with written permission by Dr Yu-Chih Chiang (2014).....	24
Figure 12 The 3D image obtained by superimposing micro-CT scans from the composite before and after polymerization. The three slices are representative of the 165 slices that were analyzed for the filler movement in the axial direction by Cho et al., 2011 (Cho et al., 2011).....	25
Figure 13 The 3D vector field image represents the filler movement direction in the bonded group by Cho et al., 2011 (Cho et al., 2011).	26

Figure 14 The investigations of the current study were based on the boundary conditions which include the cavity configuration, the bonding condition and the bonding substrate. 29

Figure 15 Overview of the different study parts. 29

Figure 16 The high resolution micro-computed tomography, μ CT 40, Scanco Medical AG, Switzerland, was used for the 3D scanning procedure of the restorations. 35

Figure 17 The prepared and filled tooth in the sample holder in the micro-CT (A), covered with a radiolucent and dark cap to avoid premature polymerization during the first scan (B). Light curing (20 s) of the composite was performed while the sample remained in the micro-CT machine (C). 35

Figure 18 Scheme of the workflow for obtaining the digital 3D-data sets from the micro-CT. 36

Figure 19 Sphere segmentation and sphere registration based on a block-matching algorithm. Sphere segmentation: set of all identified and extracted glass fillers in a same sample from the “adhesive” group (A), Sphere registration: both scans of one sample (here: "adhesive group") were superimposed. The identified glass fillers in the first scan were simply radiolucent and colorless while the corresponding glass fillers from the second scan were superimposed and color coded (B). Sphere registration was performed based on a block-matching algorithm to determine the displacement of the segmented spheres due to polymerization shrinkage. 40

Figure 20 The displacement vector field of the "adhesive" restoration, with the x-plane (A) and the z-plane (B) of the micro-CT scan in the background. Glyphs were scaled by a factor of 5 to enhance visibility. Large shrinkage vectors are seen at the lower restoration part pointing upwards. 42

Figure 21 SEM image (x200) of the “adhesive” restoration showing an intact bond at the enamel margin (A) and a defective bond “defect” at the floor of the restoration (B). One traceable glass filler is marked by the star * 42

Figure 22 The displacement vector field of the “diverging” restoration, with the x-plane (A) and z-plane (B) of the micro-CT scan in the background. Glyphs were scaled by a factor of 5 to enhance visibility. Large shrinkage vectors point downward near the free surface, and small shrinkage vectors point upward from the restoration floor. 43

Figure 23 SEM image (x200) of the “diverging" restoration, displaying a defective bond at the enamel margin (A) and an intact bond at the floor of the restoration (B). One traceable glass filler is marked by the star * 43

Figure 24 The displacement vector field in the “cylindrical” group with a predominant shrinkage pattern with the x-plane (A) and z-plane (B) of the micro-CT scan in the

background showed more vectors in the lower part, while the atypical shrinkage pattern in the “cylindrical” cavity additionally displayed large vectors in the upper restoration part. The x-plane (C) and z-plane (D) of the micro-CT scan displayed in the background. Glyphs were scaled by a factor of 5 to enhance visibility. 44

Figure 25 SEM image (x200) of the “cylindrical” restoration showing an intact bond at the enamel margin at one side (A) and a defective bond at the floor of the restoration (B). One traceable glass filler is marked by the star *..... 45

Figure 26 The probability density function of the vector lengths in the “adhesive”, “diverging” and “cylindrical” groups. The “adhesive” group had two maxima above 25 μm and a large vectors were more numerous than in the other groups. The “diverging” group had its maximum at about 25 μm which means that the majority of vectors were in that range. The “cylindrical” group had its peak at about 15 μm which means that the greatest frequency of vectors had that value..... 47

Figure 27 The probability density function of the filler movements in the z-direction in the “adhesive”, “diverging” and “cylindrical” groups. The “adhesive” group showed many peaks which related to the presence of many vectors of that value. The curve is shifted in the negative range that relates to the upward shrinkage movement at the cavity floor. The “diverging” group had a shallower curve with two maxima; the first is in the range of -20 μm that relates to the upward shrinkage at the cavity floor, while the second maximum is located at about 15 μm which can be related to the downward shrinkage seen at the free surface. The curve of the “cylindrical” cavity also has two peaks, but they are close to each other near the zero value. The first peak can be attributed to the upward movement at the lower cavity part and the second peak is related to the downward movement at the free surface..... 49

Figure 28 Possible shrinkage directions in the “diverging” cavity configuration: (A) upward shrinkage as composite at the free surface hardens first and pulls the composite upwards as soon as the adhesive bond interface to the tooth is disrupted, or (B) downward shrinkage of the free surface..... 51

Figure 29 The shrinkage of a floating specimen having no contact with any surface exhibits “free shrinkage” (A), but a specimen in contact with a surface shrinks towards it (B). 52

Figure 30 The light source in relation to the “adhesive” (A), “diverging” (B) and “cylindrical” (C) cavity configurations. In the “adhesive” cavity, light did not directly reach the resin composite below the enamel margin. In the “diverging” and “cylindrical” cavities, there was no configurational impedance to the curing-light. 54

Figure 31 The light focus of Elipar FreeLight2, 3M ESPE, in relation to the “cylindrical” cavity.	55
Figure 32 Cusp tips were flattened to allow for light-curing as close as possible to the restoration. Cavity margins were mostly located in enamel.....	57
Figure 33 The ceramic block (A) was cut into three slices into which a cylindrical cavity was prepared. The outer margin was trimmed to fit into the micro-CT sample holder and flowable composite was added as a reference landmark for the rigid registration (B).	63
Figure 34 Schematic drawing of the ceramic model.	63
Figure 35 The displacement vector field in the “ceramic+HF+silane” group with “Shrinkage Pattern-1”: downward shrinkage at the upper part of the restoration and deviation of the shrinkage vectors toward one side at the lower part, with the y-plane (A) and the z-plane (B) of the micro-CT scan in the background. Glyphs were scaled by a factor of 5 to enhance visibility.....	66
Figure 36 The displacement vector field in the “ceramic+HF+silane” group exhibited “Shrinkage Pattern-2”: downward shrinkage in the upper part of the restoration, while the lower part exhibited horizontal swirling, with the y-plane (A) and the z-plane (B) of the micro-CT scan in the background. Glyphs were scaled by a factor of 5 to enhance visibility.	67
Figure 37 SEM images (x200) of the “ceramic+HF+silane” group of the restoration margin (A) and the floor (B) showing close adaptation. One traceable glass filler is marked by the star *.	67
Figure 38 The displacement vector field in the “ceramic+HF+silane+DBA” group with downward shrinkage at the upper part of the restoration and deviation of the shrinkage vectors toward one side at the lower part, same as “Shrinkage Pattern-1” in the “ceramic+HF+silane” group, with the y-plane (A) and the z-plane (B) of the micro-CT scan in the background. Glyphs were scaled by a factor of 5 to enhance visibility.	68
Figure 39 SEM images (x200) of the “ceramic+HF+silane+DBA” group of the restoration margin (A) and floor (B) showing close adaptation. One traceable glass filler is marked by the star *.	68
Figure 40 The probability density function of the vector lengths in the groups “ceramic+HF+silane” and “ceramic+HF+silane+DBA” shows the frequency of vector length values in the groups. In the “ceramic+HF+silane” group the maximum was located at about 20 μm which can be related to the smaller vectors located majorly in the lower part of the restoration and near the cavity walls. Yet, a considerable amount of vectors was in the range below 50 μm which can be associated with the larger vectors directing downwards in	

the upper part of the cavity. In the “ceramic+HF+silane+DBA” group the distribution of vector lengths values was over a larger range than in the first group. The first maximum at 20 μm could be related to small vectors of the lower third of the restoration near the cavity floor. The second maximum had most vectors at about 45 μm that were attributed to the large downward movement at the free surface. 70

Figure 41 The probability density function of the filler movements in the z-direction in the groups “ceramic+HF+Silane” and “ceramic+HF+Silane+DBA” displays the frequency of the axial filler movement values in the groups. In the “ceramic+HF+Silane” group the maximum was located at about -10 μm which means that the greatest frequency of axial filler movement was very small and denotes upward movement. The overall quantity of axial filler movement was in the positive range which stands for downward movement. The “ceramic+HF+silane+DBA” group displays a maximum at about 13 μm that represents a greater axial downward movement than in the “ceramic+HF+silane” group. Both curves look similar to the previous group, but the “ceramic+HF+silane+DBA” group was shifted to the right into the positive range that stands for greater downward movement..... 71

Figure 42 The Teflon cylinder serving as a cavity model. Flowable composite was applied to the outer contour simulating enamel in order to serve as a reference point for the rigid registration. 79

Figure 43 Schematic drawing of the Teflon model. 79

Figure 44 The displacement vector field in a non-adhesive “Teflon” cavity with the x-plane of the micro-CT scan in the background with two different views (A) and (B). Glyphs were scaled by a factor of 5 to enhance visibility. Polymerization shrinkage vectors pointed to the center, with lateral movement greater at one side denoting the site of first detachment from the cavity walls. 80

Figure 45 The probability density function of the vector lengths in the “Teflon” group shows a multimodal distribution of the values. The first peak relates to the very small vectors that can be found close to the center of the restoration, the second peak can be linked to the small vectors at the restoration side with less movement, while the third peak stands for the main quantity of shrinkage vectors in the “Teflon” group that are directed towards the center of the restoration. 81

Figure 46 The probability density function of the filler movements in the z-direction in the “Teflon” group shows a multimodal distribution with 4 peaks (grey color). The areas below the separate peaks are joined into one area (pink color). The first and second peaks conform to upward shrinkage movement that was found at the cavity floor and the lower restoration part. The third peak constitutes the large quantity of small axial movement with slight

downward shrinkage which can be related to the middle part of the restoration where the glass beads moved mainly in horizontal direction toward the restoration center. The last peak can be linked to the downward movement of glass beads at the free surface of the restoration. 82

Figure 47 The experimental composite was placed on a Teflon disc and exhibited the “free shrinkage” and light was applied from above. Shrinkage vectors pointed toward the center of the composite and the y-plane (A) and z-plane (B) of the micro-CT scan were seen in the background. The composite in contact with the Teflon disc displayed almost no shrinkage vectors. Glyphs were scaled by a factor of 5 to enhance visibility. 85

Figure 48 Schematic drawing of composite before (A) and after (B) light-curing on the Teflon disc. A completely smooth surface would even allow for shrinkage movement on the Teflon disc surface toward the center. 86

Figure 49 Diagrammatic presentation of the “experimental” cavity with enamel at the cavity floor and dentin margins to study the effect of the bonding substrate on the shrinkage direction (A) and the “cylindrical” cavity that represents a cylindrical class I cavity (B). . 92

Figure 50 The displacement vector field of the “experimental-self-etch” cavity, with the x-plane (A) and the z-plane (B) of the micro-CT scan in the background. Glyphs were scaled by a factor of 5 to enhance visibility. Large shrinkage vectors were detected in the upper restoration part and small vectors pointed away from cavity walls. 94

Figure 51 SEM images (x200) of the “experimental-self-etch” group with a defective dentin margin (A) and an intact bond at the enamel floor (B). One traceable glass filler is marked by the star *. 94

Figure 52 The displacement vector field of the “experimental-total-etch” cavity with the x-plane (A) and the z-plane (B) of the micro-CT scan in the background. It showed downward shrinkage at the upper part of the restoration and deviation of the shrinkage vectors toward one side; at the lower part (quarter) small vectors pointed upward. Glyphs were scaled by a factor of 5 to enhance visibility. 95

Figure 53 SEM images (x200) of the “experimental-total-etch” group with both an intact dentin margin (A) and an intact bond at the enamel floor (B). One traceable glass filler is marked by the star *..... 95

Figure 54 The displacement vector field of the “cylindrical-total-etch” cavity, with the x-plane (A) and the z-plane (B) of the micro-CT scan in the background. Glyphs were scaled by a factor of 5 to enhance visibility. Downward shrinkage at the upper restoration part and smaller shrinkage upward pointing upward at the cavity floor. 96

Figure 55 SEM images (x200) of the “cylindrical-total-etch” cavity displaying an intact bond at the enamel margin (A), while the bond with the dentin floor was defective (B). One traceable glass filler is marked by the star *.....	96
Figure 56 The probability density function of the vector lengths in the four groups. The peaks of the vector length values of all groups are located in the range below 30 μm. The “experimental-total-etch” (lila) and the “cylindrical-self-etch” (orange) groups have a similar curve with greatest frequency of vectors at about 20 μm. The “cylindrical-total-etch” (green) has its peak at a lower level, but with more vectors and larger vector length values. The “experimental-self-etch” (turquoise) has the peak at about 15 μm and large vectors also in a similar distribution as in the other groups.	98
Figure 57 The probability density function of the filler movements in the z-direction in the four groups. 3 Groups have a multimodal distribution of the axial filler movement values. The “experimental-self-etch” group (turquoise) has the first peak in the negative range of small movements related to upward shrinkage found at the cavity floor, while the second peak is located in the positive range that can be attributed to the downward shrinkage of the free surface. The “experimental-total-etch” group (lila) has only one peak that is located in the negative range at about -15 μm which relates to the upward shrinkage; yet, another large portion of the values are in the positive range that conforms to the downward movement of the free restoration surface. In the “cylindrical-self-etch” group (orange) the two peaks are situated in the negative range denoting upward shrinkage. In the “cylindrical-total-etch” group (green) one peak was located in the negative values but the majority of vectors are in the positive range which indicate downward shrinkage.	100
Figure 58 Tetric EvoFlow, Ivoclar Vivadent.....	121
Figure 59 Radiolucent glass fillers, Sigmund Lindner	121
Figure 60 Adper Easy Bond, 3M ESPE	121
Figure 61 OptiBond FL, Kerr	121
Figure 62 VITA CERAMICS ETCH; VITA.....	121
Figure 63 ESPE Sil, 3M ESPE	121
Figure 64 Elipar FreeLight2, 3M ESPE	122
Figure 65 Electronic scale (Sartorius research, Germany)	122
Figure 66 Scanning electron microscope ZEISS GEMINI® FESEM, SUPRA™ 55VP, Carl Zeiss SMT AG, Oberkochen, Germany	123
Figure 67 Slow speed water-cooled diamond saw Isomet, Beuhler, Illinois, USA	123
Figure 68 Polishing machine Leco VP 100, GmbH, Neuss, Germany	123

7 Annex

7.1 Materials and equipments



Figure 58 Tetric EvoFlow, Ivoclar Vivadent

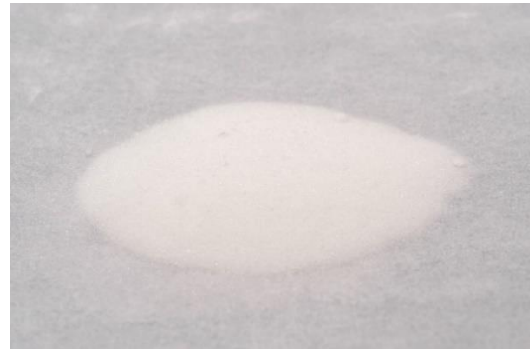


Figure 59 Radiolucent glass fillers, Sigmund Lindner

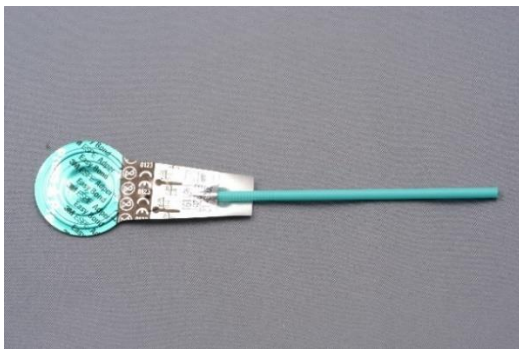


Figure 60 Adper Easy Bond, 3M ESPE



Figure 61 OptiBond FL, Kerr



Figure 62 VITA CERAMICS ETCH;
VITA

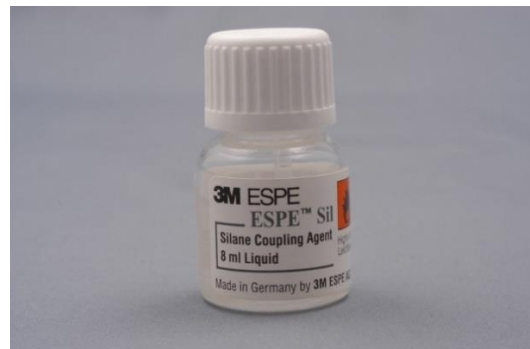


Figure 63 ESPE Sil, 3M ESPE



Figure 64 Elipar FreeLight2, 3M ESPE



Figure 65 Electronic scale (Sartorius research, Germany)

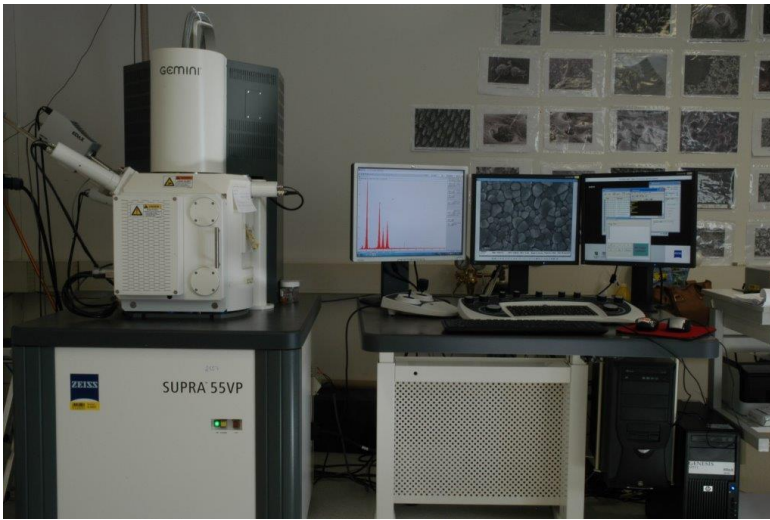


Figure 66 Scanning electron microscope ZEISS GEMINI® FESEM, SUPRA™ 55VP, Carl Zeiss SMT AG, Oberkochen, Germany






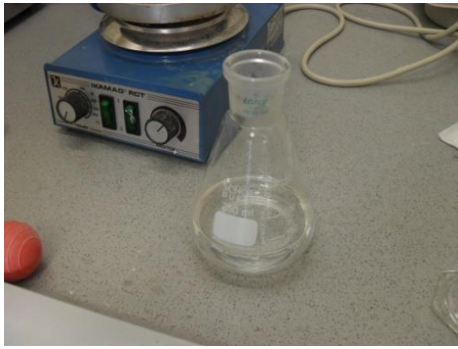
Figure 67 Slow speed water-cooled diamond saw Isomet, Beuhler, Illinois, USA



Figure 68 Polishing machine Leco VP 100, GmbH, Neuss, Germany

7.2 Protocol for the silanization of the traceable glass beads

	<p>Step 1: Glass beads 40-70 µm (Sigmund Lindner GmbH, Warmensteinach, Germany)</p>
	<p>15 g of glass beads equal 10 ml volume</p>
	<p>Step 2: Ethanol (99.9% purity) and Sil Silane Coupling Agent (3-methacryloyloxy-propyltrimethoxysilane), 3M ESPE</p>




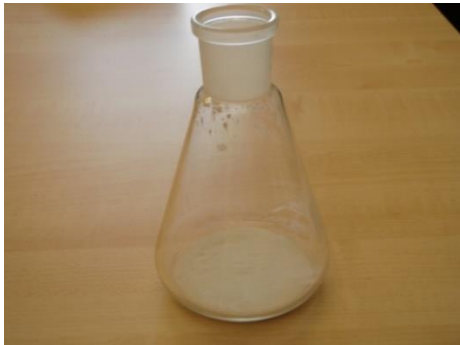


Solution mixture composed of 97 ml ethanol + 3 ml silane coupling agent



Step 3: Glass beads are added to the solution mixture, automatic stirring at room temperature for 30 min followed by stirring at 60°C for another 30 min



Step 4: Glass beads in solution are centrifuged for 10 min at 4000 rpm speed

	<p>Step 5: Silanized glass beads are washed by acetone (20 ml) three times</p>
	<p>Step 6: Silanized glass beads are left to dry overnight</p>
	<p>Step 7: Dry powder of silanized glass beads</p>
	<p>Step 8: Powder of silanized glass beads is stored in a glass container</p>

8 References

Abbas G, Fleming GJ, Harrington E, Shortall AC, Burke FJ (2003). Cuspal movement and microleakage in premolar teeth restored with a packable composite cured in bulk or in increments. *Journal of dentistry* 31(6):437-444.

Alomari QD, Reinhardt JW, Boyer DB (2001). Effect of liners on cusp deflection and gap formation in composite restorations. *Operative dentistry* 26(4):406-411.

Alster D, Feilzer AJ, de Gee AJ, Davidson CL (1997). Polymerization contraction stress in thin resin composite layers as a function of layer thickness. *Dental materials : official publication of the Academy of Dental Materials* 13(3):146-150.

Arganda-Carreras I, Sorzano CS, Marabini R, Carazo J, Ortiz-de-Solorzano C, Kybic J (2006). Consistent and Elastic Registration of Histological Sections Using Vector-Spline Regularization. In: *Computer Vision Approaches to Medical Image Analysis*. R Beichel and M Sonka editors: Springer Berlin Heidelberg, pp. 85-95.

Armstrong S, Geraldeli S, Maia R, Raposo LH, Soares CJ, Yamagawa J (2010). Adhesion to tooth structure: a critical review of "micro" bond strength test methods. *Dental materials : official publication of the Academy of Dental Materials* 26(2):e50-62.

Asmussen E, Jorgensen KD (1972). A microscopic investigation of the adaptation of some plastic filling materials to dental cavity walls. *Acta odontologica Scandinavica* 30(1):3-21.

Ausiello P, Apicella A, Davidson CL (2002). Effect of adhesive layer properties on stress distribution in composite restorations--a 3D finite element analysis. *Dental materials : official publication of the Academy of Dental Materials* 18(4):295-303.

Badole GP, Warhadpande MM, Meshram GK, Bahadure RN, Tawani SG, Tawani G *et al.* (2013). A comparative evaluation of cytotoxicity of root canal sealers: an in vitro study. *Restor Dent Endod* 38(4):204-209.

Bauer S, Wiest R, Nolte LP, Reyes M (2013). A survey of MRI-based medical image analysis for brain tumor studies. *Physics in medicine and biology* 58(13):R97-R129.

Bausch JR, de Lange K, Davidson CL, Peters A, de Gee AJ (1982). Clinical significance of polymerization shrinkage of composite resins. *The Journal of prosthetic dentistry* 48(1):59-67.

Bekkedahl N (1949). Volume dilatometry. *Journal of research of the National Bureau of Standards* 43(2):145-156.

Bouillaguet S, Gamba J, Forchelet J, Krejci I, Wataha JC (2006). Dynamics of composite polymerization mediates the development of cuspal strain. *Dental materials : official publication of the Academy of Dental Materials* 22(10):896-902.

Bouxsein ML, Boyd SK, Christiansen BA, Guldberg RE, Jepsen KJ, Muller R (2010). Guidelines for assessment of bone microstructure in rodents using micro-computed tomography. *Journal of bone and mineral research : the official journal of the American Society for Bone and Mineral Research* 25(7):1468-1486.

Bowen RL (1956). Use of epoxy resins in restorative materials. *Journal of dental research* 35(3):360-369.

Bowen RL inventor (1962). Dental filling material comprising vinyl-silane treated fused silica and a binder consisting of the reaction product of bis-phenol and glycidyl acrylate, U.S. Patent No. 3,066,112, November 27, 1962.

Bowen RL (1963). Properties of a silica-reinforced polymer for dental restorations. *Journal of the American Dental Association (1939)* 66(57-64).

Bowen RL (1967). Adhesive bonding of various materials to hard tooth tissues. VI. Forces developing in direct-filling materials during hardening. *Journal of the American Dental Association (1939)* 74(3):439-445.

Bowen RL, Nemoto K, Rapson JE (1983). Adhesive bonding of various materials to hard tooth tissues: forces developing in composite materials during hardening. *Journal of the American Dental Association (1939)* 106(4):475-477.

Braem M, Lambrechts P, Vanherle G, Davidson CL (1987). Stiffness increase during the setting of dental composite resins. *Journal of dental research* 66(12):1713-1716.

Braga RR, Ferracane JL (2002). Contraction stress related to degree of conversion and reaction kinetics. *Journal of dental research* 81(2):114-118.

Braga RR, Boaro LCC, Kuroe T, Azevedo CLN, Singer JM (2006). Influence of cavity dimensions and their derivatives (volume and 'C' factor) on shrinkage stress development and microleakage of composite restorations. *Dental Materials* 22(9):818-823.

Braga RR, Meira JB, Boaro LC, Xavier TA (2010). Adhesion to tooth structure: a critical review of "macro" test methods. *Dental materials : official publication of the Academy of Dental Materials* 26(2):e38-49.

Brekelmans WA, Poort HW, Slooff TJ (1972). A new method to analyse the mechanical behaviour of skeletal parts. *Acta orthopaedica Scandinavica* 43(5):301-317.

- Brodbelt RH, O'Brien WJ, Fan PL, Frazer-Dib JG, Yu R (1981). Translucency of human dental enamel. *Journal of dental research* 60(10):1749-1753.
- Buonocore MG (1955). A simple method of increasing the adhesion of acrylic filling materials to enamel surfaces. *Journal of dental research* 34(6):849-853.
- Buonocore MG, Wileman W, Brudevold F (1956). A Report on a Resin Composition Capable of Bonding to Human Dentin Surfaces. *Journal of dental research* 35(6):846-851.
- Cara RR, Fleming GJ, Palin WM, Walmsley AD, Burke FJ (2007). Cuspal deflection and microleakage in premolar teeth restored with resin-based composites with and without an intermediary flowable layer. *Journal of dentistry* 35(6):482-489.
- Chang HS, Cho KJ, Park SJ, Lee BN, Hwang YC, Oh WM *et al.* (2013). Thermal analysis of bulk filled composite resin polymerization using various light curing modes according to the curing depth and approximation to the cavity wall. *Journal of applied oral science : revista FOB* 21(4):293-299.
- Cheetham JJ, Palamara JE, Tyas MJ, Burrow MF (2014). Evaluation of the interfacial work of fracture of glass-ionomer cements bonded to dentin. *Journal of the mechanical behavior of biomedical materials* 29(4):427-437.
- Chen HY, Manhart J, Hickel R, Kunzelmann KH (2001). Polymerization contraction stress in light-cured packable composite resins. *Dental materials : official publication of the Academy of Dental Materials* 17(3):253-259.
- Chen HY, Manhart J, Kunzelmann KH, Hickel R (2003). Polymerization contraction stress in light-cured compomer restorative materials. *Dental materials : official publication of the Academy of Dental Materials* 19(7):597-602.
- Cheng CF, Wu KM, Chen YT, Hung SL (2013). Bacterial adhesion to antibiotic-loaded guided tissue regeneration membranes - A scanning electron microscopy study. *Journal of the Formosan Medical Association = Taiwan yi zhi*.
- Chiang YC, Roesch P, Lin CL, Hickel R, Kunzelmann K Deformation Analysis of Composite Polymerization Shrinkage from μ CT Images. Annual Meeting of the Academy of Dental Materials 2008, Wuerzburg, Germany.
- Chiang YC, Roesch P, Kunzelmann KH (2009). Polymerization Shrinkage with Light-Initiated Dental Composites. Germany, Ludwig-Maximilians-Universitaet Muenchen.
- Chiang YC, Rosch P, Dabanoglu A, Lin CP, Hickel R, Kunzelmann KH (2010). Polymerization composite shrinkage evaluation with 3D deformation analysis from microCT images. *Dental materials : official publication of the Academy of Dental Materials* 26(3):223-231.

Cho BH, Dickens SH, Bae JH, Chang CG, Son HH, Um CM (2002). Effect of interfacial bond quality on the direction of polymerization shrinkage flow in resin composite restorations. *Operative dentistry* 27(3):297-304.

Cho E, Sadr A, Inai N, Tagami J (2011). Evaluation of resin composite polymerization by three dimensional micro-CT imaging and nanoindentation. *Dental materials : official publication of the Academy of Dental Materials* 27(11):1070-1078.

Choi KK, Condon JR, Ferracane JL (2000). The effects of adhesive thickness on polymerization contraction stress of composite. *Journal of dental research* 79(3):812-817.

Chuang SF, Chen TY, Chang CH (2008). Application of Digital Image Correlation Method to Study Dental Composite Shrinkage. *Strain* 44(3):231-238.

Chuang SF, Chang CH, Chen TY (2011a). Contraction behaviors of dental composite restorations--finite element investigation with DIC validation. *Journal of the mechanical behavior of biomedical materials* 4(8):2138-2149.

Chuang SF, Chang CH, Chen TY (2011b). Spatially resolved assessments of composite shrinkage in MOD restorations using a digital-image-correlation technique. *Dental materials : official publication of the Academy of Dental Materials* 27(2):134-143.

Ciamponi AL, Del Portillo Lujan VA, Ferreira Santos JF (1994). Effectiveness of reflective wedges on the polymerization of composite resins. *Quintessence international (Berlin, Germany : 1985)* 25(9):599-602.

Clementino-Luedemann TNR, Dabanoglu A, Ilie N, Hickel R, Kunzelmann K (2006). Micro-computed tomographic evaluation of a new enzyme solution for caries removal in deciduous teeth. *Dental materials journal* 25(4):675-683.

Clementino-Luedemann TNR, Kunzelmann K (2006). Mineral concentration of natural human teeth by a commercial micro-CT. *Dental materials journal* 25(1):113-119.

Condon JR, Ferracane JL (1998). Reduction of composite contraction stress through non-bonded microfiller particles. *Dental materials : official publication of the Academy of Dental Materials* 14(4):256-260.

Cook WD, Forrest M, Goodwin AA (1999). A simple method for the measurement of polymerization shrinkage in dental composites. *Dental materials : official publication of the Academy of Dental Materials* 15(6):447-449.

Cramer NB, Stansbury JW, Bowman CN (2011). Recent advances and developments in composite dental restorative materials. *Journal of dental research* 90(4):402-416.

Davidson CL, de Gee AJ (1984). Relaxation of polymerization contraction stresses by flow in dental composites. *Journal of dental research* 63(2):146-148.

Davidson CL, de Gee AJ, Feilzer A (1984). The competition between the composite-dentin bond strength and the polymerization contraction stress. *Journal of dental research* 63(12):1396-1399.

Davidson CL, Feilzer AJ (1997). Polymerization shrinkage and polymerization shrinkage stress in polymer-based restoratives. *Journal of dentistry* 25(6):435-440.

de Gee AF, Feilzer AJ, Davidson CL (1993). True linear polymerization shrinkage of unfilled resins and composites determined with a linometer. *Dental materials : official publication of the Academy of Dental Materials* 9(1):11-14.

de Gee AJ, Davidson CL, Smith A (1981). A modified dilatometer for continuous recording of volumetric polymerization shrinkage of composite restorative materials. *Journal of dentistry* 9(1):36-42.

de la Macorra JC, Cabrera E (2012). Regional variations of microTBS of light- and chemically cured resin composite restorations in clinically relevant situations. *The journal of adhesive dentistry* 14(6):551-559.

de Melo Monteiro GQ, Montes MA, Rolim TV, de Oliveira Mota CC, de Barros Correia Kyotoku B, Gomes AS *et al.* (2011). Alternative methods for determining shrinkage in restorative resin composites. *Dental materials : official publication of the Academy of Dental Materials* 27(8):e176-185.

De Santis R, Mollica F, Prisco D, Rengo S, Ambrosio L, Nicolais L (2005). A 3D analysis of mechanically stressed dentin-adhesive-composite interfaces using X-ray micro-CT. *Biomaterials* 26(3):257-270.

DeLong R, Pintado M, Douglas WH (1985). Measurement of change in surface contour by computer graphics. *Dental materials : official publication of the Academy of Dental Materials* 1(1):27-30.

Dionysopoulos D, Papadopoulos C, Kouros P, Tsitrou E, Koliniotou-Koumpia E (2013). Temperature Rise During Photo-polymerization Under Ceramic Restorations. *Oral health and dental management* 12(4):273-278.

Donly KJ, Wild TW, Bowen RL, Jensen ME (1989). An in vitro investigation of the effects of glass inserts on the effective composite resin polymerization shrinkage. *Journal of dental research* 68(8):1234-1237.

Dullin P (1998). Development of a measuring system for the determination of the polymerization behavior of dental composite materials. "Entwicklung eines Mess-Systems

zur Untersuchung des Polymerisationsverhaltens von zahnmedizinischen Kompositfüllungswerkstoffen." (Thesis in Engineering Technology "Feinwerk und Mikrotechnik"), University of Munich.

Ernst CP, Meyer GR, Klocker K, Willershausen B (2004). Determination of polymerization shrinkage stress by means of a photoelastic investigation. *Dental materials : official publication of the Academy of Dental Materials* 20(4):313-321.

Fano V, Ortalli I, Pizzi S, Bonanini M (1997). Polymerization shrinkage of microfilled composites determined by laser beam scanning. *Biomaterials* 18(6):467-470.

Farah JW, Craig RG, Sikarskie DL (1973). Photoelastic and finite element stress analysis of a restored axisymmetric first molar. *Journal of biomechanics* 6(5):511-520.

Feilzer AJ, De Gee AJ, Davidson CL (1987). Setting stress in composite resin in relation to configuration of the restoration. *Journal of dental research* 66(11):1636-1639.

Feilzer AJ, De Gee AJ, Davidson CL (1988). Curing contraction of composites and glass-ionomer cements. *The Journal of prosthetic dentistry* 59(3):297-300.

Feilzer AJ, De Gee AJ, Davidson CL (1989). Increased wall-to-wall curing contraction in thin bonded resin layers. *Journal of dental research* 68(1):48-50.

Feilzer AJ, De Gee AJ, Davidson CL (1990). Quantitative determination of stress reduction by flow in composite restorations. *Dental materials : official publication of the Academy of Dental Materials* 6(3):167-171.

Ferracane JL (2005). Developing a more complete understanding of stresses produced in dental composites during polymerization. *Dental materials : official publication of the Academy of Dental Materials* 21(1):36-42.

Ferracane JL (2008). Buonocore Lecture. Placing dental composites--a stressful experience. *Operative dentistry* 33(3):247-257.

Filtek LS, Technical Product Profile (2007). USA: 3M ESPE Dental Products.

Filtek™ Silorane, Silorane System Adhesive, Technical Product Profile (2007). In: ME AG editor. Seefeld, Germany, pp. 40.

Fischer B, Modersitzki J (2008). Ill-posed medicine-an introduction to image registration. *Inverse Problems* 24(3):034008(034016pp).

Fleming GJ, Hall DP, Shortall AC, Burke FJ (2005). Cuspal movement and microleakage in premolar teeth restored with posterior filling materials of varying reported volumetric shrinkage values. *Journal of dentistry* 33(2):139-146.

Fleming GJ, Cara RR, Palin WM, Burke FJ (2007a). Cuspal movement and microleakage in premolar teeth restored with resin-based filling materials cured using a 'soft-start' polymerisation protocol. *Dental materials : official publication of the Academy of Dental Materials* 23(5):637-643.

Fleming GJ, Khan S, Afzal O, Palin WM, Burke FJ (2007b). Investigation of polymerisation shrinkage strain, associated cuspal movement and microleakage of MOD cavities restored incrementally with resin-based composite using an LED light curing unit. *Journal of dentistry* 35(2):97-103.

Fogleman EA, Kelly MT, Grubbs WT (2002). Laser interferometric method for measuring linear polymerization shrinkage in light cured dental restoratives. *Dental materials : official publication of the Academy of Dental Materials* 18(4):324-330.

Gonzalez-Lopez S, Lucena-Martin C, de Haro-Gasquet F, Vilchez-Diaz MA, de Haro-Munoz C (2004). Influence of different composite restoration techniques on cuspal deflection: an in vitro study. *Operative dentistry* 29(6):656-660.

Goracci C, Sadek FT, Monticelli F, Cardoso PE, Ferrari M (2004). Microtensile bond strength of self-etching adhesives to enamel and dentin. *The journal of adhesive dentistry* 6(4):313-318.

Guven EP, Yalvac ME, Kayahan MB, Sunay H, Sahin F, Bayirli G (2013). Human tooth germ stem cell response to calcium-silicate based endodontic cements. *Journal of applied oral science : revista FOB* 21(4):351-357.

Hansen EK (1982a). Visible light-cured composite resins: polymerization contraction, contraction pattern and hygroscopic expansion. *Scandinavian journal of dental research* 90(4):329-335.

Hansen EK (1982b). Contraction pattern of composite resins in dentin cavities. *Scandinavian journal of dental research* 90(6):480-483.

Hayashi T, Kobayashi S, Asakura M, Kawase M, Ueno A, Uematsu Y *et al.* (2013). Immature muscular tissue differentiation into bone-like tissue by bone morphogenetic proteins in vitro, with ossification potential in vivo. *Journal of biomedical materials research Part A*.

Hegdahl T, Gjerdet NR (1977). Contraction stresses of composite resin filling materials. *Acta odontologica Scandinavica* 35(4):191-195.

Hill DL, Batchelor PG, Holden M, Hawkes DJ (2001). Medical image registration. *Physics in medicine and biology* 46(3):R1-45.

Huang TTY, Jones AS, He LH, Darendeliler MA, Swain MV (2007). Characterisation of enamel white spot lesions using X-ray micro-tomography. *Journal of dentistry* 35(9):737-743.

Huang YH, Quan C, Tay CJ, Chen LJ (2005). Shape measurement by the use of digital image correlation. *Optical Engineering* 44(8):087011-087011.

Ikeda T, Uno S, Tanaka T, Kawakami S, Komatsu H, Sano H (2002). Relation of enamel prism orientation to microtensile bond strength. *American journal of dentistry* 15(2):109-113.

Inai N, Katahira N, Hashimoto K, Tagami J, Hirakimoto A, Marshall SJ *et al.* Microfocus X-ray CT Analysis of Shrinking Direction in Resin Composite 2002, San Diego, California; 2014.

Inoue S, Vargas MA, Abe Y, Yoshida Y, Lambrechts P, Vanherle G *et al.* (2001). Microtensile bond strength of eleven contemporary adhesives to dentin. *The journal of adhesive dentistry* 3(3):237-245.

IPS Empress CAD, Technical Product Profile (2007). In: IV AG editor. Schaan, Liechtenstein, pp. 48.

Kakaboura A, Rahiotis C, Watts D, Silikas N, Eliades G (2007). 3D-marginal adaptation versus setting shrinkage in light-cured microhybrid resin composites. *Dental materials : official publication of the Academy of Dental Materials* 23(3):272-278.

Kapferer I, Beier US, Jank S, Persson R (2013). Randomized controlled trial: lip piercing: the impact of material on microbiological findings. *Pediatric dentistry* 35(1):E23-28.

Kemp-Scholte CM, Davidson CL (1990). Complete marginal seal of Class V resin composite restorations effected by increased flexibility. *Journal of dental research* 69(6):1240-1243.

Kinomoto Y, Torii M (1998). Photoelastic analysis of polymerization contraction stresses in resin composite restorations. *Journal of dentistry* 26(2):165-171.

Kinomoto Y, Torii M, Takeshige F, Ebisu S (1999). Comparison of polymerization contraction stresses between self- and light-curing composites. *Journal of dentistry* 27(5):383-389.

- Kinomoto Y, Torii M, Takeshige F, Ebisu S (2000). Polymerization contraction stress of resin composite restorations in a model Class I cavity configuration using photoelastic analysis. *Journal of esthetic dentistry* 12(6):309-319.
- Kleverlaan CJ, Feilzer AJ (2005). Polymerization shrinkage and contraction stress of dental resin composites. *Dental materials : official publication of the Academy of Dental Materials* 21(12):1150-1157.
- Kramer N, Lohbauer U, Garcia-Godoy F, Frankenberger R (2008). Light curing of resin-based composites in the LED era. *American journal of dentistry* 21(3):135-142.
- Kullmann W (1989). [Studies on the course of polymerization shrinkage of self-cured and light-cured composites]. *Deutsche zahnärztliche Zeitschrift* 44(9):711-713.
- Kunzelmann K (1996). Analysis and quantification of wear of filling materials in vivo and in vitro. "Verschleißanalyse und -quantifizierung von Füllungsmaterialien in vivo und in vitro." ("Habilitationsschrift"), University of Munich.
- Kunzelmann KH (2008). Aufbau der Kompositfüllungswerkstoffe. In: Zahnärztliche Werkstoffe und ihre Verarbeitung, Bd 2: Werkstoffe unter klinischen Aspekten. KE Heinrich Friedrich Kappert editor. Stuttgart, Germany: Georg Thieme Verlag KG, pp. 204-241.
- Kweon HJ, Ferracane J, Kang K, Dhont J, Lee IB (2013). Spatio-temporal analysis of shrinkage vectors during photo-polymerization of composite. *Dental materials : official publication of the Academy of Dental Materials* 29(12):1236-1243.
- Kwon O-H, Park S-H (2012). Evaluation of internal adaptation of dental adhesive restorations using micro-CT. *Restor Dent Endod* 37(1):41-49.
- Kwon Y, Ferracane J, Lee IB (2012). Effect of layering methods, composite type, and flowable liner on the polymerization shrinkage stress of light cured composites. *Dental materials : official publication of the Academy of Dental Materials* 28(7):801-809.
- Kybic J, Unser M (2003). Fast parametric elastic image registration. *Image Processing, IEEE Transactions on* 12(11):1427-1442.
- Labella R, Lambrechts P, Van Meerbeek B, Vanherle G (1999). Polymerization shrinkage and elasticity of flowable composites and filled adhesives. *Dental materials : official publication of the Academy of Dental Materials* 15(2):128-137.
- Lai JH, Johnson AE (1993). Measuring polymerization shrinkage of photo-activated restorative materials by a water-filled dilatometer. *Dental materials : official publication of the Academy of Dental Materials* 9(2):139-143.

Lang H, Rampado M, Mullejans R, Raab WH (2004). Determination of the dynamics of restored teeth by 3D electronic speckle pattern interferometry. *Lasers in surgery and medicine* 34(4):300-309.

Lee HL, Jr., Swartz ML, Smith FF (1969). Physical properties of four thermosetting dental restorative resins. *Journal of dental research* 48(4):526-535.

Lee IB, Cho BH, Son HH, Um CM (2005). A new method to measure the polymerization shrinkage kinetics of light cured composites. *Journal of oral rehabilitation* 32(4):304-314.

Lee IB, Min SH, Seo DG (2012). A new method to measure the polymerization shrinkage kinetics of composites using a particle tracking method with computer vision. *Dental materials : official publication of the Academy of Dental Materials* 28(2):212-218.

Lee MR, Cho BH, Son HH, Um CM, Lee IB (2007). Influence of cavity dimension and restoration methods on the cusp deflection of premolars in composite restoration. *Dental materials : official publication of the Academy of Dental Materials* 23(3):288-295.

Leprince JG, Palin WM, Hadis MA, Devaux J, Leloup G (2013). Progress in dimethacrylate-based dental composite technology and curing efficiency. *Dental materials : official publication of the Academy of Dental Materials* 29(2):139-156.

Li J, Fok AS, Satterthwaite J, Watts DC (2009). Measurement of the full-field polymerization shrinkage and depth of cure of dental composites using digital image correlation. *Dental materials : official publication of the Academy of Dental Materials* 25(5):582-588.

Li J, Li H, Liu X, Fok A A glass model cavity system for shrinkage stress assessment. IADR/AADR/CADR 89th General Session 2011, San Diego, Calif.;1578.

Lindberg A, Peutzfeldt A, van Dijken JW (2004). Curing depths of a universal hybrid and a flowable resin composite cured with quartz tungsten halogen and light-emitting diode units. *Acta odontologica Scandinavica* 62(2):97-101.

Liu Q, Ding J, Chambers DE, Debnath S, Wunder SL, Baran GR (2001). Filler-coupling agent-matrix interactions in silica/polymethylmethacrylate composites. *Journal of biomedical materials research* 57(3):384-393.

Lopes HB, Santos TD, de Oliveira FS, Freitas GP, de Almeida AL, Gimenes R *et al.* (2013). Poly(vinylidene-trifluoroethylene)/ barium titanate composite for in vivo support of bone formation. *Journal of biomaterials applications*.

Lu H, Stansbury JW, Dickens SH, Eichmiller FC, Bowman CN (2004a). Probing the origins and control of shrinkage stress in dental resin composites. II. Novel method of simultaneous

measurement of polymerization shrinkage stress and conversion. *Journal of biomedical materials research Part B, Applied biomaterials* 71(1):206-213.

Lu H, Stansbury JW, Dickens SH, Eichmiller FC, Bowman CN (2004b). Probing the origins and control of shrinkage stress in dental resin-composites: I. Shrinkage stress characterization technique. *Journal of materials science Materials in medicine* 15(10):1097-1103.

Lung CY, Matinlinna JP (2012). Aspects of silane coupling agents and surface conditioning in dentistry: an overview. *Dental materials : official publication of the Academy of Dental Materials* 28(5):467-477.

Lutz F, Luescher B, Ochsenbein H, Muehleman HR (1976). *Adhaesive Zahnheilkunde* Zurich: Juris Druck und Verlag.

Lutz F, Luscher B, Ochsenbein H (1977). [In vitro evaluation of the adaptation and quality of the margins in various composite systems]. *Schweizerische Monatsschrift fur Zahnheilkunde = Revue mensuelle suisse d'odonto-stomatologie / SSO* 87(8):752-763.

Lutz F, Phillips RW (1983). A classification and evaluation of composite resin systems. *The Journal of prosthetic dentistry* 50(4):480-488.

Lutz F, Krejci I, Luescher B, Oldenburg TR (1986). Improved proximal margin adaptation of Class II composite resin restorations by use of light-reflecting wedges. *Quintessence international (Berlin, Germany : 1985)* 17(10):659-664.

Magne P (2007). Efficient 3D finite element analysis of dental restorative procedures using micro-CT data. *Dental materials : official publication of the Academy of Dental Materials* 23(5):539-548.

Meira JB, Braga RR, de Carvalho AC, Rodrigues FP, Xavier TA, Ballester RY (2007). Influence of local factors on composite shrinkage stress development--a finite element analysis. *The journal of adhesive dentistry* 9(6):499-503.

Meleo D, Manzon L, Pecci R, Zuppante F, Bedini R (2012). A proposal of microtomography evaluation for restoration interface gaps. *Annali dell'Istituto superiore di sanita* 48(1):83-88.

Meredith N, Setchell DJ (1997). In vitro measurement of cuspal strain and displacement in composite restored teeth. *Journal of dentistry* 25(3-4):331-337.

Miletic V, Manojlovic D, Mitrovic N, Stankovic TS, Maneski T (2011). Analysis of local shrinkage patterns of self-adhering and flowable composites using 3D digital image correlation. *Quintessence international (Berlin, Germany : 1985)* 42(9):797-804.

Moorthy A, Hogg CH, Dowling AH, Grufferty BF, Benetti AR, Fleming GJ (2012). Cuspal deflection and microleakage in premolar teeth restored with bulk-fill flowable resin-based composite base materials. *Journal of dentistry* 40(6):500-505.

Morin DL, Douglas WH, Cross M, DeLong R (1988). Biophysical stress analysis of restored teeth: experimental strain measurement. *Dental materials : official publication of the Academy of Dental Materials* 4(1):41-48.

Mungara J, Philip J, Joseph E, Rajendran S, Elangovan A, Selvaraju G (2013). Comparative evaluation of fluoride release and recharge of pre-reacted glass ionomer composite and nano-ionomeric glass ionomer with daily fluoride exposure: an in vitro study. *Journal of the Indian Society of Pedodontics and Preventive Dentistry* 31(4):234-239.

Naoum SJ, Ellakwa A, Morgan L, White K, Martin FE, Lee IB (2012). Polymerization profile analysis of resin composite dental restorative materials in real time. *Journal of dentistry* 40(1):64-70.

Oliveira KM, Consani S, Goncalves LS, Brandt WC, Ccahuana-Vasquez RA (2012). Photoelastic evaluation of the effect of composite formulation on polymerization shrinkage stress. *Brazilian oral research* 26(3):202-208.

Onose H, Sano H, Kanto H, Ando S, Hasuike T (1985). Selected curing characteristics of light-activated composite resins. *Dental materials : official publication of the Academy of Dental Materials* 1(2):48-54.

Opdam NJ, Feilzer AJ, Roeters JJ, Smale I (1998). Class I occlusal composite resin restorations: in vivo post-operative sensitivity, wall adaptation, and microleakage. *American journal of dentistry* 11(5):229-234.

Pabis LV, Xavier TA, Rosa EF, Rodrigues FP, Meira JB, Lima RG *et al.* (2012). A method to investigate the shrinkage stress developed by resin-composites bonded to a single flat surface. *Dental materials : official publication of the Academy of Dental Materials* 28(4):e27-34.

Palin WM, Fleming GJ, Nathwani H, Burke FJ, Randall RC (2005). In vitro cuspal deflection and microleakage of maxillary premolars restored with novel low-shrink dental composites. *Dental materials : official publication of the Academy of Dental Materials* 21(4):324-335.

Park JW, Ferracane JL (2005). Measuring the residual stress in dental composites using a ring slitting method. *Dental materials : official publication of the Academy of Dental Materials* 21(9):882-889.

Park JW, Ferracane JL (2006). Residual Stress in Composites with the Thin-ring-slitting Approach. *Journal of dental research* 85(10):945-949.

Pearson GJ, Hegarty SM (1989). Cusp movement of molar teeth with composite filling materials in conventional and modified MOD cavities. *British dental journal* 166(5):162-165.

Penn RW (1986). A recording dilatometer for measuring polymerization shrinkage. *Dental materials : official publication of the Academy of Dental Materials* 2(2):78-79.

Pereira RA, Araujo PA, Castaneda-Espinosa JC, Mondelli RF (2008). Comparative analysis of the shrinkage stress of composite resins. *Journal of applied oral science : revista FOB* 16(1):30-34.

Phillips RW, Lutz F, Roulet JF (1983). [Lateral tooth composites--an assessment of the situation]. *Schweizerische Monatsschrift fur Zahnheilkunde = Revue mensuelle suisse d'odonto-stomatologie / SSO* 93(8):666-673.

Porte A, Lutz F, Lund MR, Swartz ML, Cochran MA (1984). Cavity designs for composite resins. *Operative dentistry* 9(2):50-56.

Price RB, Felix CA, Andreou P (2004). Effects of resin composite composition and irradiation distance on the performance of curing lights. *Biomaterials* 25(18):4465-4477.

Price RB, Fahey J, Felix CM (2010a). Knoop microhardness mapping used to compare the efficacy of LED, QTH and PAC curing lights. *Operative dentistry* 35(1):58-68.

Price RB, Felix CM, Whalen JM (2010b). Factors affecting the energy delivered to simulated class I and class v preparations. *Journal (Canadian Dental Association)* 76(a94).

Price RB, Labrie D, Rueggeberg FA, Felix CM (2010c). Irradiance differences in the violet (405 nm) and blue (460 nm) spectral ranges among dental light-curing units. *Journal of esthetic and restorative dentistry : official publication of the American Academy of Esthetic Dentistry [et al]* 22(6):363-377.

Price RB, McLeod ME, Felix CM (2010d). Quantifying light energy delivered to a Class I restoration. *Journal (Canadian Dental Association)* 76(a23).

Price RB, Rueggeberg FA, Labrie D, Felix CM (2010e). Irradiance uniformity and distribution from dental light curing units. *Journal of esthetic and restorative dentistry : official publication of the American Academy of Esthetic Dentistry [et al]* 22(2):86-101.

Price RB, Labrie D, Whalen JM, Felix CM (2011). Effect of distance on irradiance and beam homogeneity from 4 light-emitting diode curing units. *Journal (Canadian Dental Association)* 77(b9).

Price RB, Sullivan B, Labrie D, Kostylev I Matching the Light Beam Profile to Resin Microhardness Maps. IADR/AADR/CADR 91st General Session 2013, Seattle, Washington;290.

Puckett AD, Smith R (1992). Method to measure the polymerization shrinkage of light-cured composites. *The Journal of prosthetic dentistry* 68(1):56-58.

Qualtrough AJ, Cramer A, Wilson NH, Roulet JF, Noack M (1991). An in vitro evaluation of the marginal integrity of a porcelain inlay system. *The International journal of prosthodontics* 4(6):517-523.

Qvist V, Qvist J (1985). Replica patterns on composite restorations performed in vivo with different acid-etch restorative procedures. *Scandinavian journal of dental research* 93(4):360-370.

Rees JS, Jacobsen PH (1989). The polymerization shrinkage of composite resins. *Dental materials : official publication of the Academy of Dental Materials* 5(1):41-44.

Rees JS, Jagger DC, Williams DR, Brown G, Duguid W (2004). A reappraisal of the incremental packing technique for light cured composite resins. *Journal of oral rehabilitation* 31(1):81-84.

Roberson TM (2006a). In: Sturdevant's Art and Science of Operative Dentistry. TM Roberson, HO Heymann and EJJ Swift editors: Mosby Elsevier, pp. 92-94.

Roberson TM (2006b). In: Sturdevant's Art and Science of Operative Dentistry. TM Roberson, HO Heymann and EJJ Swift editors: Mosby Elsevier, pp. 243-280.

Rodrigues FP, Li J, Silikas N, Ballester RY, Watts DC (2009). Sequential software processing of micro-XCT dental-images for 3D-FE analysis. *Dental Materials* 25(6):e47-e55.

Rodrigues FP, Silikas N, Watts DC, Ballester RY (2012). Finite element analysis of bonded model Class I 'restorations' after shrinkage. *Dental materials : official publication of the Academy of Dental Materials* 28(2):123-132.

Rodriguez VI, Abate PF, Macchi RL (2006). Immediate polymerization shrinkage in light cured restorative resins. *Acta odontologica latinoamericana : AOL* 19(1):3-7.

Rösch P, Chiang YC, Kunzelmann K (2009). Quantification of local polymerisation shrinkage from 3D micro CT images of dental composites. *International Journal of Computer assisted Radiology and Surgery* 4 (Suppl. 1)(200-201.

Roulet JF, Salchow B, Wald M (1991). Margin analysis of posterior composites in vivo. *Dental materials : official publication of the Academy of Dental Materials* 7(1):44-49.

- Rullmann I, Schattenberg A, Marx M, Willershausen B, Ernst CP (2012). Photoelastic determination of polymerization shrinkage stress in low-shrinkage resin composites. *Schweizer Monatsschrift für Zahnmedizin = Revue mensuelle suisse d'odonto-stomatologie = Rivista mensile svizzera di odontologia e stomatologia / SSO* 122(4):294-299.
- Sakaguchi RL, Sasik CT, Bunczak MA, Douglas WH (1991). Strain gauge method for measuring polymerization contraction of composite restoratives. *Journal of dentistry* 19(5):312-316.
- Sakaguchi RL, Peters MC, Nelson SR, Douglas WH, Poort HW (1992). Effects of polymerization contraction in composite restorations. *Journal of dentistry* 20(3):178-182.
- Sakaguchi RL, Versluis A, Douglas WH (1997). Analysis of strain gage method for measurement of post-gel shrinkage in resin composites. *Dental materials : official publication of the Academy of Dental Materials* 13(4):233-239.
- Sakaguchi RL, Wiltbank BD, Murchison CF (2004a). Contraction force rate of polymer composites is linearly correlated with irradiance. *Dental materials : official publication of the Academy of Dental Materials* 20(4):402-407.
- Sakaguchi RL, Wiltbank BD, Shah NC (2004b). Critical configuration analysis of four methods for measuring polymerization shrinkage strain of composites. *Dental materials : official publication of the Academy of Dental Materials* 20(4):388-396.
- Sakaguchi RL, Powers JM (2012). *Craig's Restorative Dental Materials*. Philadelphia: Elsevier/Mosby, pp. 161-198.
- Sandholzer MA, Walmsley AD, Lumley PJ, Landini G (2013). Radiologic evaluation of heat-induced shrinkage and shape preservation of human teeth using micro-CT. *Journal of Forensic Radiology and Imaging* 0).
- Scherrer SS, Cesar PF, Swain MV (2010). Direct comparison of the bond strength results of the different test methods: a critical literature review. *Dental materials : official publication of the Academy of Dental Materials* 26(2):e78-93.
- Schneider LF, Cavalcante LM, Silikas N (2010). Shrinkage Stresses Generated during Resin-Composite Applications: A Review. *Journal of dental biomechanics* 2010(
- Schwass DR, Swain MV, Purton DG, Leichter JW (2009). A system of calibrating microtomography for use in caries research. *Caries Res* 43(4):314-321.
- Schweikl H, Hiller KA, Carl U, Schweiger R, Eidt A, Ruhl S *et al.* (2013). Salivary protein adsorption and *Streptococcus gordonii* adhesion to dental material surfaces. *Dental materials : official publication of the Academy of Dental Materials* 29(10):1080-1089.

Scientific Documentation Tetric EvoCeram® Bulk Fill (2013). In: IV AG editor. Schaan, Liechtenstein, pp. 39.

Sharp LJ, Choi IB, Lee TE, Sy A, Suh BI (2003). Volumetric shrinkage of composites using video-imaging. *Journal of dentistry* 31(2):97-103.

Simon Y, Mortier E, Dahoun A, Gerdolle DA (2008). Video-controlled characterization of polymerization shrinkage in light-cured dental composites. *Polymer Testing* 27(6):717-721.

Smith DL, Schoonover IC (1953). Direct filling resins: dimensional changes resulting from polymerization shrinkage and water sorption. *Journal of the American Dental Association (1939)* 46(5):540-544.

Soltesz U, Bath P, Klaiber B (1986). Dimensional behavior of dental composites due to polymerization shrinkage and water sorption. In: Biological and Biomechanical Performance of Biomaterials. P Christel, A Meunier and A Lee editors. Amsterdam: Elsevier, pp. 123-128.

Sorzano COS, Thevenaz P, Unser M (2005). Elastic registration of biological images using vector-spline regularization. *Biomedical Engineering, IEEE Transactions on* 52(4):652-663.

Suh BI, Wang Y (2001). Determining the direction of shrinkage in dental composites by changes in surface contour for different bonding configurations. *American journal of dentistry* 14(2):109-113.

Suliman AA, Boyer DB, Lakes RS (1993a). Interferometric measurements of cusp deformation of teeth restored with composites. *Journal of dental research* 72(11):1532-1536.

Suliman AA, Boyer DB, Lakes RS (1993b). Cusp movement in premolars resulting from composite polymerization shrinkage. *Dental materials : official publication of the Academy of Dental Materials* 9(1):6-10.

Suliman AH, Boyer DB, Lakes RS (1994). Polymerization shrinkage of composite resins: comparison with tooth deformation. *The Journal of prosthetic dentistry* 71(1):7-12.

Sun J, Lin-Gibson S (2008). X-ray microcomputed tomography for measuring polymerization shrinkage of polymeric dental composites. *Dental materials : official publication of the Academy of Dental Materials* 24(2):228-234.

Sun J, Eidelman N, Lin-Gibson S (2009a). 3D mapping of polymerization shrinkage using X-ray micro-computed tomography to predict microleakage. *Dental materials : official publication of the Academy of Dental Materials* 25(3):314-320.

Sun J, Fang R, Lin N, Eidelman N, Lin-Gibson S (2009b). Nondestructive quantification of leakage at the tooth-composite interface and its correlation with material performance parameters. *Biomaterials* 30(27):4457-4462.

Suzuki K, Anada T, Miyazaki T, Miyatake N, Honda Y, Kishimoto KN *et al.* (2014). Effect of addition of hyaluronic acids on the osteoconductivity and biodegradability of synthetic octacalcium phosphate. *Acta biomaterialia* 10(1):531-543.

Swanson TK, Feigal RJ, Tantbirojn D, Hodges JS (2008). Effect of Adhesive Systems and Bevel on Enamel Margin Integrity in Primary and Permanent Teeth. *Pediatric dentistry* 30(2):134-140.

Swennen GRJ, Barth EL, Eulzer C, Schutyser F (2007). The use of a new 3D splint and double CT scan procedure to obtain an accurate anatomic virtual augmented model of the skull. *International journal of oral and maxillofacial surgery* 36(2):146-152.

Swift EJ, Jr., Perdigao J, Heymann HO (1995). Bonding to enamel and dentin: a brief history and state of the art, 1995. *Quintessence international (Berlin, Germany : 1985)* 26(2):95-110.

Tagami J, Nikaido T, Nakajima M, Shimada Y (2010). Relationship between bond strength tests and other in vitro phenomena. *Dental materials : official publication of the Academy of Dental Materials* 26(2):e94-99.

Taha NA, Palamara JE, Messer HH (2009). Cuspal deflection, strain and microleakage of endodontically treated premolar teeth restored with direct resin composites. *Journal of dentistry* 37(9):724-730.

Takahashi H, Finger WJ, Wegner K, Utterodt A, Komatsu M, Wostmann B *et al.* (2010). Factors influencing marginal cavity adaptation of nanofiller containing resin composite restorations. *Dental materials : official publication of the Academy of Dental Materials* 26(12):1166-1175.

Takahashi N, Kitagami T, Komori T (1980). Behaviour of teeth under various loading conditions with finite element method. *Journal of oral rehabilitation* 7(6):453-461.

Tantbirojn D, Versluis A, Pintado MR, DeLong R, Douglas WH (2004). Tooth deformation patterns in molars after composite restoration. *Dental materials : official publication of the Academy of Dental Materials* 20(6):535-542.

Thresher RW, Saito GE (1973). The stress analysis of human teeth. *Journal of biomechanics* 6(5):443-449.

Toefco Engineered Coating Systems I (2013).

Tornavoi DC, Agnelli JA, Panzeri H, Reis AC (2013). Color change of composite resins subjected to accelerated artificial aging. *Indian journal of dental research : official publication of Indian Society for Dental Research* 24(5):605-609.

van Dijken JW, Horstedt P, Meurman JH (1985). SEM study of surface characteristics and marginal adaptation of anterior resin restorations after 3-4 years. *Scandinavian journal of dental research* 93(5):453-462.

Van Ende A, De Munck J, Van Landuyt KL, Poitevin A, Peumans M, Van Meerbeek B (2013). Bulk-filling of high C-factor posterior cavities: effect on adhesion to cavity-bottom dentin. *Dental materials : official publication of the Academy of Dental Materials* 29(3):269-277.

Van Meerbeek B, De Munck J, Yoshida Y, Inoue S, Vargas M, Vijay P *et al.* (2003). Buonocore memorial lecture. Adhesion to enamel and dentin: current status and future challenges. *Operative dentistry* 28(3):215-235.

Versluis A, Douglas WH, Cross M, Sakaguchi RL (1996). Does an incremental filling technique reduce polymerization shrinkage stresses? *Journal of dental research* 75(3):871-878.

Versluis A, Tantbirojn D, Douglas WH (1998). Do dental composites always shrink toward the light? *Journal of dental research* 77(6):1435-1445.

Versluis A, Tantbirojn D, Douglas WH (2004a). Distribution of transient properties during polymerization of a light-initiated restorative composite. *Dental materials : official publication of the Academy of Dental Materials* 20(6):543-553.

Versluis A, Tantbirojn D, Pintado MR, DeLong R, Douglas WH (2004b). Residual shrinkage stress distributions in molars after composite restoration. *Dental materials : official publication of the Academy of Dental Materials* 20(6):554-564.

Wagner DW, Lindsey DP, Beaupre GS (2011). Deriving tissue density and elastic modulus from microCT bone scans. *Bone* 49(5):931-938.

Watts DC, Amer O, Combe EC (1984). Characteristics of visible-light-activated composite systems. *British dental journal* 156(6):209-215.

Watts DC, Cash AJ (1991). Determination of polymerization shrinkage kinetics in visible-light-cured materials: methods development. *Dental materials : official publication of the Academy of Dental Materials* 7(4):281-287.

Watts DC, Hindi AA (1999). Intrinsic 'soft-start' polymerisation shrinkage-kinetics in an acrylate-based resin-composite. *Dental Materials* 15(1):39-45.

Watts DC, Marouf AS (2000). Optimal specimen geometry in bonded-disk shrinkage-strain measurements on light-cured biomaterials. *Dental materials : official publication of the Academy of Dental Materials* 16(6):447-451.

Watts DC, Marouf AS, Al-Hindi AM (2003). Photo-polymerization shrinkage-stress kinetics in resin-composites: methods development. *Dental materials : official publication of the Academy of Dental Materials* 19(1):1-11.

Watts DC, Satterthwaite JD (2008). Axial shrinkage-stress depends upon both C-factor and composite mass. *Dental materials : official publication of the Academy of Dental Materials* 24(1):1-8.

Weinmann W, Thalacker C, Guggenberger R (2005). Siloranes in dental composites. *Dental materials : official publication of the Academy of Dental Materials* 21(1):68-74.

Wilson HJ (1978). Properties of Radiation-Cured Restorative Resins. London: Franklin Scientific Projects.

Yamamoto A, Miyazaki M, Rikuta A, Kurokawa H, Takamizawa T (2007). Comparison of two methods for measuring the polymerization characteristics of flowable resin composites. *Dental materials : official publication of the Academy of Dental Materials* 23(7):792-798.

Yamamoto T, Ferracane JL, Sakaguchi RL, Swain MV (2009). Calculation of contraction stresses in dental composites by analysis of crack propagation in the matrix surrounding a cavity. *Dental Materials* 25(4):543-550.

Yamamoto T, Kubota Y, Momoi Y, Ferracane JL (2012). Polymerization stresses in low-shrinkage dental resin composites measured by crack analysis. *Dental materials : official publication of the Academy of Dental Materials* 28(9):e143-149.

Yu B, Ahn JS, Lee YK (2009). Measurement of translucency of tooth enamel and dentin. *Acta odontologica Scandinavica* 67(1):57-64.

Zeiger DN, Sun J, Schumacher GE, Lin-Gibson S (2009). Evaluation of dental composite shrinkage and leakage in extracted teeth using X-ray microcomputed tomography. *Dental materials : official publication of the Academy of Dental Materials* 25(10):1213-1220.

Zou W, Gao J, Jones AS, Hunter N, Swain MV (2009). Characterization of a novel calibration method for mineral density determination of dentine by X-ray microtomography. *Analyst* 134(1):72-79.

Eidesstattliche Versicherung

Kaisarly, Dalia Adel Mahmoud

Ich erkläre hiermit an Eides statt,

dass ich die vorliegende Dissertation mit dem Thema

“The Effect of Boundary Conditions on the Polymerization Shrinkage Vectors of Light-Cured Dental Resin Composites”

selbständig verfasst, mich außer der angegebenen keiner weiteren Hilfsmittel bedient und alle Erkenntnisse, die aus dem Schrifttum ganz oder annähernd übernommen sind, als solche kenntlich gemacht und nach ihrer Herkunft unter Bezeichnung der Fundstelle einzeln nachgewiesen habe.

Ich erkläre des Weiteren, dass die hier vorgelegte Dissertation nicht in gleicher oder in ähnlicher Form bei einer anderen Stelle zur Erlangung eines akademischen Grades eingereicht wurde.

München, den 29.07.2014